INTERNATIONAL SCIENTIFIC JOURNAL

GEOGRAPHICA PANNONICA

Impact factor: 1.8 | CiteScore: 3.1

Volume 28, Issue 1 (March 2024)

UNIVERSITY OF NOVI SAD, FACULTY OF SCIENCES

DEPARTMENT OF GEOGRAPHY, TOURISM AND HOTEL MANAGEMENT

UNIVERSITY OF NOVI SAD | FACULTY OF SCIENCES
DEPARTMENT OF GEOGRAPHY, TOURISM & HOTEL MANAGEMENT

INTERNATIONAL SCIENTIFIC JOURNAL

GEOGRAPHICA PANNONICA

Impact factor: 1.8 | CiteScore: 3.1

Volume 28, Issue 1, March 2024

ISSN 0354-8724 (hard copy) | ISSN 1820-7138 (online) | UDC 05:91(497.1)=20

ISSN 0354-8724 (hard copy) | ISSN 1820-7138 (online) | UDC 05:91(497.1)=20

INTERNATIONAL SCIENTIFIC JOURNAL

GEOGRAPHICA PANNONICA

UNIVERSITY OF NOVI SAD | FACULTY OF SCIENCES | DEPARTMENT OF GEOGRAPHY, TOURISM & HOTEL MANAGEMENT

EDITORIAL OFFICE

Faculty of Sciences
Department of Geography, Tourism and Hotel Management
Trg Dositeja Obradovića 3, 21000 Novi Sad, Serbia
tel. +381 21 450-105
fax +381 21 459-696
Official site: www.dgt.uns.ac.rs

CONTACTS

Lazar Lazić, PhD, full professor
Department of Geography, Tourism and Hotel Management, Serbia, lazar.lazic@dgt.uns.ac.rs

Dragan Milošević, teaching assistant
Department of Geography, Tourism and Hotel Management, Serbia, dragan.milosevic@dgt.uns.ac.rs

Official mail of the Journal
gpscijournal@dgt.uns.ac.rs

Internet portal
www.dgt.uns.ac.rs/pannonica.html

Instructions to authors
www.dgt.uns.ac.rs/pannonica/instructions.htm

Contents

Hamza Bendechou, Ahmed Akakba, Mohammed Issam Kalla, Abderrahmane Ben Salem Hachi

Monitoring and Predicting Land Use/Land Cover Dynamics in Djelfa City, Algeria, using Google Earth Engine and a Multi Layer Perceptron Markov Chain Model 1

doi: 10.5937/gp28-47299

Ádám Gyurkó, Zoltán Bujdosó, Al Fauzi Rahmat, Lóránt Dénes Dávid

Characterisation of Hungary's Regional Tourism and Economic Performance between 2004 and 2022 in the Light of EU Funding 21

doi: 10.5937/gp28-48906

Nusret Drešković, Samir Đug, Muniba Osmanović

NDVI and NDBI Indexes as Indicators of the Creation of Urban Heat Islands in the Sarajevo Basin 34

doi: 10.5937/gp28-48216

Tamara Jovanović, Katarina Otašević, Ljubica Ivanović Bibić, Jelena Milanković Jovanov, Anđelija Ivkov Džigurski, Aleksandra Dragin, Smiljana Đukičin Vučković, Stefan Stajić, Aco Lukić, Lazar Kotorčević

Which Psychological Characteristics Make a Good Geography Teacher in High School? 44

doi: 10.5937/gp28-47894

Waleed Babiker, Guirong Tan, Mohamed Abdallah Ahmed Alriah, Ayman M. Elameen

Evaluation and Correction Analysis of the Regional Rainfall Simulation by CMIP6 over Sudan 53

doi: 10.5937/gp28-46565

Shivanjali Mohite, Meenal Surawar

Assessing Pedestrian Thermal Comfort to Improve Walkability in the Urban Tropical Environment of Nagpur City 71

doi: 10.5937/gp28-48166

INTERNATIONAL SCIENTIFIC JOURNAL
GEOGRAPHICA PANNONICA
Volume 28, Issue 1, 1–20 (March 2024)
Contents lists available at ScienceDirect
Journal homepage: http://www.dgt.uns.ac.rs/en/homepage/pannonica/

Monitoring and Predicting Land Use/Land Cover Dynamics in Djelfa City, Algeria, using Google Earth Engine and a Multi Layer Perceptron Markov Chain Model

Hamza Bendechou[A*], Ahmed Akakba[A], Mohammed Issam Kalla[A], Abderrahmane Ben Salem Hachi[B]

[A] *Laboratory of natural hazards and spatial planning (LRNAT), Earth and Universe Sciences Institute, University of Batna 2, Batna, Algeria; h.bendechou@univ-batna2.dz, a.akakba@univ-batna2.dz, m.kalla@univ-batna2.dz*

[B] *Department of Earth and Universe Sciences, University Ziane Achour of Djelfa, Djelfa, Algeria; iha2007hachi@gmail.com*

KEYWORDS

Land use/land cover
Google Earth Engine
Support vector machine
Multi Layer Perceptron
Markov Chain
Djelfa city

ABSTRACT

Understanding the historical and projected changes in land use and land cover (LULC) in Djelfa city is crucial for sustainable land management, considering both natural and human influences. This study employs Landsat images from the Google Earth Engine and the support vector machine (SVM) technique for LULC classification in 1990, 2005, and 2020, achieving over 90% accuracy and kappa coefficients above 88%. The Land Change Modeler (LCM) was used for detecting changes and predicting future LULC patterns, with Markov Chain (MC) and Multi Layer Perceptron (MLP) techniques applied for 2035 projections, showing an average accuracy of 83.96%. Key findings indicate a substantial urban expansion in Djelfa city, from 924.09 hectares in 1990 to 2742.30 hectares in 2020, with a projected increase leading to 1.6% of nonurban areas transitioning to urban by 2035. There has been significant growth in steppe areas, while forested, agricultural, and barren lands have seen annual declines. Projections suggest continued degradation of bare land and a slight reduction in steppe areas by 2035. These insights underscore the need for reinforced policies and measures to enhance land management practices within the region to cater to its evolving landscape and promote sustainable development.

Introduction

Land Use/Land Cover Change (LULCC) resulting from human activities is a well-recognized global phenomenon that has significantly transformed the Earth's terrestrial surface. Over the period from 1960 to 2019, approximately one-third of the Earth's land area underwent alterations (Winkler et al., 2021). While human-induced changes to land have been practised for thousands of years, the scale and pace of LULCC in recent times have escalated significantly, exerting profound effects at local, regional, and global scales. These changes are crucial for understanding the altered landscape, ecological stewardship, and future-oriented environmental planning (Dwivedi et al., 2005; Fan et al., 2007a; Zhao et al., 2004). In the last three centuries, global LULCC has been characterized by the expansion of agriculture at the expense of forested areas (Kolb et al., 2013; Pérez-Vega et al., 2012). This trend is particularly evident in Africa, where natural vegetation has given way to anthropogenic land uses (Barnieh et al., 2020;

* Corresponding author: Hamza Bendechou; email: bendechou@gmail.com

doi: 10.5937/gp28-47299

Received: October 23, 2023 | Revised: January 08, 2024 | Accepted: February 06, 2024

Bullock et al., 2021; Findell et al., 2017). Between 2012 and 2017, Africa experienced a substantial reduction in natural vegetation and an increase in impervious areas, primarily due to population growth and soil desiccation driven by climate change (Nowak & Greenfield, 2020). Various factors, including population growth, economic expansion, and physical variables like topography, climate, and soil composition, significantly influence land use and land cover changes (Skole & Tucker, 1993).

Choosing appropriate prediction and validation time intervals significantly influences the accuracy of predictions (Chen & Pontius, 2010). The accuracy of predictions can be influenced by the pace and nature of transitions within the selected time intervals. Utilizing a broader temporal scale for modeling land cover change might lead to an inadequate understanding of landscape change patterns, potentially compromising the overall performance of the model (Alvarez Martinez et al., 2011). Many research studies focusing on future land cover change tend to adopt relatively short to intermediate historical time scales, typically spanning 5 to 15 years.

Land use change is intricately linked to historical processes, reflecting how communities interact with and utilize their landscapes. In contemporary times, land use has evolved beyond habitation to encompass industrial ventures and tourism (Mather, 1986). Analyzing LULC changes is crucial for understanding global transformations across spatial and temporal dimensions (Lambin, 1997) and provides insights into human activities within specific environments (López et al., 2001).

However, the rapid global population growth has placed substantial pressure on land resources, leading to complex interactions among environmental factors (Green et al., 1994). Land use change is a dynamic process with nonlinear patterns that can initiate intricate feedback loops, affecting living conditions and community vulnerability. Therefore, evaluating land use change trajectories and projecting future scenarios is essential for establishing sustainable conditions.

Remote sensing technology offers a rapid and effective means of monitoring LULC changes due to its broad spatial coverage, frequent updates, and abundant data availability (Homer et al., 2020; Zhao et al., 2016). However, processing remote sensing data traditionally can be time-consuming and resource-intensive, especially for large-scale LULC information extraction. The emergence of cloud storage and computing technology, such as Google Earth Engine (GEE), has revolutionized the handling of extensive remote sensing data, making it a pivotal tool for monitoring land use changes (Gorelick et al., 2017). Satellite imagery, in particular, facilitates comprehensive monitoring of deforestation and landscape dynamics on a global scale (Noma et al., 2013; Oliveira, 2017).

The adoption of cloud-based platforms like GEE is essential for handling large-scale data efficiently, enabling the analysis of expansive spatial regions without the need for extensive data downloads (Fadli et al., 2019).

Many scholars have conducted research using GEE to monitor LULC changes, water resources, eco-environmental quality, and agricultural resources (Dong et al., 2016; Ermida et al., 2020; Hu et al., 2018; Li et al., 2021; MAO & LI, 2021; Wang et al., 2020; Xiong et al., 2017; Xiong et al., 2021).

Land Change Models, such as the Markov Chain Model (MC), Artificial Neural Networks (ANN), and the Land Change Modeler (LCM), play a significant role in environmental and geomatics research related to LULCC (Camacho Olmedo et al., 2015). Monitoring and analyzing LULC changes are essential for understanding current land use patterns and their alterations, facilitating sustainable development initiatives (Fan et al., 2007b). These models enhance our understanding of land use modifications driven by human activities (Brown et al., 2004).

Several methods, including the Markov chain (MC), artificial neural network (ANN), cellular automata (CA), CA-Markov, binary logistic regression (BLR), and similarity-weighted instance-based machine learning algorithms (MLA), are commonly employed to predict and simulate future LULC changes (Anand et al., 2018; Azari et al., 2016; Islam et al., 2018; Liu et al., 2017; Mozumder et al., 2016; Sinha et al., 2015). LCM stands out for its significance in capturing land cover changes and its applicability in various contexts (Halmy et al., 2015). However, no single model is superior to others, and the choice depends on specific research objectives (Alqadhi et al., 2021).

The integration of Multi Layer Perceptron (MLP) algorithms into LCM frameworks allows researchers to harness the power of MLP's ability to learn from historical data and generate projections for future land cover scenarios. MLP neural networks, with their input, hidden, and output layers, excel at capturing complex, nonlinear relationships (Siroosi et al., 2020). They are particularly useful when prior knowledge is limited, accommodating missing data and operating without stringent requirements, unlike some other models (Pontius et al., 2008).

Incorporating both natural and human factors into LULC dynamics is essential for projecting potential future scenarios. These driving forces can manifest as direct or indirect influences, making their consideration crucial for optimizing land use and sustainable planning (Behera et al., 2012).

The MLPNN algorithm was employed to map the significant potential transitions between different LULC classes (Larbi et al., 2019). As per Eastman (2020), MLP neural networks have been identified as the most robust approach for mapping transition potentials. While the logistic regression method remains a viable option, MLP neural networks offer the advantage of simultaneously modeling

multiple or even all transitions, making them highly adept at capturing nonlinear relationships (Eastman, 2020).

This study focuses on Djelfa city, Algeria, which has experienced significant growth and land use changes since its establishment in 1962. However, a comprehensive evaluation of these changes using remote sensing and GIS technology is lacking. Such an assessment is crucial for effective urban planning to address the challenges posed by rapid urbanization. The study aims to analyze land use transformations in Djelfa city, document temporal shifts, identify driving factors, and examine initiatives for managing these changes. Ultimately, the research seeks to provide valuable insights for sustainable urban planning and land management in Djelfa city.

Historical satellite images are used to monitor and analyze LULC changes, with a focus on predicting future changes under a business-as-usual scenario. Understanding past, current, and projected LULC changes is vital for effective land management in Djelfa city, considering ongoing socioeconomic transformations. The study utilizes GEE for SVM supervised classification, a high-performance machine learning algorithm renowned for its accuracy in LULC classification.

While existing research in Djelfa city using remote sensing images on the GEE platform is limited, this study fills the gap by providing a comprehensive 45-year assessment of land use changes, thus contributing valuable empirical data for land use policies and sustainable planning in the region. The research is instrumental in understanding the spatial dynamics of land use changes, preventing resource misallocation, and enhancing land management in Algeria.

Materials and methods

Study area

The study is focused on the capital city of Djelfa Province, situated in the central region of northern Algeria. It is positioned approximately 300 km south of the country's capital. The city is located within the geographic coordinates of 34° 31' to 34° 48' North latitude and 3° 4' to 3° 21' East longitude. Encompassing an area of 542.17 km², the study area exhibits distinct climatic features, predominantly classified as semi-arid. The prevailing climatic conditions in the study area are indicative of a semi-arid climate, characterized by an annual average precipitation ranging between 200 mm and 500 mm. The climate is typified by hot semi-arid summers, with maximum temperatures reaching up to 33 °C, contrasted by cold subtropical winters, during which temperatures can drop below 0°C. Geographically, the study area is situated within a region marked by plateaus, varying in altitude between 900 m and 1400 m (D.P.S.B, 2020) (Figure 1).

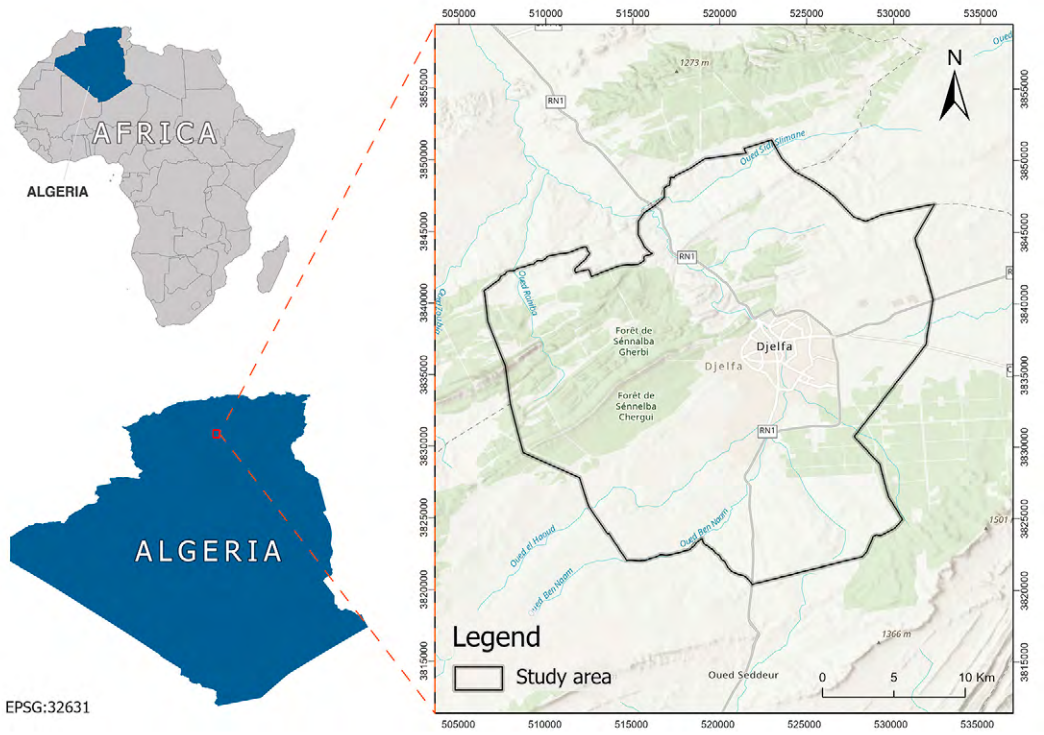

Figure 1. The study area
Source: ESRI Map including World Topographic Map and World Hillshade

Data collection

This study utilized data primarily from Landsat TM/OLI for remote sensing imagery, digital elevation model (DEM) for topographic analysis, and various geographic and socioeconomic datasets (Table 1). Specifically, we employed Landsat 5 TM for 1990 and 2005, and Landsat 8 OLI for 2020 due to their relevance in LULC analysis, detailed in Table 2. These images facilitate the identification of land use and land cover transitions (Midekisa et al., 2017) and were utilized as inputs for the analysis of land use and land cover changes. To clarify, classification was conducted on three individual years within the specified period (Feng et al., 2020; Rawat & Kumar, 2015), avoiding any implication of continuous annual study.

The term 'ground truth data' refers to actual observations used as training samples to develop the land classification model, detailed in Table 3. This includes data from field surveys and digitized high-resolution images from Google Earth. The employment of these ground truth data was critical in developing three distinct classified images for the respective years, reflecting the diverse LULC classes within Djelfa city (Wagle et al., 2020; Zadbagher et al., 2018).

Image preprocessing

In this study, GEE was utilized for its extensive repository of satellite imagery, known for radiometric and geometric corrections. Our preprocessing involved specific scaling

Table 1. Factors influencing the LULC changes.

Type	Code	Name	Source
Socioeconomic factors	TMI	Topographic map index	https://www.earthdata.nasa.gov/sensors/srtm Shuttle Radar Topography Mission (SRTM)
	DFR	Distance from roads	https://www.openstreetmap.org/ Downloaded the shapefile of Road Open Street distance method Map Road network (Town plan for the wilaya of Djelfa 2023)
	DFB	Distance from the built up land	https://earthexplorer.usgs.gov/ Downloaded the shapefile of built up area (Town plan for the wilaya of Djelfa 2023)
Natural factors	DFS	Distance to stream	https://www.hydrosheds.org/ Download toposheet map of study area
	SLP	Slope gradients	https://www.earthdata.nasa.gov/sensors/srtm Shuttle Radar Topography Mission (SRTM)
	ELV	Elevation	https://www.earthdata.nasa.gov/sensors/srtm Shuttle Radar Topography Mission (SRTM)

Table 2. Landsat image collections used for classification

Year	Satellite	Sensor	RBG composite bands	Spatial resolution	Period of collection
1990	Landsat	5-TM	3-4-5	30m	01/01/90–31/12/90
2005	Landsat	5-TM	3-4-5	30m	01/01/05–31/12/05
2020	Landsat	8-OLI	4-5-6	30m	01/01/20–31/12/20
TM Thematic Mapper, OLI Operational Land Image					

Source: USGS

Table 3. Number of Training samples of LULC units for 1990, 2005, and 2020

LULC units	Number of Training samples		
	1990	2005	2020
Urban Area	28	30	29
Agricultural Land	23	31	31
Forest Land	46	46	44
Steppe	29	29	29
Bare land	44	44	43
Total	170	180	176

techniques to adjust image values for true surface reflectance, crucial for accurate land cover classification (Carneiro et al., 2021; Mugiraneza et al., 2020; Roy et al., 2020). Cloud masking was conducted using a Landsat Simple Cloud Score algorithm, as influenced by the approaches outlined in (Carneiro et al., 2021). To further enhance the classification process, NDVI and NDBI indices were computed, serving as supplementary attributes to enrich the dataset with vital details on vegetation and built-up areas (Barnieh et al., 2020; Feng et al., 2016; Hackman et al., 2017, 2020; Prasomsup et al., 2020; Yu et al., 2014).

Topographic Analysis

In our methodology, the Topographic Index (TI) was calculated using the widely accepted formula developed by (Beven et al., 1984), utilizing Aster GDEM data. TI, which quantifies relative humidity, is integral to understanding moisture dynamics and their implications on land characteristics.

Analysis of Spatial Variables

The analysis of spatial variables was conducted using Cramer's V to distinguish between static and dynamic properties. Specifically, distance from roads and distance from settlements were identified as dynamic factors, while other variables were considered static. The derived Cramer's V values were adopted as weighting factors for the spatial variables and incorporated into the MC model for future projections. The transformation of categorical maps into continuous maps was facilitated using the Evidence Likelihood transformation, aiding in a more refined and comprehensive analysis of land cover transitions (Mas et al., 2014).

Image classification and accuracy assessment

In this study, we employed the GEE, an open-access cloud-based platform, for image collection, supervised classification, and accuracy assessment, utilizing AI machine learning algorithms. Specifically, the SVM classifier was used within the GEE for accurate LULC classification (Mantero et al., 2004; Wahap & Shafri, 2020). The GEE code editor was a valuable tool for analysis and customization via programming code. Training samples were crucial for this process and are detailed in Table 3. For each year, 70% of the samples were used for training the SVM classification algorithm, and the remaining 30% for testing, focusing on SVM's capability to minimize misclassified pixels (Shaharum et al., 2020). Quantitative accuracy of the classified LULC maps was measured using two key metrics: Overall Accuracy (OA) and the Kappa index (K). OA is the ratio of correctly classified pixels to the total number of pixels, and it's calculated using equation (1). The Kappa index measures agreement by chance in the classification process, and it's represented by equation (2).

$$OA = \left(\frac{\sum_{i=1}^{n} x_i}{N} \right) \cdot 100 \quad (1)$$

Where x_i represents the number of correctly classified pixels for each class and N is the total number of pixels.

$$K = \frac{\sum a - \sum ef}{N - \sum ef} \quad (2)$$

Where a is the frequency of correct classifications for each category, ef is the expected frequency of correct classifications by chance, and N is the total number of pixels.

We also implemented the MLP model to refine the land cover classification process, training it with 75% of the data and testing with the remaining 25%. This ensured robust predictive performance, with the optimal MLP training parameters detailed in Table 8. Support vectors in the SVM framework were instrumental in defining the hyperplane, thereby maximizing the separation between classes (Liu et al., 2020). This process and the resulting classified images are visualized in Figure 2.

Change detection and transition analysis using LCM

We utilized the LCM integrated with IDRISI Selva software to analyze and predict land use changes in Djelfa city for the periods 1990-2005 and 2005-2020, employing categorized maps from Landsat imagery (Abijith & Saravanan, 2022; Mishra et al., 2018; Shawul & Chakma, 2019). The LCM's application included:

- Calculating annual rate of change for each LULC class.
- Generating FROMTO change maps and spatial trend maps using a third-degree polynomial function (Eastman, 2020).
- Determining the extent of land surface change between LULC states to understand the dynamics over the designated periods (Singh, 1989).

In-depth evaluations of land use dynamics and biodiversity impacts were conducted, with the findings offering insights into the anthropogenic influences on various LULC classes. The percentage change is computed using Equation (3) to quantify the extent of changes (Hussien et al., 2023).

$$p = \frac{(AI - Ae) \cdot 100}{Ae} \quad (3)$$

Where AI is the area in a later LULC map, and Ae is the area in an earlier LULC map. The analysis utilized the post-classification approach for a comprehensive evaluation of LULC dynamics. The specific methodologies and

outcomes of LCM within the context of Djelfa city are now detailed and precise, addressing the need for specificity.

Consolidated Modeling and Prediction Analysis

For our LULC change prediction, the MLP and MC models were utilized (Mishra & Rai, 2016). The MLP model, noted for its 83.96% accuracy rate, facilitated the creation of potential change maps as crucial inputs for further MC analysis, aiming to project future land cover changes with associated probabilities (Gashaw et al., 2018). Initial modeling involved using transition potential images from key historical years as part of the predictive groundwork.

The study also integrated various natural and anthropogenic factors affecting land cover, utilizing a combination of topographic, demographic, and environmental data (Kim & Newman, 2020; Mirici et al., 2018). This integration was critical in predicting transition potentials and understanding the implications of various land cover drivers on future land use scenarios. An empirical analysis of shifts in land cover was conducted, focusing on quantifying changes and predicting future scenarios (Eastman, 2015; Karul & Soyupak, 2003). A rigorous validation phase followed the initial modeling to ensure the model's predictive accuracy (Chaudhuri & Clarke, 2014).

The simulation results from these models aimed to provide a nuanced understanding of the LULC changes over time. This involved mapping the gains and losses within distinct LULC classes to offer insights into the dynamics of land use changes and the effectiveness of our modeling approach (Hasan et al., 2020; Shaharum et al., 2020).

Model validation

The reliability of our predictive models was ensured through a rigorous validation process subsequent to the initial calibration phase. This involved a two-step approach where model parameters were first fine-tuned, followed by a rigorous assessment of predictive accuracy. The validation phase primarily utilized the Kappa coefficient, a widely recognized metric for measuring the accuracy of predictive models (Congalton, 1991; Singh et al., 2018). The process involved comparing forecasted LULC data gener-

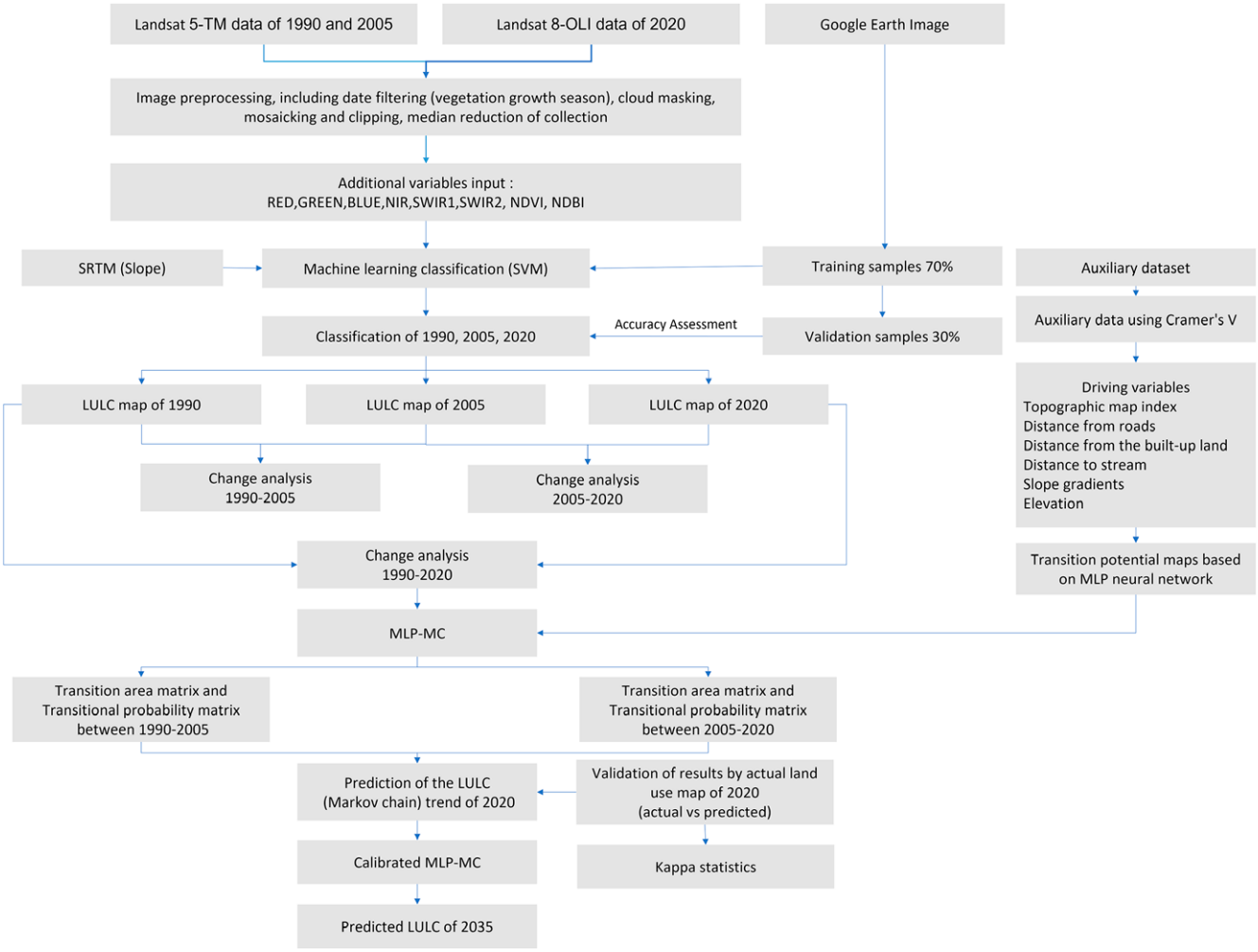

Figure 2. Overview of the methodology of LULC maps classification and prediction in the Djelfa city

ated by the model against a set of reference data to evaluate the model's predictions (Bununu, 2017; Congalton, 1991). Insights gained from this validation phase contributed to understanding the potential to project LULC scenarios for future years, thereby extending the applicability and relevance of the study's findings.

Results

Our key findings and conclusions can be summarized as follows:

LULC Mapping and Accuracy

The study conducted multitemporal LULC mapping for 1990, 2005, and 2020 with overall accuracies of 90%, 94%, and 94% respectively. Kappa coefficients indicated high reliability across all years. The SVM classification, visualized in Figure 3, and the detailed proportions in Table 4, revealed significant land cover dynamics over the three decades. A notable trend was the decrease in Bare land and an increase in Urban Area and Steppe, indicating a shift towards anthropogenic land use. The classification and transitions are detailed in the confusion matrix (Table 5) and visualized changes (Figures 4 and 5). The detailed weighting values of explanatory variables and transitions between LULC classes are provided in Table 6 and Table 7, with the driving forces and their significance presented in Table 8.

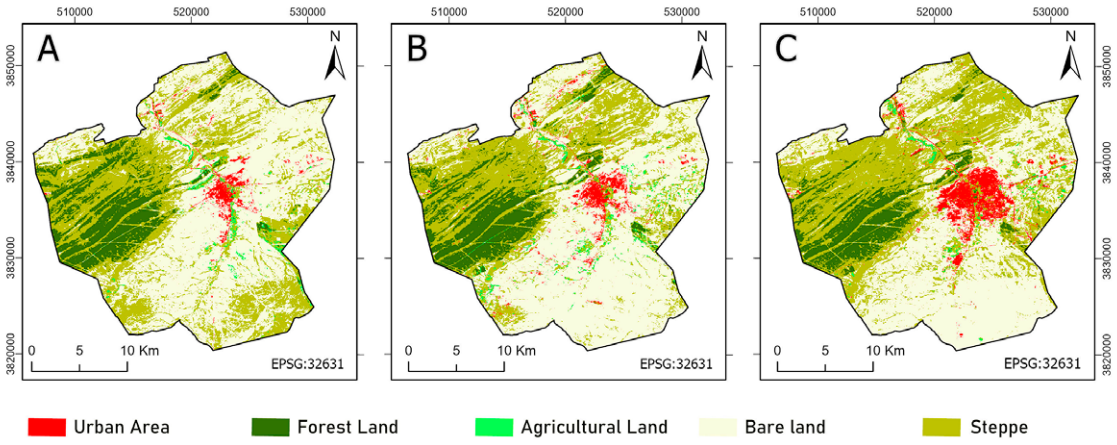

Figure 3. SVM classification results in GEE of (A) 1990, (B) 2005 and (C) 2020.

Table 4. Proportion of LULC units in 1990, 2005 and 2020

LULC unit	1990		2005		2020	
	Area (Ha)	Area (%)	Area (Ha)	Area (%)	Area (Ha)	Area (%)
Urban Area	924.09	1.75	1405.12	2.66	2742.30	5.20
Forest Land	6174.25	11.70	6128.76	11.61	5344.06	10.12
Agricultural Land	768.25	1.46	1051.47	1.99	547.05	1.04
Bare land	27944.39	52.94	28632.48	54.24	24976.58	47.32
Steppe	16974.66	32.16	15567.96	29,49	19175.79	36.33
Total	52785.64	100.00	52785.79	100.00	52785.79	100.00

Table 5. Confusion matrix of the LULC classification in 1990, 2005 and 2020

LULC 1990					
	Urban Area	Forest Land	Agricultural Land	Bare Land	Steppe
Urban Area	17	0	0	0	0
Forest Land	0	31	0	0	3
Agricultural Land	0	0	14	0	0
Bare land	0	0	1	32	3
Steppe	0	1	0	3	16
LULC 2005					
	Urban Area	Forest Land	Agricultural Land	Bare Land	Steppe
Urban Area	21	0	0	0	0
Forest Land	0	28	0	0	1
Agricultural Land	0	0	23	0	1
Bare land	1	0	2	26	1
Steppe	0	0	0	1	15
LULC 2020					
	Urban Area	Forest Land	Agricultural Land	Bare Land	Steppe
Urban Area	22	0	0	0	0
Forest Land	0	25	0	0	4
Agricultural Land	0	0	13	0	0
Bare land	0	0	0	27	0
Steppe	0	0	0	2	23

Table 6. Markov transitional probability matrix of land use types in Djelfa city based on (1990 to 2005), (2005 to 2020)

		LULC 1990				
		Urban Area	Forest Land	Agricultural Land	Bare Land	Steppe
LULC 2005	Urban Area	0.68	0.00	0.01	0.24	0.07
	Forest Land	0.00	0.84	0.00	0.00	0.16
	Agricultural Land	0.02	0.10	0.30	0.27	0.31
	Bare Land	0.02	0.00	0.02	0.84	0.12
	Steppe	0.01	0.05	0.02	0.28	0.64
		LULC 2005				
		Urban Area	Forest Land	Agricultural Land	Bare Land	Steppe
LULC 2020	Urban Area	0.71	0.01	0.01	0.13	0.14
	Forest Land	0.00	0.81	0.00	0.00	0.18
	Agricultural Land	0.05	0.05	0.16	0.21	0.53
	Bare Land	0.05	0.00	0.01	0.78	0.16
	Steppe	0.01	0.02	0.01	0.14	0.82

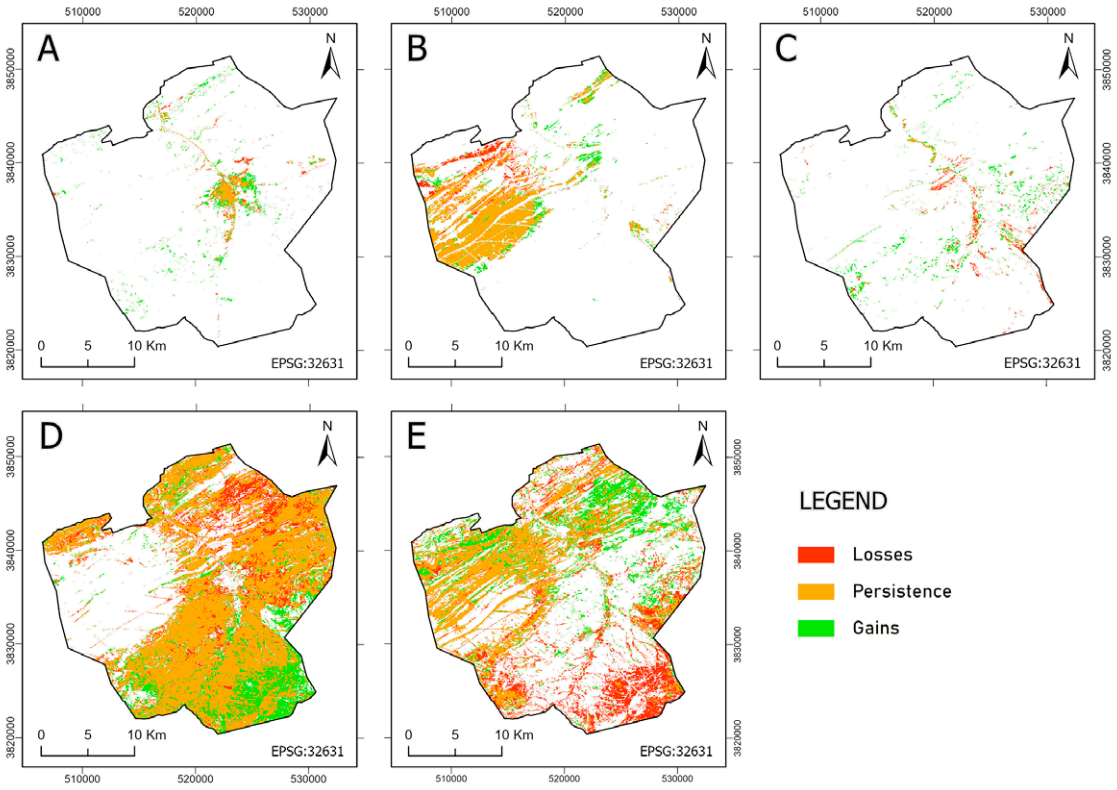

Figure 4. Gains and losses in various LULC between 1990 and 2005: (A) Urban Area, (B) Forest Land, (C) Agricultural Land, (D) Bare land, and (E) Steppe

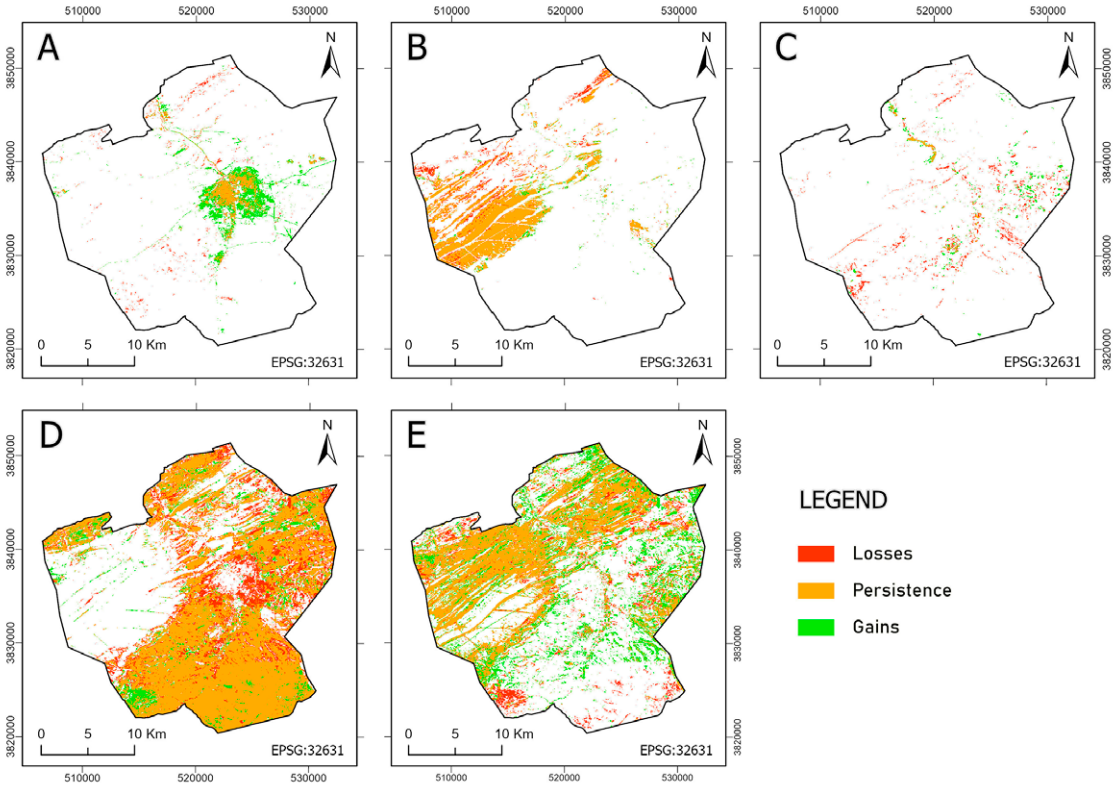

Figure 5. Gains and losses in various LULC between 2005 and 2020: (A) Urban Area, (B) Forest Land, (C) Agricultural Land, (D) Bare land, and (E) Steppe

Table 7. Driving forces with Cramer's V

Driving force	Cramer's V
Topographic map index	0.44
Distance from roads	0.49
Distance from the built up land	0.41
Distance to stream	0.27
Slope gradients	0.39
Elevation	0.62

Table 8. MLP model variable value and accuracy rate

Variables	Results
Hidden layer nodes	17
Start learning rate	0.01
End learning rate	0.001
Momentum factor	0.5
RMS	0.01
Iteration	10000
Training RMS	1
Testing RMS	1
Accuracy rate (%)	83.96
Skill measure	0.6791

Modeling LULC Transformation

The MLP method was employed for modeling the transformation potential for each LULC class. To facilitate this, an input dataset for the MultiLayer Perceptron, including spatial variables like elevation, distance from roads, and topographic index, was compiled and is illustrated in Figure 6. This groundwork led to the identification of nine significant transformations, which were then modeled and visualized in Figures 7 and 8. The process involved using the spatial variables mentioned earlier, leading to the generation of transition probability maps. These transitions underscore the region's dynamic land use, with a particular focus on the expansion of urban areas and the transformation of natural land cover types.

Model Validation

The validation process assessed the model's predictive accuracy using the Kappa coefficient (Table 9), comparing forecasted data with actual classified maps (Figure 9). The high Kappa value obtained signifies a robust fit and reliability of the model's predictions, suggesting the model's efficacy in forecasting future land cover dynamics. The kappa index values of the simulated LULC map for 2020, demonstrating the effectiveness of our model predictions, are presented in Table 10. This validation confirms the models' applicability for future LULC projections and the robustness of their predictions (Pontius, 2000).

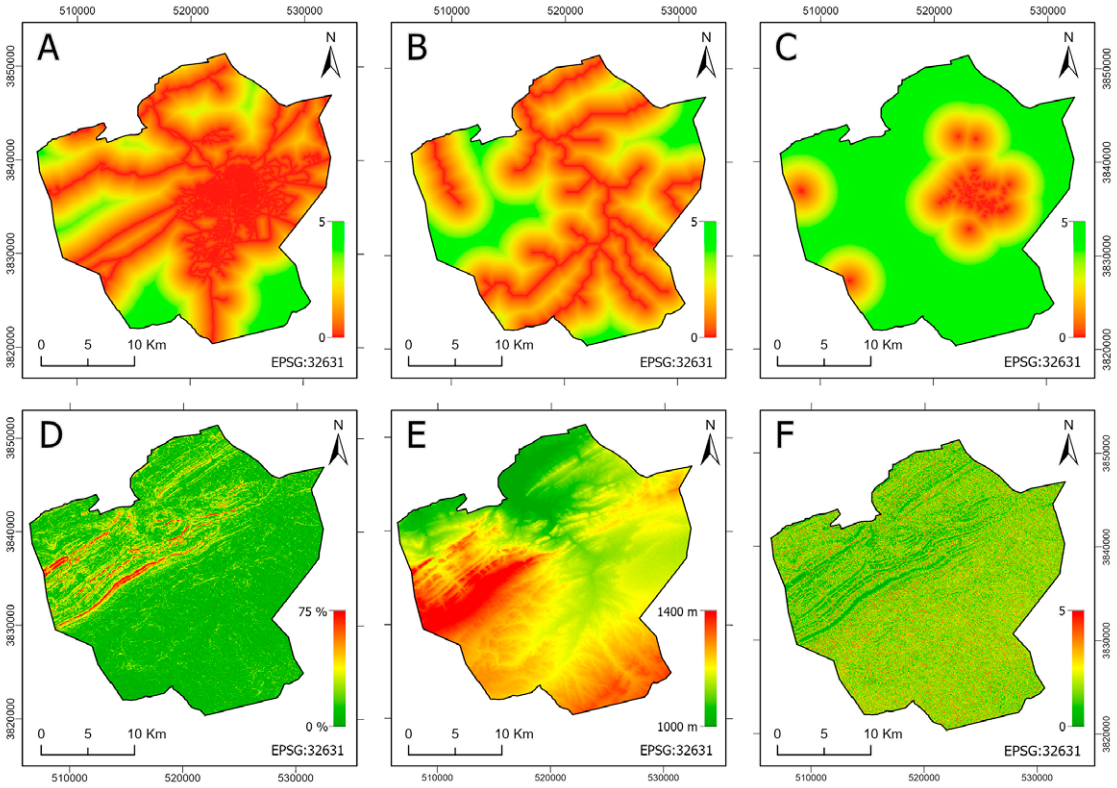

Figure 6. Input dataset for MultiLayer Perceptron: (A) Distance Road, (B) Distance stream hydro, (C) Distance urban, (D) Slope, (E) Elevation (DEM), and (F) Topographic map index

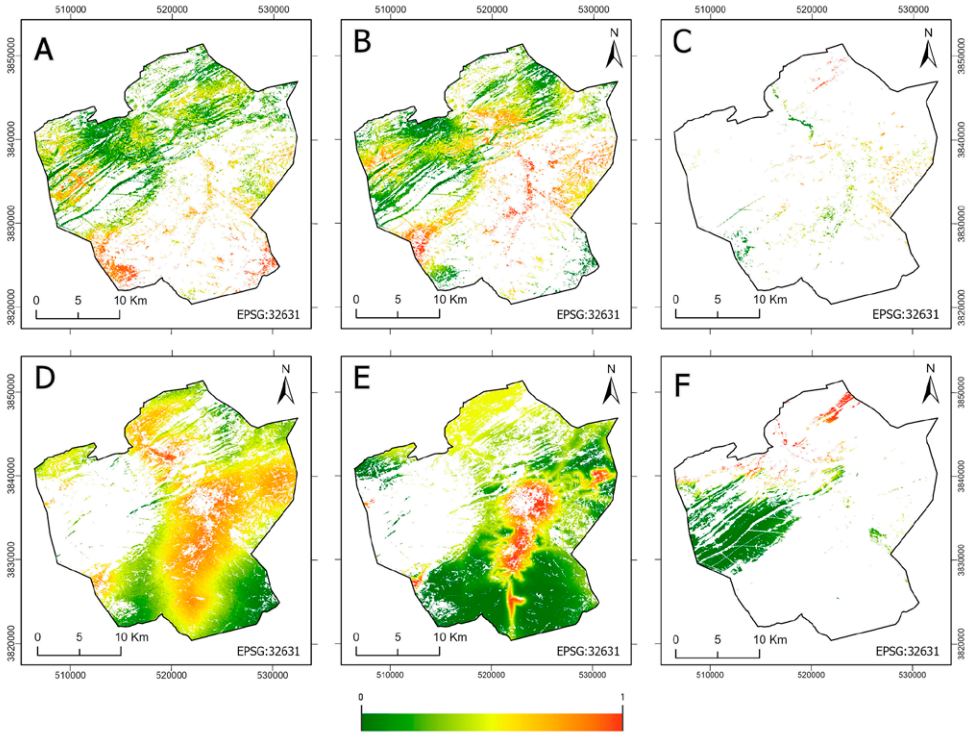

Figure 7. Major transformation. during 1990 to 2005; (A) from steppe to Bare land, (B) from steppe to Agricultural Land, (C) from Agricultural Land to Forest Land, (D) from Bare land to Agricultural Land, (E) from Bare land to Urban Area and (F) from Forest Land to steppe

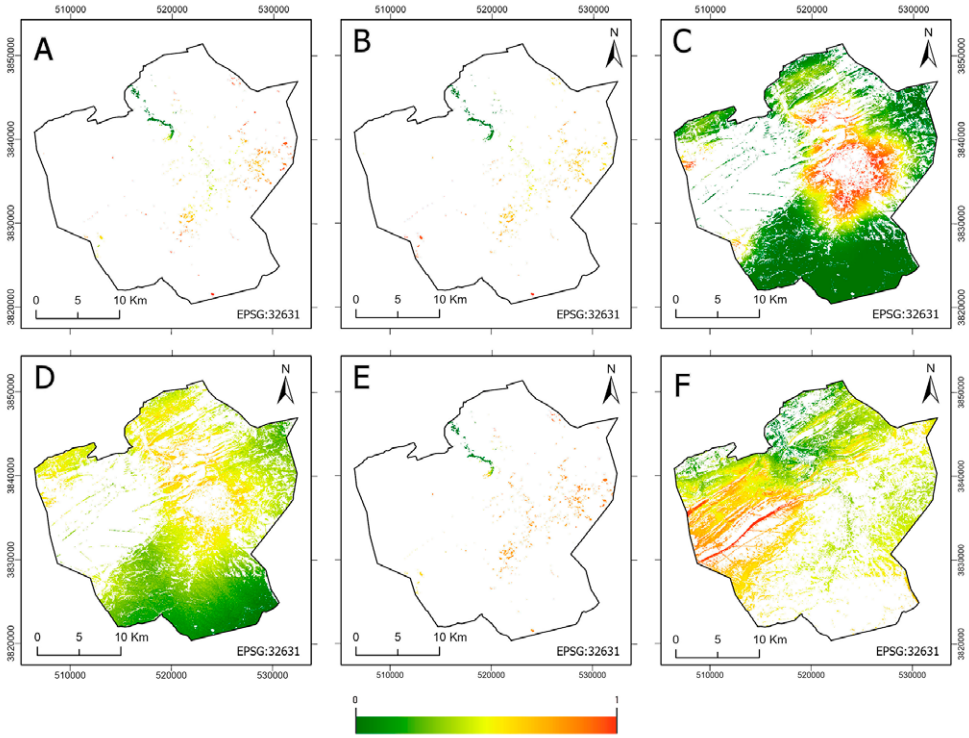

Figure 8. Major transformation. during 2005 to 2020; (A) from Agricultural Land to steppe, (B) from Agricultural Land to Forest Land, (C) from Bare land to Urban Area, (D) from Bare land to steppe, (E) from Agricultural Land to Urban Area and (F) from Forest Land to steppe

Table 9. LULC change prediction validation based on the actual and projected 2020 LULC

LULC Types	Projected 2020		Actual 2020	
	Area (Ha)	Area (%)	Area (Ha)	Area (%)
Urban Area	2742,30	5,20	2607,71	4,94
Agricultural Land	5344,06	10,12	5568,87	10,55
Forest Land	547,05	1,04	580,47	1,10
Steppe	24976,58	47,32	24862,69	47,10
Bare Land	19175,79	36,33	19166,05	36,31
Total	52785,79	100,00	52785,79	100,00

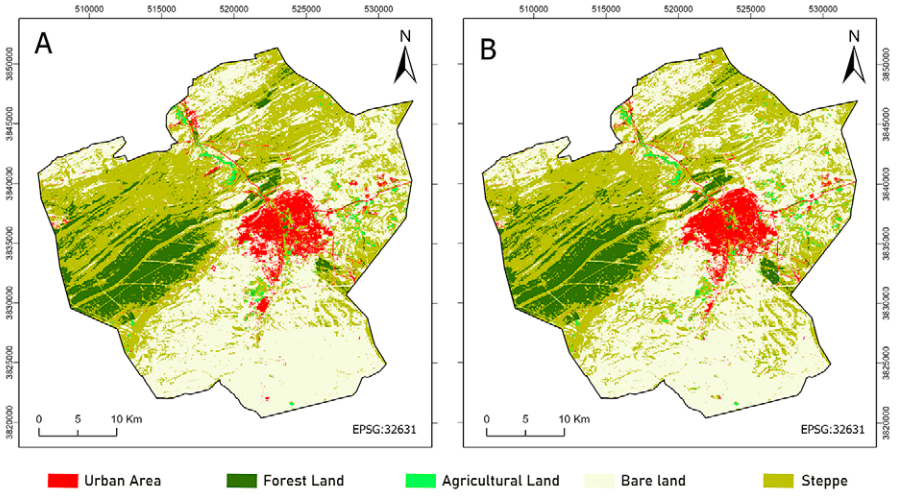

Figure 9. Observed and predicted LULC maps: (A) 2020 LULC observed, (B) 2020 LULC predicted

Table 10. The k index values of the simulated LULC map of 2020

Index	Value
Kno	0.9155
Klocation	0.8999
KlocationStrata	0.8999
Kstandard	0.8930

Future LULC Prediction

Future predictions using the MC model and LCM were validated and projected for 2035. Noteworthy transformations were categorized based on historical trends, with a particular increase in forested areas. The future LULC map for 2035, derived from the model, is presented in Figure 10, with a projected increase in Steppe and Urban Area, reflecting ongoing land rehabilitation efforts and urban expansion. The LULC coverage of classified and simulated images, which provides a comparative view of actual versus predicted land cover scenarios, is detailed in Table 11.

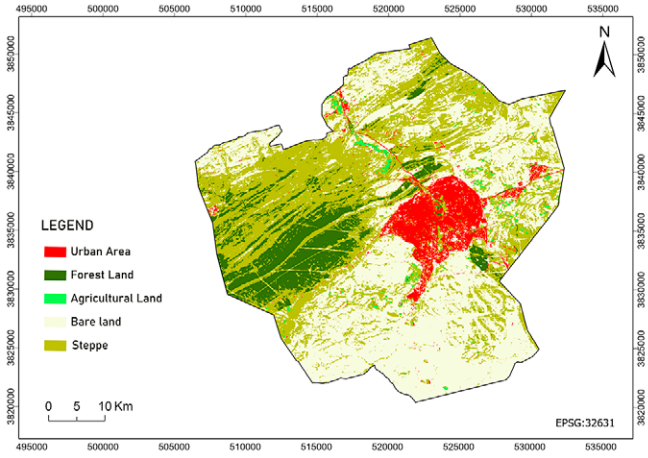

Figure 10. Predicted LULC map for 2035

Table 11. LULC coverage of classified and simulated images

LULC units	1990		2005		2020		2035	
	Area (Ha)	Area (%)	Area (Ha)	Area (%)	Area (Ha)	Area (%)	Area (Ha)	Area (%)
Urban Area	924.09	1.75	1405.12	2.66	2742.30	5.20	3588.93	6.80
Forest Land	6174.25	11.70	6128.76	11.61	5344.06	10.12	5576.99	10.57
Agricultural Land	768.25	1.46	1051.47	1.99	547.05	1.04	547.42	1.04
Bare Land	27944.39	52.94	28632.48	54.24	24976.58	47.32	24061.95	45.58
Steppe	16974.66	32.16	15567.96	29.49	19175.79	36.33	19010.48	36.01
Total	52785.64	100.00	52785.79	100.00	52785.79	100.00	52785.79	100.00

Discussion

In our study of multitemporal LULC mapping using SVM classification of Landsat imagery and auxiliary data within the GEE platform, we achieved high classification accuracy, underscoring the SVM method's robustness (Li et al., 2017). However, certain disparities in urban patterns between 1990 and 2005 were observed, notably in some urban areas undergoing significant changes. These variations may be attributed to challenges in acquiring high-quality images in dense cloud cover areas and phenological changes between seasons (Gong et al., 2016). Additionally, while employing images from December 2015 for our analysis, we postulated minimal land-cover change from our last ground truth sampling in May 2015, a factor that might have influenced our results.

The classification system occasionally diverged from global definitions, possibly leading to the misclassification of orchards and dense mixed crops as forests, particularly relevant in our ecological assessments (Gong et al., 2013). Recognizing such discrepancies is vital as they could contribute to the observed alterations in urban and other land cover categories. Despite these challenges, the overall accuracy rates of over 82.0% and corroborative visual observations of the maps emphasize SVM's significant utility and efficacy as a tool for LULC classification.

We reaffirm the strength and high accuracy of SVM classification in producing precise and consistent LULC maps and recognize the need for ongoing research. Future studies should explore the nuanced challenges and limitations encountered, particularly in urban area classification. Addressing these challenges will enhance the reliability and applicability of LULC maps, contributing to a more comprehensive understanding and management of land use and cover changes (Li et al., 2017). This continued effort is invaluable in advancing our understanding and appreciation of the dynamic and complex nature of land use classification.

Understanding LULC transitions is crucial for effective ecological and environmental management and gaining insights into future land use changes. Djelfa city, often referred to as the gateway to the Sahara or the capital of the steppes, provides a unique context for studying these transitions. Its landscape is marked by the Sennalba forest to the west, expansive steppe lands in the north, urban expansion to the east, and potential urban hubs in the south. Our study focused on analyzing LULC dynamics in Djelfa city over the past three decades and predicting future changes up to 2035. We employed various methodologies, including remote sensing, Geographic Information Systems (GIS), and a Multi-Layer Perceptron Neural Network (MLPNN)-based MC model, to comprehensively examine these dynamics.

The results revealed that Djelfa County has experienced a notable increase in urban expansion, driven by population growth and rural-to-urban migration This trend was particularly pronounced from 1990 to 2005 when the urban area expanded by 0.91% (D.P.S.B, 2020). Between 1987 and 1998, the population of Djelfa increased from 83,162 to 158,644 inhabitants, representing an annual growth rate of 6.67%. This surge can be partially attributed to the security situation between 1992 and 2001, which led rural residents and those from neighboring communities to migrate towards the city of Djelfa. From 1998 to 2008, the population growth accelerated, with the number rising to 311,931 inhabitants, at a growth rate of 6.6%—significantly higher than the national average. This growth was due to improved social conditions as evidenced by increased birth rates and decreased mortality rates. Moreover, the National Office of Statistics reports a positive internal migratory balance of 7,676 individuals and a positive external migratory balance of 1,660 individuals for Djelfa during this decade (ONS, 2011). These statistics not only substantiate a population increase but also support the urban expansion observed, correlating with the demographic growth and migration patterns.

Bare land, which covered a significant portion of the study area in 1990, experienced changes due to soil degradation, overgrazing, and pressures on rangelands. These changes may have been influenced not only by local land

management practices but also by broader environmental changes, including climate change, which can exacerbate soil erosion and desertification processes (IPCC, 2019; UN-OHRLLS, 2015). Agricultural land increased modestly from 1990 to 2005, mainly due to the abandonment of agropastoral activities during economic and security crises.

The forested area exhibited a decline, primarily attributed to anthropogenic pressures like illicit logging and overgrazing, while steppe areas witnessed significant expansion, partly due to land rehabilitation and silvicultural reclamation initiatives. Over the last decade to fifteen years, substantial rehabilitation efforts have been undertaken by the High Commission for Steppe Development (HCDS) and the National Forest Research Institute (INRF) Djelfa station. However, it's worth noting that this expansion isn't solely due to rehabilitation activities; microclimatic factors within the study area have also played a role in fostering steppe regeneration (Dudley & Phillips, 2006; World Economic Forum, 2023). The observed changes in our study area align with broader regional trends noted in other research, which have documented similar shifts in land cover types due to a combination of human activities and environmental changes (Alvarez Martinez et al., 2011).

The LULC classification and change analysis results corroborate the conversion of bare land into larger urban areas and steppe regions, with minor changes observed in agricultural and forested lands. This rise in steppe areas can be attributed to the aforementioned anthropogenic pressures, alongside the mentioned rehabilitation and silvicultural reclamation initiatives. Further research is needed to disentangle the relative impacts of these factors and to understand their interaction with climate change (Hart & Mouton, 2005; Keohane & Victor, 2011; Senge, 2008)

The observed land cover changes in our study from 2005 to 2020, such as decreasing forest cover and expanding urban and steppe areas, occur within a broader context of ecological fragility characteristic of arid and semi-arid regions. These regions, accounting for about 40% of Earth's land surface and including parts of North Africa, are particularly vulnerable to environmental changes (White & Nackoney, 2003; Yan et al., 2019). The trends noted in our study area are reflective of the challenges and dynamics experienced in these ecologically sensitive regions and align with documented patterns in similar contexts (Hishe et al., 2021). We acknowledge the importance of considering these broader ecological and geographical characteristics in our analysis and will further explore how these general trends manifest specifically in Algeria or Northwest Africa.

The projected LULC map for 2035 forecasts a further increase in urban areas, underscoring urbanization's continued influence on land use dynamics. This projection integrates a multi-index approach that improves the differentiation between urban build-up and bare soils, significantly enhancing classification accuracy, particularly in semi-arid regions like Djelfa. Notably, our model respects natural and man-made constraints, avoiding urban expansion into impractical areas such as the protected forest of Senelba, which aligns with the current concentric and compact urban form of Djelfa and similar cities within the Algerian steppe. Additionally, incorporating scenarios such as ecological protection, as suggested by (Xu et al., 2019), indicates a restrained urban spread compared to historical trends, which further confirms our projections' alignment with sustainable development practices. The precision of these projections could be improved with more detailed demographic data, yet the incorporation of various spectral indices and the consideration of geographical constraints assure the general reliability of our results. Future expansions are modeled to occur in viable areas, avoiding slopes or other inaccessible regions, thus reflecting a realistic trajectory of urban growth.

Our study highlights the dynamic nature of LULC changes in Djelfa city over the past 30 years and provides valuable insights for future land use planning. Sustainable urban development and effective land management strategies are essential to mitigate the environmental and social consequences of these changes. Monitoring and managing the pace and extent of urban expansion are critical to achieving sustainable development while preserving the environment. Furthermore, the integration of demographic data into future studies would provide a more holistic understanding of the drivers behind these changes, contributing to informed decision-making and effective management practices. Our use of ANN techniques has improved the reliability of our findings, reducing potential expert bias and inaccuracies in land cover analysis. However, it's important to note that the MLPNNMC approach may not cover all possible LULC transitions, and further research may be needed for applications involving a wider range of transitions, particularly in semi-natural areas.

Conclusion

In conclusion, this study utilized geospatial techniques and remote sensing data to analyze the temporal evolution of land use and land cover patterns in Djelfa city. By employing Landsat 5 and Landsat 8 imagery and employing advanced models, we projected land use changes up to 2035. Our validation process demonstrated the robustness of our approach, with an accuracy exceeding 83%, affirming the predictive capabilities of our composite model.

The integration of remote sensing, GIS, and land use change models proved to be a powerful tool for compre-

hensively mapping and monitoring land use transitions. Through SVM algorithms in GEE we generated accurate land use maps for pivotal years, highlighting the influence of auxiliary variables like elevation, roads, and settlement patterns on future land use changes.

Our analysis revealed a dominant trend towards urban expansion, resulting in a projected 6.80% increase in built-up areas by 2035. Additionally, our implementation of the Multi-Layer Perceptron MC model effectively estimated future land use dynamics, emphasizing the potential of remote sensing and GIS integration in land use analysis and prediction.

While our findings underscore the significance of our methodology for sustainable development and land management, we acknowledge the limitations related to the moderate resolution of Landsat imagery. This suggests room for improvement in image quality and prediction techniques for future research.

In summary, this research contributes to understanding and addressing the complex dynamics of land use in Djelfa city. By advocating for more comprehensive datasets, including climate, political, and urban development factors, we can enhance the accuracy of our predictive models. Replicating this methodology in other urban contexts will further enrich our insights into land use changes, guiding informed decisions for sustainable development while mitigating the environmental impacts of urban growth.

Acknowledgements

We extend our gratitude to the anonymous reviewers whose insightful feedback and constructive critiques significantly enhanced the quality of this manuscript. Our sincere appreciation also goes to the United States Geological Survey (USGS) for granting free access to the Landsat images utilized in this study.

Funding: *The research described in this study was not supported by any external funding sources.*

Conflicts of Interest: *The authors of this study have stated that there are no competing interests present.*

Disclosure: *The authors have no relevant financial or non-financial disclosures to report.*

Data Availability: *The datasets utilized and/or assessed in this study can be obtained by contacting the corresponding author upon reasonable request.*

Ethical approval: *All authors named in the manuscript have provided their consent for authorship, thoroughly reviewed and approved the manuscript, and granted permission for its submission and subsequent publication. The order of authorship was agreed upon by all listed authors before the manuscript was submitted.*

Ethical standards: *The manuscript has not been previously published, in part or in full, in any journal. It adheres to the ethical standards of this journal.*

References

Abijith, D., & Saravanan, S. (2022). Assessment of land use and land cover change detection and prediction using remote sensing and CA Markov in the northern coastal districts of Tamil Nadu, India. *Environmental Science and Pollution Research*, 29(57), 86055–86067. https://doi.org/10.1007/s11356-021-15782-6

Alqadhi, S., Mallick, J., Balha, A., Bindajam, A., Singh, C. K., & Hoa, P. V. (2021). Spatial and decadal prediction of land use/land cover using multi-layer perceptron-neural network (MLP-NN) algorithm for a semi-arid region of Asir, Saudi Arabia. *Earth Science Informatics*, 14(3), 1547–1562. https://doi.org/10.1007/s12145-021-00633-2

Alvarez Martinez, J. M., Suarez-Seoane, S., & De Luis Calabuig, E. (2011). Modelling the risk of land cover change from environmental and socio-economic drivers in heterogeneous and changing landscapes: The role of uncertainty. *Landscape and Urban Planning*, 101(2), 108–119. https://doi.org/10.1016/j.landurbplan.2011.01.009

Anand, J., Gosain, A. K., & Khosa, R. (2018). Prediction of land use changes based on Land Change Modeler and attribution of changes in the water balance of Ganga basin to land use change using the SWAT model. *Science of the Total Environment*, 644, 503–519. https://doi.org/10.1016/j.scitotenv.2018.07.017

Azari, M., Tayyebi, A., Helbich, M., & Reveshty, M. A. (2016). Integrating cellular automata, artificial neural network, and fuzzy set theory to simulate threatened orchards: Application to Maragheh, Iran. *GIScience and Remote Sensing*, 53(2), 183–205. https://doi.org/10.1080/15481603.2015.1137111

Barnieh, B. A., Jia, L., Menenti, M., Zhou, J., & Zeng, Y. (2020). Mapping land use land cover transitions at different spatiotemporal scales in West Africa. *Sustainability*, 12(20), 1–52. https://doi.org/10.3390/su12208565

Behera, M. D., Borate, S. N., Panda, S. N., Behera, P. R., & Roy, P. S. (2012). Modelling and analyzing the watershed dynamics using Cellular Automata (CA)-Mark-

ov model - A geo-information based approach. *Journal of Earth System Science*, 121(4), 1011–1024. https://doi.org/10.1007/s12040-012-0207-5

Beven, K. J., Kirkby, M. J., Schofield, N., & Tagg, A. F. (1984). Testing a Physically-Based Flood Forecasting Model (Topmodel) for Three U. K. Catchments. *Journal of Hydrology*, 69(1–4), 119–143.

Brown, D. G., Walker, R., Manson, S., & Seto, K. (2004). Modeling Land Use and Land Cover Change BT. In G. Gutman, A. C. Janetos, C. O. Justice, E. F. Moran, J. F. Mustard, R. R. Rindfuss, D. Skole, B. L. Turner, & M. A. Cochrane (Eds.), *Land Change Science: Observing, Monitoring and Understanding Trajectories of Change on the Earth's Surface* (pp. 395–409). Netherlands: Springer. https://doi.org/10.1007/978-1-4020-2562-4_23

Bullock, E. L., Healey, S. P., Yang, Z., Oduor, P., Gorelick, N., Omondi, S., Ouko, E., & Cohen, W. B. (2021). Three decades of land cover change in East Africa. *Land*, 10(2), 1–15. https://doi.org/10.3390/land10020150

Bununu, Y. A. (2017). Integration of Markov chain analysis and similarity-weighted instance-based machine learning algorithm (SimWeight) to simulate urban expansion. *International Journal of Urban Sciences*, 21(2), 217–237. https://doi.org/10.1080/12265934.2017.1284607

Camacho Olmedo, M. T., Pontius, R. G., Paegelow, M., & Mas, J. F. (2015). Comparison of simulation models in terms of quantity and allocation of land change. *Environmental Modelling and Software*, 69, 214–221. https://doi.org/10.1016/j.envsoft.2015.03.003

Carneiro, E., Lopes, W., & Espindola, G. (2021). Urban land mapping based on remote sensing time series in the google earth engine platform: A case study of the teresina-timon conurbation area in Brazil. *Remote Sensing*, 13(7). https://doi.org/10.3390/rs13071338

Chaudhuri, G., & Clarke, K. C. (2014). Temporal Accuracy in Urban Growth Forecasting: A Study Using the SLEUTH Model. *Transactions in GIS*, 18(2), 302–320. https://doi.org/10.1111/tgis.12047

Chen, H., & Pontius, R. G. (2010). Diagnostic tools to evaluate a spatial land change projection along a gradient of an explanatory variable. *Landscape Ecology*, 25(9), 1319–1331. https://doi.org/10.1007/s10980-010-9519-5

Congalton, R. G. (1991). A review of assessing the accuracy of classifications of remotely sensed data. *Remote Sensing of Environment*, 37(1), 35–46. https://doi.org/10.1016/0034-4257(91)90048-B

D.P.S.B. (2020). *Monograph of the wilaya of Djelfa*. Djelfa: Department of Budget Programming and Monitoring (3–11 pp).

Dong, J., Xiao, X., Menarguez, M. A., Zhang, G., Qin, Y., Thau, D., Biradar, C., & Moore, B. (2016). Mapping paddy rice planting area in northeastern Asia with Landsat 8 images, phenology-based algorithm and Google Earth Engine. *Remote Sensing of Environment*, 185, 142–154. https://doi.org/10.1016/j.rse.2016.02.016

Dudley, N., & Phillips, A. (2006). Forests and protected areas: guidance on the use of the IUCN protected area management categories. In Forests and protected areas : guidance on the use of the IUCN protected area management categories (Issue 12). https://doi.org/10.2305/iucn.ch.2006.pag.12.en

Dwivedi, R. S., Sreenivas, K., & Ramana, K. V. (2005). Land-use/land-cover change analysis in part of Ethiopia using Landsat Thematic Mapper data. *International Journal of Remote Sensing*, 26(7), 1285–1287. https://doi.org/10.1080/01431160512331337763

Eastman, J. R. (2015). *TerrSet Geospatial Monitoring and Modeling Software*. Clark University. https://clarklabs.org/terrset/

Eastman, J. R. (2020). *TerrSet Geospatial Monitoring and Modeling Software*. Clark University. https://clarklabs.org/terrset/

Ermida, S. L., Soares, P., Mantas, V., Göttsche, F. M., & Trigo, I. F. (2020). Google earth engine open-source code for land surface temperature estimation from the landsat series. *Remote Sensing*, 12(9), 1–21. https://doi.org/10.3390/RS12091471

Fadli, A. H., Kosugo, A., Ichii, K., & Ramli, R. (2019). Satellite-based monitoring of forest cover change in indonesia using google earth engine from 2000 to 2016. *Journal of Physics: Conference Series*, 1317(1), 012046. https://doi.org/10.1088/1742-6596/1317/1/012046

Fan, F., Weng, Q., & Wang, Y. (2007a). Land use and land cover change in Guangzhou, China, from 1998 to 2003, based on Landsat TM /ETM+ imagery. *Sensors*, 7(7), 1323–1342. https://doi.org/10.3390/s7071323

Fan, J. P. H., Wong, T. J., & Zhang, T. (2007b). Politically connected CEOs, corporate governance, and Post-IPO performance of China's newly partially privatized firms. *Journal of Financial Economics*, 84(2), 330–357. https://doi.org/10.1016/j.jfineco.2006.03.008

Feng, D., Zhao, Y., Yu, L., Li, C., Wang, J., Clinton, N., Bai, Y., Belward, A., Zhu, Z., & Gong, P. (2016). Circa 2014 African land-cover maps compatible with FROM-GLC and GLC2000 classification schemes based on multi-seasonal Landsat data. *International Journal of Remote Sensing*, 37(19), 4648–4664. https://doi.org/10.1080/01431161.2016.1218090

Feng, Y., Lei, Z., Tong, X., Gao, C., Chen, S., Wang, J., & Wang, S. (2020). Spatially-explicit modeling and intensity analysis of China's land use change 2000–2050. *Journal of Environmental Management*, 263, 110407. https://doi.org/10.1016/j.jenvman.2020.110407

Findell, K. L., Berg, A., Gentine, P., Krasting, J. P., Lintner, B. R., Malyshev, S., Santanello, J. A., & Shevliakova, E. (2017). The impact of anthropogenic land use and land cover change on regional climate extremes. *Na-*

ture Communications, 8(1), 1–9. https://doi.org/10.1038/s41467-017-01038-w

Gashaw, T., Tulu, T., Argaw, M., & Worqlul, A. W. (2018). Modeling the hydrological impacts of land use/land cover changes in the Andassa watershed, Blue Nile Basin, Ethiopia. *Science of the Total Environment*, 619–620, 1394–1408. https://doi.org/10.1016/j.scitotenv.2017.11.191

Gong, P., Wang, J., Yu, L., Zhao, Y., Zhao, Y., Liang, L., Niu, Z., Huang, X., Fu, H., Liu, S., Li, C., Li, X., Fu, W., Liu, C., Xu, Y., Wang, X., Cheng, Q., Hu, L., Yao, W., Zhang, H., Zhu, P., Zhao, Z, Zhang, H., Zheng, Y., Ji, L., Zhang, Y., Chen, H., Yan, A., Guo, J., Yu, L., Wang, L., Liu, X., Shi, T., Zhu, M., Chen, Y., Yang, G., Tang, P., Xu, B., Giri, C., Clinton, N., Zhu, Z., & Chen, J. (2013). Finer resolution observation and monitoring of global land cover: First mapping results with Landsat TM and ETM+ data. *International Journal of Remote Sensing*, 34(7), 2607–2654. https://doi.org/10.1080/01431161.2012.748992

Gong, P., Yu, L., Li, C., Wang, J., Liang, L., Li, X., Ji, L., Bai, Y., Cheng, Y., & Zhu, Z. (2016). A new research paradigm for global land cover mapping. *Annals of GIS*, 22(2), 87–102. https://doi.org/10.1080/19475683.2016.1164247

Gorelick, N., Hancher, M., Dixon, M., Ilyushchenko, S., Thau, D., & Moore, R. (2017). Google Earth Engine: Planetary-scale geospatial analysis for everyone. *Remote Sensing of Environment*, 202(2016), 18–27. https://doi.org/10.1016/j.rse.2017.06.031

Green, K., Kempka, D., & Lackey, L. (1994). Using remote sensing to detect and monitor land-cover and land-use change. *Photogrammetric Engineering and Remote Sensing*, 60, 331–337.

Hackman, K. O., Gong, P., & Wang, J. (2017). New land-cover maps of Ghana for 2015 using landsat 8 and three popular classifiers for biodiversity assessment. *International Journal of Remote Sensing*, 38(14), 4008–4021. https://doi.org/10.1080/01431161.2017.1312619

Hackman, K. O., Li, X., Asenso-Gyambibi, D., Asamoah, E. A., & Nelson, I. D. (2020). Analysis of geo-spatiotemporal data using machine learning algorithms and reliability enhancement for urbanization decision support. *International Journal of Digital Earth*, 13(12), 1717–1732. https://doi.org/10.1080/17538947.2020.1805036

Halmy, M. W. A., Gessler, P. E., Hicke, J. A., & Salem, B. B. (2015). Land use/land cover change detection and prediction in the north-western coastal desert of Egypt using Markov-CA. *Applied Geography*, 63, 101–112. https://doi.org/10.1016/j.apgeog.2015.06.015

Hart, T., & Mouton, J. (2005). Indigenous knowledge and its relevance for agriculture: a case study in Uganda. *Indilinga African Journal of Indigenous Knowledge Systems*, 4(1), 249–263.

Hasan, S., Shi, W., Zhu, X., Abbas, S., & Khan, H. U. A. (2020). Future simulation of land use changes in rapidly urbanizing South China based on land change modeler and remote sensing data. *Sustainability*, 12(11), 4–6. https://doi.org/10.3390/su12114350

Hishe, H., Giday, K., Van Orshoven, J., Muys, B., Taheri, F., Azadi, H., Feng, L., Zamani, O., Mirzaei, M., & Witlox, F. (2021). Analysis of Land Use Land Cover Dynamics and Driving Factors in Desa'a Forest in Northern Ethiopia. *Land Use Policy*, 101, 105039. https://doi.org/10.1016/j.landusepol.2020.105039

Homer, C., Dewitz, J., Jin, S., Xian, G., Costello, C., Danielson, P., Gass, L., Funk, M., Wickham, J., & Stehman, S. (2020). Conterminous United States land cover change patterns 2001–2016 from the 2016 national land cover database. *ISPRS Journal of Photogrammetry and Remote Sensing*, 162, 184–199.

Hu, Y., Dong, Y., & Batunacun. (2018). An automatic approach for land-change detection and land updates based on integrated NDVI timing analysis and the CVAPS method with GEE support. ISPRS *Journal of Photogrammetry and Remote Sensing*, 146, 347–359. https://doi.org/10.1016/j.isprsjprs.2018.10.008

IPCC. (2019). Climate Change and Land: an IPCC special report. Climate Change and Land: An IPCC Special Report on Climate Change, Desertification, Land Degradation, Sustainable Land Management, Food Security, and Greenhouse Gas Fluxes in Terrestrial Ecosystems, 1–864. https://www.ipcc.ch/srccl/

Islam, K., Rahman, M. F., & Jashimuddin, M. (2018). Modeling land use change using Cellular Automata and Artificial Neural Network: The case of Chunati Wildlife Sanctuary, Bangladesh. *Ecological Indicators*, 88, 439–453. https://doi.org/10.1016/j.ecolind.2018.01.047

Karul, C., & Soyupak, S. (2003). A Comparison between Neural Network Based and Multiple Regression Models for Chlorophyll-a Estimation BT. In F. Recknagel (Ed.), *Ecological Informatics: Understanding Ecology by Biologically-Inspired Computation* (pp. 249–263). Berlin Heidelberg: Springer. https://doi.org/10.1007/978-3-662-05150-4_13

Keohane, R. O., & Victor, D. G. (2011). The regime complex for climate change. *Perspectives on Politics*, 9(1), 7–23.

Kim, Y., & Newman, G. (2020). Advancing scenario planning through integrating urban growth prediction with future flood risk models. *Computers, Environment and Urban Systems*, 82, 101498. https://doi.org/10.1016/j.compenvurbsys.2020.101498

Kolb, M., Mas, J. F., & Galicia, L. (2013). Evaluating drivers of land-use change and transition potential models in a complex landscape in Southern Mexico. *International Journal of Geographical Information Science*, 27(9), 1804–1827. https://doi.org/10.1080/13658816.2013.770517

Lambin, E. F. (1997). Modelling and monitoring land-cover change processes in tropical regions. *Progress in Physical Geography*, 21(3), 375–393. https://doi.org/10.1177/030913339702100303

Larbi, I., Forkuor, G., Hountondji, F. C. C., Agyare, W. A., & Mama, D. (2019). Predictive Land Use Change under Business-As-Usual and Afforestation Scenarios in the Vea Catchment, West Africa. *International Journal of Advanced Remote Sensing and GIS*, 8(1), 3011–3029. https://doi.org/10.23953/cloud.ijarsg.416

Li, C., Gong, P., Wang, J., Zhu, Z., Biging, G. S., Yuan, C., Hu, T., Zhang, H., Wang, Q., Li, X., Liu, X., Xu, Y., Guo, J., Liu, C., Hackman, K. O., Zhang, M., Cheng, Y., Yu, L., Yang, J., Huang, H., & Clinton, N. (2017). The first all-season sample set for mapping global land cover with Landsat-8 data. *Science Bulletin*, 62(7), 508–515. https://doi.org/10.1016/j.scib.2017.03.011

Li, J., Knapp, D. E., Lyons, M., Roelfsema, C., Phinn, S., Schill, S. R., & Asner, G. P. (2021). Automated global shallowwater bathymetry mapping using google earth engine. *Remote Sensing*, 13(8). https://doi.org/10.3390/rs13081469

Liu, C., Li, W., Zhu, G., Zhou, H., Yan, H., & Xue, P. (2020). Land use/land cover changes and their driving factors in the northeastern tibetan plateau based on geographical detectors and google earth engine: A case study in gannan prefecture. *Remote Sensing*, 12(19), 1–18. https://doi.org/10.3390/RS12193139

Liu, G., Jin, Q., Li, J., Li, L., He, C., Huang, Y., & Yao, Y. (2017). Policy factors impact analysis based on remote sensing data and the CLUE-S model in the Lijiang River Basin, China. *Catena*, 158, 286–297. https://doi.org/10.1016/j.catena.2017.07.003

López, E., Bocco, G., Mendoza, M., & Duhau, E. (2001). Predicting land-cover and land-use change in the urban fringe. *Landscape and Urban Planning*, 55(4), 271–285. https://doi.org/10.1016/s0169-2046(01)00160-8

Mantero, P., Moser, G., & Serpico, S. B. (2004). Partially supervised classification of remote sensing images using SVM-based probability density estimation. *IEEE Transactions on geoscience and remote sensing*, 43(3), 559-570. https://doi.org/10.1109/WARSD.2003.1295212

Mao, L., & Li, M. (2021). Integrating Sentinel Active and Passive Data to Map Land Cover in a National Park from GEE Platform. *Geomatics and Information Science of Wuhan University*, 48(5), 756-764.

Mas, J. F., Kolb, M., Paegelow, M., Camacho Olmedo, M. T., & Houet, T. (2014). Inductive pattern-based land use/cover change models: A comparison of four software packages. *Environmental Modelling and Software*, 51, 94–111. https://doi.org/10.1016/j.envsoft.2013.09.010

Mather., A. S. (1986). *Land use*. Longman.

Midekisa, A., Holl, F., Savory, D. J., Andrade-Pacheco, R., Gething, P. W., Bennett, A., & Sturrock, H. J. W. (2017). Mapping land cover change over continental Africa using Landsat and Google Earth Engine cloud computing. *PLoS ONE*, 12(9), 1–15. https://doi.org/10.1371/journal.pone.0184926

Mirici, M. E., Berberoglu, S., Akin, A., & Satir, O. (2018). Land use/cover change modelling in a mediterranean rural landscape using multi-layer perceptron and markov chain (MLP-MC). *Applied Ecology and Environmental Research*, 16(1), 467–486. https://doi.org/10.15666/aeer/1601_467486

Mishra, V. N., & Rai, P. K. (2016). A remote sensing aided multi-layer perceptron-Markov chain analysis for land use and land cover change prediction in Patna district (Bihar), India. *Arabian Journal of Geosciences*, 9(4). https://doi.org/10.1007/s12517-015-2138-3

Mishra, V. N., Rai, P. K., Prasad, R., Punia, M., & Nistor, M. M. (2018). Prediction of spatio-temporal land use/land cover dynamics in rapidly developing Varanasi district of Uttar Pradesh, India, using geospatial approach: a comparison of hybrid models. *Applied Geomatics*, 10(3), 257–276. https://doi.org/10.1007/s12518-018-0223-5

Mozumder, C., Tripathi, N. K., & Losiri, C. (2016). Comparing three transition potential models: A case study of built-up transitions in North-East India. *Computers, Environment and Urban Systems*, 59, 38–49. https://doi.org/10.1016/j.compenvurbsys.2016.04.009

Mugiraneza, T., Nascetti, A., & Ban, Y. (2020). Continuous monitoring of urban land cover change trajectories with landsat time series and landtrendr-google earth engine cloud computing. *Remote Sensing*, 12(18). https://doi.org/10.3390/RS12182883

Noma, A., Korting, T. S., & Fonseca, L. M. G. (2013). Uma Comparação entre Classificadores usando Regiões e Perfis EVI para Agricultura. *Anais XVI Simpósio Brasileiro de Sensoriamento Remoto, São José dos Campos: Instituto Nacional de Pesquisas Espaciais*, 2250-2257. http://urlib.net/dpi.inpe.br/marte2/2013/05.28.23.34

Nowak, D. J., & Greenfield, E. J. (2020). The increase of impervious cover and decrease of tree cover within urban areas globally (2012–2017). *Urban Forestry and Urban Greening*, 49. https://doi.org/10.1016/j.ufug.2020.126638

Oliveira, J. P. (2017). Detecção de áreas desmatadas na porção sul do estado do Amazonas, utilizando técnicas de extração de características e redes neurais artificiais. Master thesis. Manaus: Universidade Federal do Amazonas, Faculdade de Technologia.

ONS. (2011). L'armature urbaine RGPH 2008 - Collections Statistiques n° 163/2011 [The urban framework RGPH 2008 - Statistics Collections n° 163/2011]. 220. https://www.ons.dz/IMG/pdf/armature_urbaine_2008.pdf

Pérez-Vega, A., Mas, J. F., & Ligmann-Zielinska, A. (2012). Comparing two approaches to land use/cover change modeling and their implications for the assessment of biodiversity loss in a deciduous tropical forest. *Environmental Modelling and Software*, 29(1), 11–23. https://doi.org/10.1016/j.envsoft.2011.09.011

Pontius, R. G. (2000). Quantification error versus location error in comparison of categorical maps. *Photogrammetric Engineering and Remote Sensing*, 67(5), 540-540.

Pontius, R. G., Boersma, W., Castella, J. C., Clarke, K., Nijs, T., Dietzel, C., Duan, Z., Fotsing, E., Goldstein, N., Kok, K., Koomen, E., Lippitt, C. D., McConnell, W., Mohd Sood, A., Pijanowski, B., Pithadia, S., Sweeney, S., Trung, T. N., Veldkamp, A. T., & Verburg, P. H. (2008). Comparing the input, output, and validation maps for several models of land change. *Annals of Regional Science*, 42(1), 11–37. https://doi.org/10.1007/s00168-007-0138-2

Prasomsup, W., Piyatadsananon, P., Aunphoklang, W., & Boonrang, A. (2020). Extraction technic for built-up area classification in Landsat 8 imagery. *International Journal of Environmental Science and Development*, 11(1), 15–20. https://doi.org/10.18178/ijesd.2020.11.1.1219

Rawat, J. S., & Kumar, M. (2015). Monitoring land use/cover change using remote sensing and GIS techniques: A case study of Hawalbagh block, district Almora, Uttarakhand, India. *Egyptian Journal of Remote Sensing and Space Science*, 18(1), 77–84. https://doi.org/10.1016/j.ejrs.2015.02.002

Roy, S., Pandit, S., Eva, E. A., Bagmar, M. S. H., Papia, M., Banik, L., Dube, T., Rahman, F., & Razi, M. A. (2020). Examining the nexus between land surface temperature and urban growth in Chattogram Metropolitan Area of Bangladesh using long term Landsat series data. *Urban Climate*, 32, 100593. https://doi.org/10.1016/j.uclim.2020.100593

Senge, P. (2008). The necessary revolution: How individuals and organisations are working together to create a sustainable world. *Management Today*, 24(10), 54–57.

Shaharum, N. S. N., Shafri, H. Z. M., Ghani, W. A. W. A. K., Samsatli, S., Al-Habshi, M. M. A., & Yusuf, B. (2020). Oil palm mapping over Peninsular Malaysia using Google Earth Engine and machine learning algorithms. *Remote Sensing Applications: Society and Environment*, 17, 100287. https://doi.org/10.1016/j.rsase.2020.100287

Shawul, A. A., & Chakma, S. (2019). Spatiotemporal detection of land use/land cover change in the large basin using integrated approaches of remote sensing and GIS in the Upper Awash basin, Ethiopia. *Environmental Earth Sciences*, 78(5), 1–13. https://doi.org/10.1007/s12665-019-8154-y

Singh, A. (1989). Review Articlel: Digital change detection techniques using remotely-sensed data. *International Journal of Remote Sensing*, 10(6), 989–1003. https://doi.org/10.1080/01431168908903939

Singh, S. K., Laari, P. B., Mustak, S. K., Srivastava, P. K., & Szabó, S. (2018). Modelling of land use land cover change using earth observation data-sets of Tons River Basin, Madhya Pradesh, India. *Geocarto International*, 33(11), 1202–1222.

Sinha, S., Sharma, L. K., & Nathawat, M. S. (2015). Improved Land-use/Land-cover classification of semi-arid deciduous forest landscape using thermal remote sensing. *Egyptian Journal of Remote Sensing and Space Science*, 18(2), 217–233. https://doi.org/10.1016/j.ejrs.2015.09.005

Siroosi, H., Heshmati, G., & Salmanmahiny, A. (2020). Can empirically based model results be fed into mathematical models? MCE for neural network and logistic regression in tourism landscape planning. *Environment, Development and Sustainability*, 22(4), 3701–3722. https://doi.org/10.1007/s10668-019-00363-y

Skole, D., & Tucker, C. (1993). Tropical deforestation and habitat fragmentation in the amazon: Satellite data from 1978 to 1988. *Science*, 260(5116), 1905–1910. https://doi.org/10.1126/science.260.5116.1905

UN-OHRLLS. (2015). The Impact of Climate Change, Desertification and Land Degradation on the Development Prospects of Landlocked Developing Countries. 1–59. http://unohrlls.org/custom-content/uploads/2015/11/Impact_Climate_Change_2015.pdf

Wagle, N., Acharya, T. D., Kolluru, V., Huang, H., & Lee, D. H. (2020). Multi-temporal land cover change mapping using google earth engine and ensemble learning methods. *Applied Sciences*, 10(22), 1–20. https://doi.org/10.3390/app10228083

Wahap, N. A., & Shafri, H. Z. M. (2020). Utilization of Google Earth Engine (GEE) for land cover monitoring over Klang Valley, Malaysia. *IOP Conference Series: Earth and Environmental Science*, 540(1). https://doi.org/10.1088/1755-1315/540/1/012003

Wang, J., Wu, J., Wang, Z., Gao, F., & Xiong, Z. (2020). Understanding Urban Dynamics via Context-Aware Tensor Factorization with Neighboring Regularization. IEEE *Transactions on Knowledge and Data Engineering*, 32(11), 2269–2283. https://doi.org/10.1109/TKDE.2019.2915231

White, R. P., & Nackoney, J. (2003). *Drylands, people, and ecosystem goods and services*. World resources institute.

Winkler, K., Fuchs, R., Rounsevell, M., & Herold, M. (2021). Global land use changes are four times greater than previously estimated. *Nature Communications*, 12(1), 1–10. https://doi.org/10.1038/s41467-021-22702-2

World Economic Forum. (2023). The Global Risks Report 2023 (18.a). In The WEF. https://www.weforum.org/reports/global-risks-report-2023

Xiong, J., Thenkabail, P. S., Gumma, M. K., Teluguntla, P., Poehnelt, J., Congalton, R. G., Yadav, K., & Thau, D. (2017). Automated cropland mapping of continental Africa using Google Earth Engine cloud computing. *ISPRS Journal of Photogrammetry and Remote Sensing*, 126, 225–244. https://doi.org/10.1016/j.isprsjprs.2017.01.019

Xiong, Y., Xu, W., Lu, N., Huang, S., Wu, C., Wang, L., Dai, F., & Kou, W. (2021). Assessment of spatial–temporal changes of ecological environment quality based on RSEI and GEE: A case study in Erhai Lake Basin, Yun-

nan province, China. *Ecological Indicators*, 125, 107518. https://doi.org/10.1016/j.ecolind.2021.107518

Xu, C., McDowell, N. G., Fisher, R. A., Wei, L., Sevanto, S., Christoffersen, B. O., Weng, E., & Middleton, R. S. (2019). Increasing impacts of extreme droughts on vegetation productivity under climate change. *Nature Climate Change*, 9(12), 948–953. https://doi.org/10.1038/s41558-019-0630-6

Yan, Q., Le, P. V. V., Woo, D. K., Hou, T., Filley, T., & Kumar, P. (2019). Three-Dimensional Modeling of the Coevolution of Landscape and Soil Organic Carbon. *Water Resources Research*, 1218–1241. https://doi.org/10.1029/2018WR023634

Yu, L., Liang, L., Wang, J., Zhao, Y., Cheng, Q., Hu, L., Liu, S., Yu, L., Wang, X., Zhu, P., Li, X., Xu, Y., Li, C., Fu, W., Li, X., Li, W., Liu, C., Cong, N., Zhang, H., Fangdi, S., Xinfang, B., Xin, Q., Li, D., Yan, D., Zhu, Z., Goodchild, M. F. & Gong, P. (2014). Meta-discoveries from a synthesis of satellite-based land-cover mapping research. *International Journal of Remote Sensing*, 35(13), 4573–4588. https://doi.org/10.1080/01431161.2014.930206

Zadbagher, E., Becek, K., & Berberoglu, S. (2018). Modeling land use/land cover change using remote sensing and geographic information systems: case study of the Seyhan Basin, Turkey. *Environmental Monitoring and Assessment*, 190(8). https://doi.org/10.1007/s10661-018-6877-y

Zhao, G. X., Lin, G., & Warner, T. (2004). Using Thematic Mapper data for change detection and sustainable use of cultivated land: A case study in the Yellow River delta, China. *International Journal of Remote Sensing*, 25(13), 2509–2522. https://doi.org/10.1080/0143116031000161957 1

Zhao, Z., Meng, Y., Yue, A., Huang, Q., Kong, Y., Yuan, Y., Liu, X., Lin, L., & Zhang, M. (2016). Review of remotely sensed time series data for change detection. *Yaogan Xuebao/Journal of Remote Sensing*, 20(5), 1110–1125. https://doi.org/10.11834/jrs.20166170

INTERNATIONAL SCIENTIFIC JOURNAL
GEOGRAPHICA PANNONICA
Volume 28, Issue 1, 21–33 (March 2024)
Contents lists available at ScienceDirect
Journal homepage: http://www.dgt.uns.ac.rs/en/homepage/pannonica/

Characterisation of Hungary's Regional Tourism and Economic Performance between 2004 and 2022 in the Light of EU Funding

Ádám Gyurkó[A*], Zoltán Bujdosó[B], Al Fauzi Rahmat[B], Lóránt Dénes Dávid[C]

[A] *Eszterházy Károly Catholic University, Hungary; gyurko.adam@uni-eszterhazy.hu*
[B] *Hungarian University of Agriculture and Life Sciences, Hungary; Bujdoso.Zoltan@uni-mate.hu; rahmat.al.fauzi@phd.uni-mate.hu*
[C] *John von Neumann University, Faculty of Economics and Business, Hungary*
Hungarian University of Agriculture and Life Sciences, Hungary; david.lorant.denes@uni-neumann.hu

KEYWORDS

economic performance
regional differences
regional tourism performance
tourism situation assessment
tourism development

ABSTRACT

The objective of the study is to show the regional differences in Hungary in terms of economic determination and tourism performance. The overdominance of Budapest can be identified in most socio-economic indicators. The consequence of the capital's "hydrocephalus" is that Hungary's peripheral regions have developed serious economic challenges, and reducing regional disparities in these areas is key. From a tourism perspective in particular, the capital's hydrocephalus is also an opportunity, as the spill-over effect can increase the popularity of other destinations in the country. The Balaton and Western Transdanubia regions are the main beneficiaries of this effect. In addition to the analysis of regional disparities, the study also looks at the impact on tourism of the crisis periods caused by the 2008 global economic crisis and the pandemic that unfolded in 2020-2021, which led to a historic low in the tourism sector, notably the pandemic, by analysing longer time series data. The balance between international and domestic tourism is key to the resilience of tourism to the crisis. Multi-directional tourism can reduce exposure to external factors and contribute to the stability of the tourism industry.

Introduction

There is a high correlation between economic performance and the spatial concentration of tourist destinations (Bohlin et al., 2022; Gyurkó, 2022; Káposzta & Nagy, 2022; Priatmoko et al., 2021) in most destinations. Budapest, as the country's capital, stands out by far in terms of economic and social development indicators and determines the dynamics of the country's economic development. In terms of international tourism to the country, Budapest's hydrocephalus can also be identified. As a result, the country's peripheral regions are struggling to keep up and regional disparities are widening.

Even the European Union cohesion development funds that have been coming to Hungary since 2004 have not been able to mitigate the excessive dominance of Budapest in reducing regional disparities (Dobó & Pintér, 2023). As a consequence, the peripheral regions of the country have been facing serious economic challenges, which may lead not only to economic problems but also to social tensions

* Corresponding author: Ádám Gyurkó, email: gyurko.adam@uni-eszterhazy.hu
doi: 10.5937/gp28-48906
Received: January 25, 2024 | Revised: February 28, 2024 | Accepted: March 05, 2024

and depopulation, which threaten rural areas in the long term.

Further support for regional development policies and investments is therefore crucial for Hungary's economic and tourism development (Gyurkó, 2020), as tourism determination in European destinations shows a high and even correlation with overall socio-economic well-being indicators (Çaglayan & Sak, 2012; García-Sánchez et al., 2021). The reduction of regional disparities should be a priority in the coming years in order to achieve a more even and sustainable development of the country, both economically and in terms of tourism.

The relationship between socio-economic disparities and tourism performance

There is a very strong correlation between socio-economic development and tourism performance (Sam et al., 2014; Stec & Grzebyk, 2022). Countries with the highest tourism indicators also have strong economic indicators. The positive impact of tourism on economic growth is evident in both developed and underdeveloped economies (Dávid et al., 2007; Paramati et al., 2017). The most common of the economic impacts of tourism is its ability to create jobs, as this sector requires a large human resource (Dayananda, 2014; Manzoor et al., 2019; Scheyvens & Hughes, 2021). Despite the advances in technology and the spread of automation, it will require a large human workforce in the long run. Investment in tourism will greatly increase the number of jobs, thereby contributing to the reduction of unemployment, which will generate savings and revenue for the state. In the case of salaries, the private sector covers the contributions, while in the event of unemployment, the state pays the benefits. For these reasons, job creation is one of the most important economic impacts of tourism. However, job creation does not only have an economic effect, but it also has a positive social impact. It has the potential to make workers a valuable and active part of the local society and also contributes to the wider provision of livelihoods (Aykac, 2010; Dávid et al., 2003; Leonard, 2015).

Socio-economic differences have a major impact on the performance of a tourist destination. One of the most prominent influencing factors is the economic development of a given region, which largely determines the attractiveness and performance of individual attractions and destinations. Itis because economically stronger regions are often able to offer higher quality tourism services and are more attractive to tourists through more frequent and better-quality infrastructure development. In contrast, less developed regions tend to have more limited tourism opportunities, resulting in less competitiveness (Cárdenas-García et al., 2015). The most commonly used measure of economic performance and regional socio-economic disparities is gross domestic product (GDP) (Cracolici et al, 2010; Giannetti et al., 2015) The relationships between this indicator and tourism performance are rather complex, but in general, it can be said that the economic situation of a region, as determined by its GDP, has a significant impact on tourism development and vice versa. The links are, therefore, two-way, i.e., the tourism sector can contribute to the economic development of a region through the efficient use of its resources, provided that long-term plans are developed. In this way, it can increase the income-generating capacity of the region under study, which can contribute to the sustainable development of the local economy and, at the same time, the national economy (Assadzadeh & Nasab, 2012; Khan et al., 2020).

The importance of balance and diversification in tourism resilience

There is a high correlation between economic performance and the spatial concentration of tourist destinations (Antonakakis et al., 2015) in most destinations. The periods of crisis in the 21st century – the 2008 global economic crisis and the coronavirus pandemic that unfolded in 2020 – have clearly shown that the key to the resilience of the tourism sector to crises is the balance between international and domestic tourism (Arbulú, et al., 2021; Bui & Wickens, 2021; Litvinova-Kulikova, et al., 2023; Fekete & Fábián, 2022). It has proven the tourism industry to be resilient to negative events and has managed to recover, adapt, and innovate in the face of uncertainty (Sulhaini et al., 2023). Its aforementioned success is because a high level of tourist arrivals from several directions can reduce the sector's exposure to external factors and contribute to the stability of the industry. In the epidemic period, however, the Shumpeterian thesis of economic development – not sacrificing long-term interests for short-term goals – was inevitably pushed into the background during the pandemic, as the primary global objective was to minimise the epidemic risk. For crisis resilience, it is of paramount importance that the destination has a diversified tourism product offer, as socio-economic crises can restructure demand temporarily or even in the longer term. It can even lead to regional disparities, especially in small regions (Christofakis et al., 2019; Đokić et al, 2016).

In addition, the need to react quickly to changing consumer demands in times of crisis is a key pillar of maintaining competitiveness (Csugány & Tánczos, 2019), and it should maintain such economic, social, and environmental ways to continue to compete in the global tourism market (Díaz-Padilla et al., 2023). Therefore, it is crucial for destinations to focus on re-orienting the tourism system, regenerating tourism growth, and investing in infrastructure, product development, market development, and structural reforms (Varghese & Chennattuserry, 2022), as well as the role of stakeholders is highlighted in disaster

management from external roots to ensure tourism resilience and restore its image (Berbekova et al., 2021). Therefore, tourism destinations must follow a diversification strategy without dependence on one destination to mitigate future risks, thereby requiring the development of new attractions (Tömöri & Staniscia, 2023). In Hungary, this process was observed during the coronavirus epidemic, when destinations based on health tourism services suffered a much larger decline in turnover. However, another important factor is that the crisis in health tourism services has been affected not only by travel restrictions on foreign tourists, but also by the high proportion of elderly tourists. In Hungary, the example of the Western Transdanubia region is an excellent illustration of how a stable – with a more significant domestic but dominant international interest – and diversified tourism product offer shows a higher degree of crisis resilience.

Thus, maintaining a balance between domestic and foreign visitors and a diversity of tourist attractions is key to achieving tourism sustainability and stability. On this basis, the development and diversification of the tourism sector are also vital to improving Hungary's tourism competitiveness and increasing its resilience to crises.

The emergence of EU development funds in tourism development in Hungary

The European Union has recognised the positive economic and social effects of integration, such as job creation, development of peripheral regions, strengthening of transnational cooperation, social cohesion, etc. (Abbott & Wallace, 2014; Gwiaździńska-Goraj et al., 2022; Popa, 2012). The recognition of these positive effects is demonstrated by the fact that the European Union has launched several international programmes for the general development of the sector, such as the European Year of Tourism, Philoxenia, and Calypso.

In Hungary, EU development funds have been present in the country's territorial development even before its accession in 2004. After the 1990s, the most significant domestic tourism development measure was the Széchenyi Plan 2000-2003. The programme aimed to improve the quality of tourism, based on the stimulation of domestic and international tourism and the increase of tourism performance. The biggest achievement of the development plan was the increase of the domestic tourist season from 221 to 316 days, which seemed to revitalise a tourism sector that had been in decline for decades. The expansion is mainly due to the significant development of health tourism, which has become the leading tourism product in the domestic tourism sector and is still the most dominant in Hungary today. In the following decades, the tourism sector has been consistently perceived as a priority sector.

The EU provided significant financial support to Hungary and the other Eastern European accession countries in the years following the change of regime, with the aim of promoting economic and social cohesion and ensuring territorial development (Börzel, 2010; Suurna, & Kattel, 2010). These support funds were indirectly linked to tourism development.

From 2004 onwards, the objectives for the use of aid funds were defined in the development plans (2004-2006 NFT, 2007-2010 ÚMFT, 2010-2013 ÚSZT, 2014-2020 Széchenyi 2020) and the associated operational programmes, which defined the periods for the use of aid funds. The so-called convergence regions, which are able to generate less than 75% of the EU average GDP, have received the largest amounts of funding for the development periods. In Hungary, all but the Central Hungary region fall into this category. There have been several debates and doubts about the success of the use of development funds, which basically question the absorption capacity of NUTS II regions.

The European Commission approved the Partnership Agreement with Hungary for the period 2021-2027 in December 2022. This agreement is worth nearly €22 billion and will allow for investments from these EU cohesion funds. However, in order for Hungary to be able to implement cohesion policy programmes, it is necessary to meet the eligibility criteria. Since December 2009, tourism policy has had its own legal basis, but it does not have its own budget in the current Multiannual Financial Framework for the period 2021-2027 (Körtvélyesi, 2023).

Methods

The following study of economic determination and tourism performance in different regions of Hungary has used reliable data sources originating from three databases, namely Eurostat, Hungarian Central Statistical Office (KSH), and Supported project search by additional sources. Firstly, the Eurostat was initiated from the official statistical office of the European Union, which provides reliable and comparable data on various economic and tourism indicators of the EU Member States, including the number of nights spent, the number of tourists, the receipts from accommodation fees and GDP. In addition, this research involved the Hungarian Central Statistical Office (KSH), which is the source of the most important indicators of the Hungarian economy and society, including regional and national tourism and economic data. Lastly, this study obtained data by supported project search, such as the database available at https://www.palyazat.gov.hu/tamogatott_projektkereso which provides the most important

information on European Union development funds coming to Hungary from 2004 onwards. For the present study, the analysis of the database was relevant for the analysis of the grants awarded for tourism development in Hungary.

A comprehensive database was compiled from the data available between 2004 and 2022, which included the following data sets:

- Average gross earnings per capita (HUF)
- Gross domestic product per capita (GDP per capita, thousand HUF)
- Number of nights spent in commercial accommodation (number)
- Gross domestic revenue from accommodation in commercial accommodation (HUF 1 000)
- Total gross foreign turnover from accommodation in commercial hotels (HUF 1 000)
- Total gross receipts from commercial hotels (HUF 1 000)
- Number of foreign guests in commercial accommodation (persons)
- European Union (ERDF) aid granted for tourism development (HUF)
- Number of guests in commercial accommodation (persons)

The data series were analysed for the period 2004 to 2022. On a territorial basis, the EU-25 Member States (excluding Cyprus and Malta) have been analysed for the number of nights spent, the whole territory of Hungary for the other indicators and the NUT2 and NUT3 administrative units for some indicators.

The methods of analysis based on the indicators used in the study were essentially descriptive. The analysis of the annual number of overnight stays, the number of tourists and the time trends of the absolute values of the gross receipts from accommodation allowed a deeper understanding of the evolution of the tourism performance. The tourism development subsidies, also analysed in absolute figures and in a descriptive way, provide a good indication of the tourism potential of a municipality or region, its development direction and the embeddedness of the tourism sector in the local economy. The fundamental objective of such aid is to develop and maintain a sustainable and prosperous tourism industry. The study analyses GDP per capita at NUTS3 level, compared with average gross earnings per capita and tourism and traffic indicators. The analysis contributes to understanding the regional specificities of economic performance and to exploring the links with tourism indicators.

The study also aims at inferring the regional conditions of tourism competitiveness by defining tourism GDP as a factor of tourism in the regions of Hungary. One of the tourism GDP factors was defined by the authors with the following indicator.

- Tourism development: Total gross revenue from commercial accommodation/permanent population

To illustrate the regional differences, a distorted map was produced using QGIS software, which shows the economic performance of each region in terms of GDP per capita based on the territorial coverage of NUTS2 regions, thus highlighting regional differences.

Results

Tourism performance of Hungary in the European Union, 2004-2022

The growth of tourism in Europe has had a significant and far-reaching impact on national economies across the globe. Europe, including the Member States of the European Union, has consistently emerged as a leader in the tourism market. This can be attributed to the region's captivating history, diverse cultural heritage, and awe-inspiring natural landscapes. These factors combine to create a unique and irresistible allure that positions Europe as a top tourist destination. The tourism industry in Europe continues to thrive, attracting millions of visitors each year and generating substantial economic benefits for the countries within the region.

The tourism sector in the European Union plays a significant role in the overall economy, contributing to the GDP both at the national and integration levels. The revenue generated from tourism activities supports various sectors, including hospitality, transportation, and entertainment, creating employment opportunities and stimulating economic growth.

One of the key factors driving the growth of tourism in Europe is the well-developed transport infrastructure and tourist services network. The Schengen Agreement, which allows for the free movement of people across many EU countries, has greatly facilitated travel for EU citizens. This seamless mobility has made it easier and more convenient for tourists to explore multiple destinations within Europe, contributing to the overall growth of the tourism industry.

Furthermore, Europe boasts a highly efficient and interconnected transportation system. Airports, railway stations, and transport networks are well-developed, ensuring smooth connectivity between various cities and regions. This accessibility enhances mobility for both domestic and international tourists, making it easier for them to navigate and explore the diverse attractions that Europe has to offer.

The objective of this study is to characterise Hungary's regional tourism and economic performance between 2004 and 2022 in the light of the European Union's tourism resources. In European terms, Hungary's tourism performance can be considered as medium. In 2019, a record year for tourism, the country's tourist arrivals exceeded 33 million nights, making Hungary the 15th most visited of the EU-27 Member States. In tourism terms, Hungary cannot be called a tourism powerhouse due to its lack of high mountains, coastline and global attractions. In line with this characteristic, the country's tourism is based more on the demand for built and natural cultural heritage, food and drink, spas and wellness services. The interest in Hungarian history and culture, as well as the numerous thermal and spa springs, renowned for their healing properties, are also important attractions. In terms of international tourists, the main visitors come from neighbouring Member States, but there is also an increasing number of tourists from Asia and the USA. A significant part of tourism in Hungary is based around the capital, Budapest and the Lake Balaton region, but rural regions are also dynamically developing destinations, both on the demand and supply sides.

Figure 1 shows the number of nights spent in commercial accommodation in the European Union in 2022. Due to a lack of data, the map does not include the EU-27 Member States of Malta and Cyprus. The most visited destinations in 2022, based on the tourism indicators, which include both domestic and international nights, were Spain, France, Germany, and Italy. These countries reached 400 million overnight stays, mainly due to their potential for classic beach holidays, with the exception of Germany.

Hungary's regional tourism performance between 2004 and 2022

Hungary's tourism industry has developed significantly over the past decades. In 2004, Hungary joined the European Union, which created new opportunities for tourism. Tourism in Budapest plays a very important role in Hungary's tourism. The capital has seen significant investments in tourism infrastructure and superstructure in recent decades. In addition, the capital offers a number of attractions of international interest, such as the Parliament, the Fisherman's Bastion, the Danube embankment and the famous Gellért and Széchenyi spas. As a result, Budapest attracts an increasing number of tourists every year. In a record year in 2019, the capital's visitor numbers exceeded 10.7 million overnight stays, generated by a total of 4.6 million tourists, of which almost 4 million were foreigners.

Figure 2 shows the number of nights spent in commercial accommodation in the NUTS 2 regions of Hungary in 2022. The map shows that Budapest remains the country's most popular tourist destination with over 8.6 million overnight stays. The capital offers a wide range of cultur-

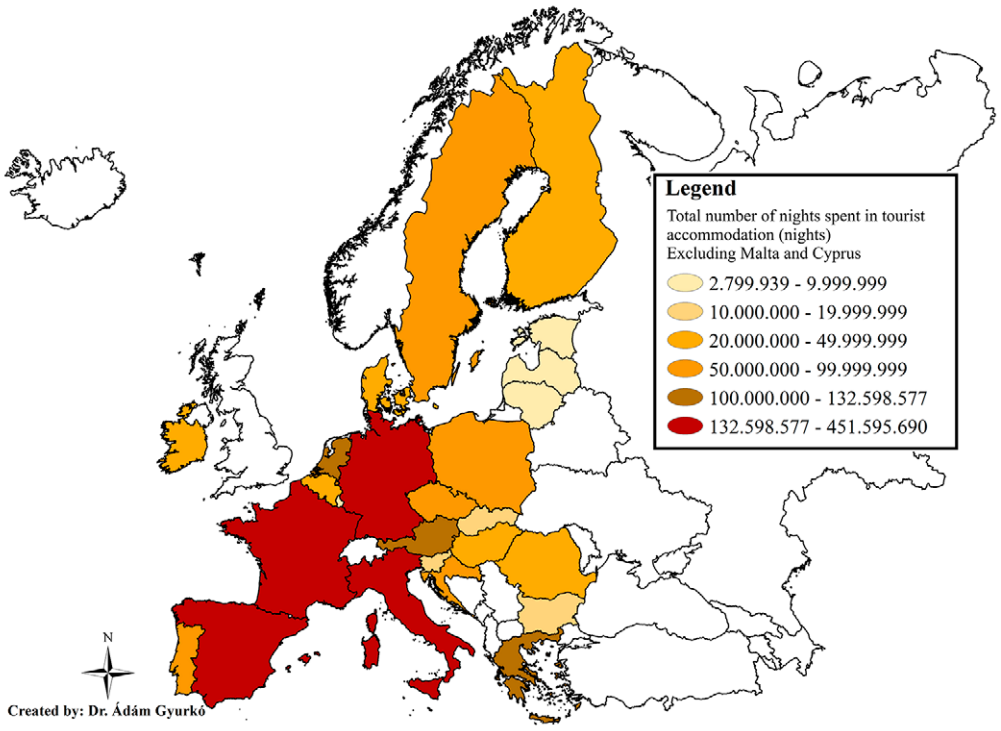

Figure 1. Number of nights spent in commercial accommodation in the European Union (EU-25, excluding Malta and Cyprus) in 2022
Source: Eurostat Database, 2023 based on own edits

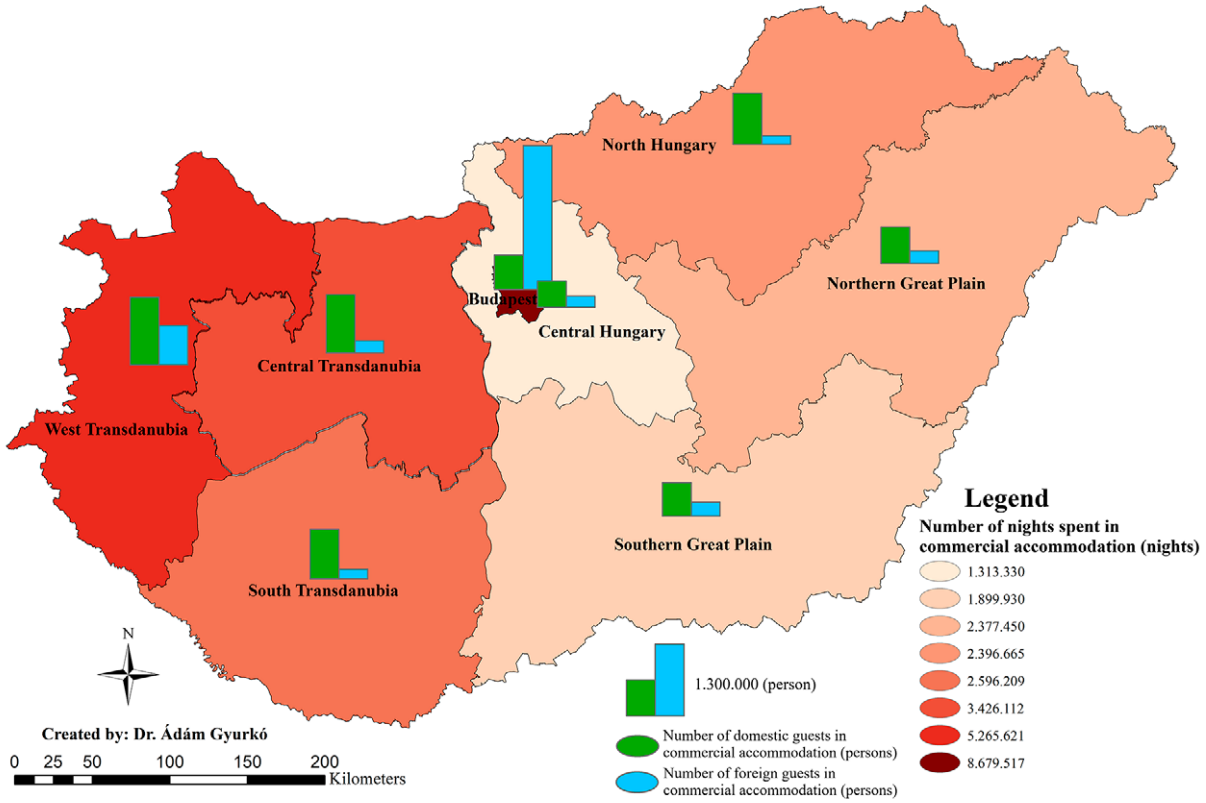

Figure 2. Regional tourism in Hungary in 2022 (NUTS2)
Source: KSH Database, 2023 based on own editing

al and historical attractions that attract a large number of foreign tourists (Schultz & Somodi, 2021). Budapest is virtually the only truly international destination in Hungary. The number and proportion of foreign visitors are also outstanding in national terms. In 2022, 2.5 million foreign tourists generated 6.8 million overnight stays, which exceeds the total number of international tourists arriving in other parts of the country.

At NUTS 2 level, the West Transdanubia region is the second most important Hungarian destination in terms of tourism performance (5.2 million overnight stays). The region attracts visitors with its natural beauties, its historical towns, but most of all with its spas (Hévíz, Zalaegerszeg, Sárvár, Bükfürdő, etc.). The number and proportion of foreign visitors is quite high, mainly due to the proximity of the Austrian border. The Central Transdanubia region was the third most visited destination in Hungary in 2022, with 3.4 million overnight stays. The tourism potential of the region is mainly due to the northern shore of Lake Balaton. In the South Transdanubia region, Lake Balaton also generates the highest number of visitors in the region.

The eastern part of the country is becoming less and less of a priority region in tourism terms as it moves away from solvent demand. However, in recent decades, these regions have also experienced a strong upsurge, with the number of overnight stays almost doubling in both the Northern Hungary and Northern Great Plain regions.

In tourism terms, in 2019, the share of tourism-specific activities in the gross output of the total national economy was 6.4% in Hungary, similar to the previous year, while the multiplier effect of production was 10%. The value added of tourism-related sectors was 6.8% of the national economy as a whole, or 11% including the multiplier effect. The two main sectors of the tourism sector, accommodation and food services, together accounted for about 2.1% of domestic production. At the historical low in 2020, the share of tourism-specific activities in the gross output of the total national economy fell to 5.4%, 7.9% including multiplier production effects. The value added of tourism-related sectors was 5.5% of the national economy as a whole, reaching 8.1% including the multiplier effect. The two main sectors of the tourism sector, accommodation and food services, together accounted for around 1.6% of gross domestic production, compared with 2.1% the previous year.

The tourism development indicator in national terms experienced a dynamic upswing from 2004 to 2019 (Figure 3), which was interrupted by the global economic crisis in 2008, pushing it into a declining, stagnant state until 2011.

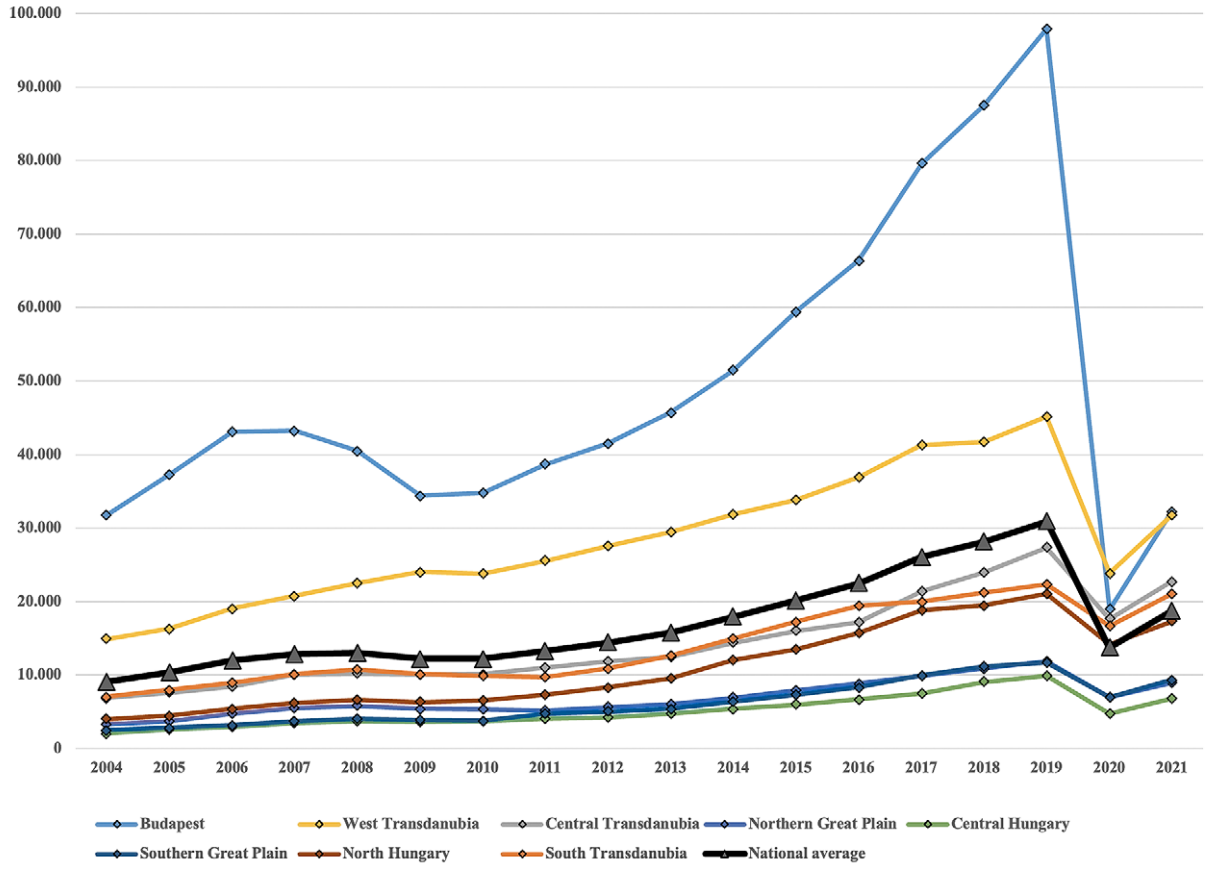

Figure 3. Tourism development (total revenue of accommodation establishments/permanent population) of commercial accommodation in Hungarian regions between 2004 and 2022
Source: KSH Database, 2023 based on own editing

The indicators allow objective, comparable performance assessment at both micro and macro levels. The indicator helps quantify the profitability of tourism in the target areas, understand the contribution of tourism to the local economy, and understand the impact tourism can have on the population of the area. The global crisis has mainly affected Budapest's destination in terms of the tourism development indicator, with a lack of mass international travel. During the pandemic that unfolded in 2020, the Budapest destination suffered an even more pronounced decline, with tourism development falling below the level of the Western Transdanubian region. At the same time, the coronavirus epidemic not only affected international travel, but the restrictive measures introduced also caused domestic tourism to plummet to a historic low. As a result, all regions, and thus the national average, experienced a significant decline in tourism development.

Budapest is Hungary's most dominant tourist destination due to its historical and cultural heritage, vibrant cultural life, well-developed infrastructure and affordable prices, which has led to regional differences in Hungary's tourism. In tourism terms, the existence of regional differences is not necessarily a disadvantage for a country. The dominance of Budapest in Hungarian tourism can have a spill-over effect on other destinations in the country. The capital's popularity could increase interest in Hungary on the international market, which could in particular have a positive impact on the Balaton and Western Transdanubia regions. By exploiting the spill-over effect, Hungary could become an even more important player on the European tourism map.

Regional economic characteristics of Hungary and the regional distribution of EU funds and its impact on tourism development

This chapter analyses the distribution and use of EU funds for tourism development in Hungary between 2004 and 2022, with the aim of examining the financing of tourism development projects and the regional distribution of EU funds, and the resulting impact on the Hungarian tourism sector and the overall economic conditions. Using economic data and tourism statistics, the study analyses the regional distribution of GDP, GDP per capita and number of overnight stays. From 2004 onwards, EU funds in Hungary offer significant potential for supporting tourism development and reducing disparities between regions.

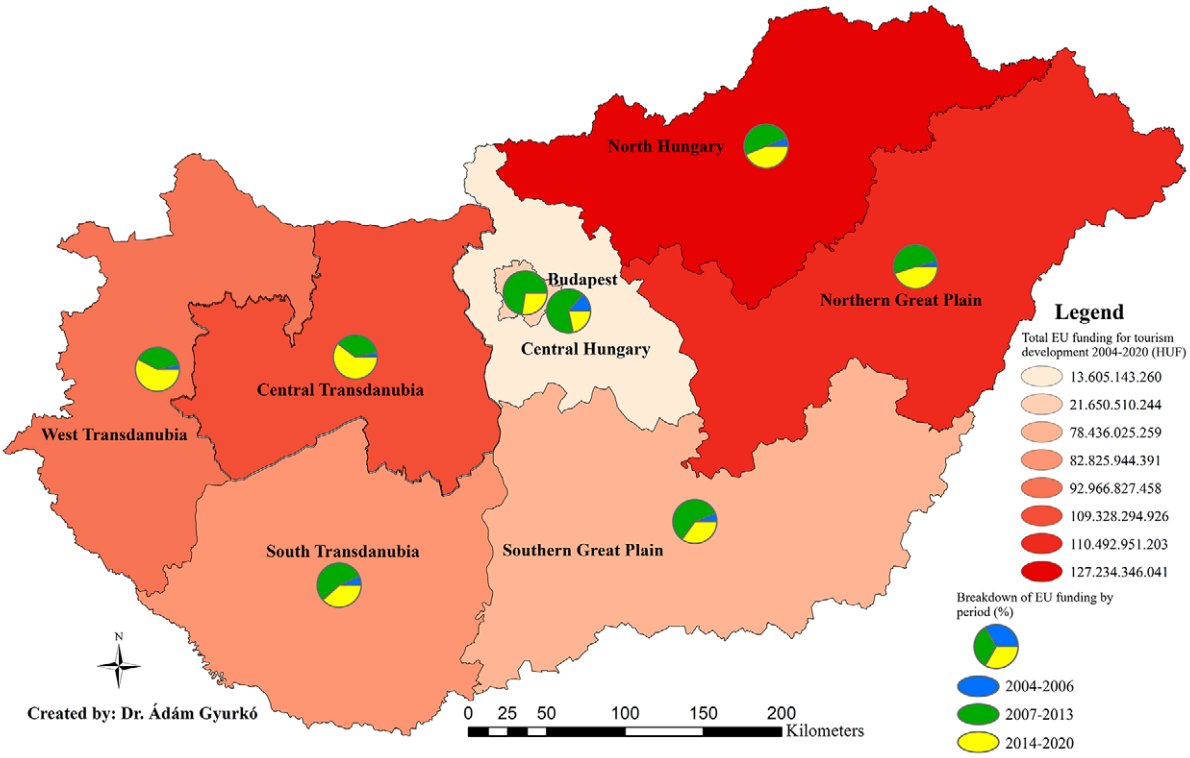

Figure 4. European Union funds (ERDF) granted under the tourism incentive in the regions of Hungary between 2004 and 2020
Source: https://www.palyazat.gov.hu/tamogatott_projektkereso Database, 2023 based on own editing

Figure 4 shows that, nationally, the North-Hungary region received the most financial resources for tourism development between 2004 and 2020. This is due to the high tourism potential of the region (settlements rich in cultural and historical values, thermal waters, impressive natural formations, etc.) and the EU cohesion policy, which gives priority to the development of less developed regions within the integration process. Based on these two factors, the North-Hungary region has been the most prioritised area for tourism development in recent planning periods.

Figure 5 shows the average gross earnings per capita (HUF) at the NUT3 level and the gross domestic product per capita (HUF thousands) at the NUT2 level in Hungary in 2021. For both indicators, outliers can be identified in Budapest, which is a good indicator of Hungary's water-headedness. Generally speaking, capital cities always have a higher GDP per capita due to a number of factors, including their central role, high quantity and quality of jobs, concentration of research and development centres, transport and other infrastructure advantages, and high number and quality of cultural and educational institutions. The economic structure of the country is therefore capital-centred, but an NW-SE economic axis can be identified, which makes the western part of the country a prosperous region compared to the eastern part. As a result, the western counties and regions have higher GDP per capita and average earnings than the national average. The counties of Fejér and Győr-Moson-Sopron exceed the national average for both indicators.

In general, there is a positive correlation between GDP per capita and average earnings. However, it is important to understand that this correlation is not always clear and linear. Several factors influence the relationship between the two indicators and the correlation may vary between countries, regions and time periods. In general, countries and regions with higher economic activity tend to have higher GDP per capita and, as a consequence, often higher average earnings.

A number of other factors may also underlie the relationship, such as economic growth, productivity, labour market conditions, industry composition, education levels and labour market policies, etc. Higher GDP per capita creates opportunities for higher wages and earnings, provided that this is accompanied by higher economic growth and productivity. Thus, a number of socio-economic factors combine to influence the extent to which GDP per capita determines the evolution of average earnings.

Figure 6 shows the specific weight of each region in Hungary in the country's economic performance. If we relate the size of the country's regions to the volume of its gross domestic product (GDP), we can see how water-headed the country is, with Budapest accounting for

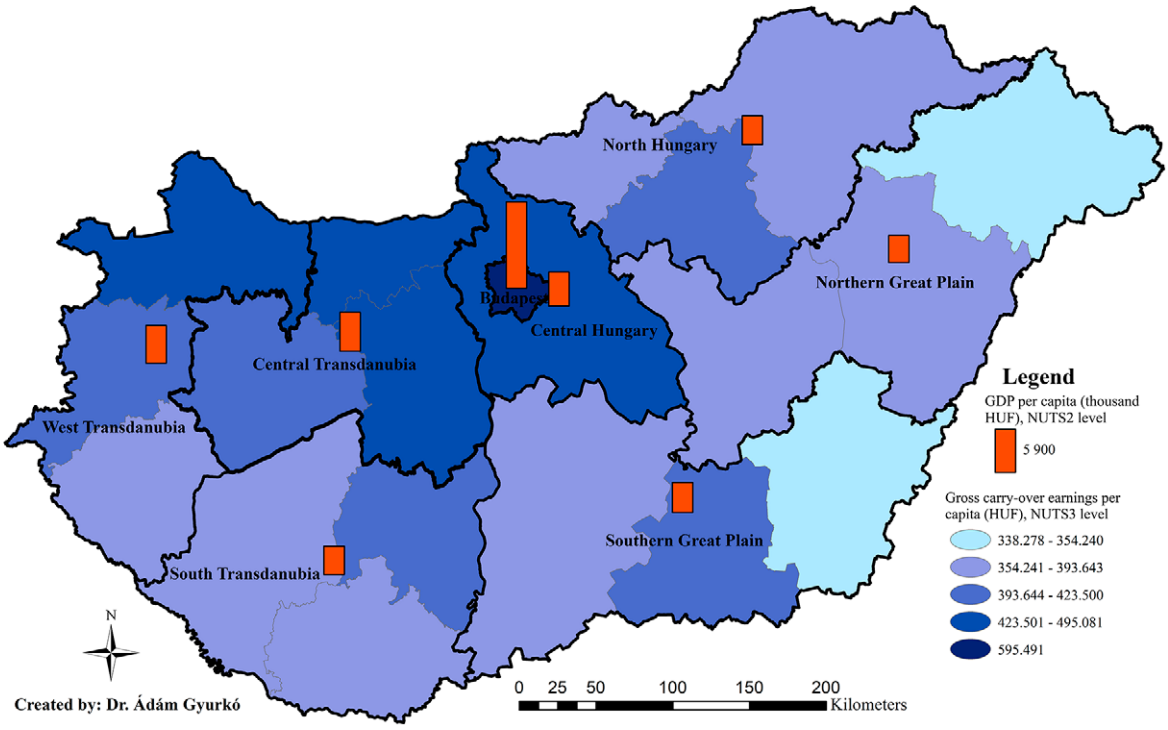

Figure 5. Average gross earnings per capita (HUF) at the NUT3 level and gross domestic product per capita (thousand HUF) at the NUT2 level in Hungary in 2021
Source: KSH Database, 2023 based on own editing

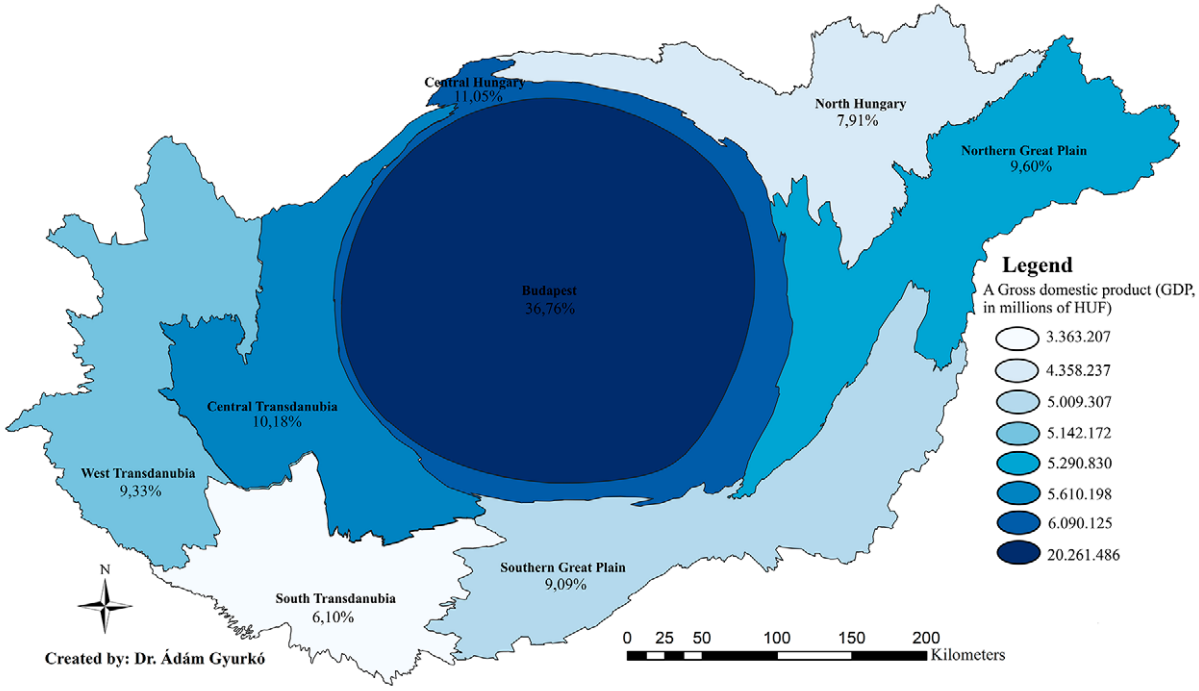

Figure 6. Hungary's NUTS2 regions as a share of gross domestic product (GDP)
Source: KSH Database, 2023 based on own editing

more than a third of the country's GDP. The GDP per capita in the capital is more than twice the national average (Figure 5) and almost five times as much as in Szabolcs-Szatmár-Bereg or Somogy counties.

In Hungary, the regional disparities in terms of GDP have not changed significantly between 2004 and 2021. The capital, Budapest, remains a prominent economic centre, while in other regions the industrial, agricultural or service sectors are more pronounced. Reducing regional disparities and promoting more equitable economic development remains a major challenge in Hungary, with regional development policies and investments requiring additional financial support. In their absence, inequality between rural, less-developed areas and prosperous regions will become even more pronounced.

Accounting for just over a third of Hungary's economic output, Budapest is also a major tourist attraction, a rarity in Europe and the world. No radical change in this indicator can be predicted, as there is no clear counterpart to the capital within the national borders, without which regional disparities are guaranteed to persist.

Regional differences in the performance of tourism, in terms of the share of nights spent in commercial accommodation, also reflect the overweight of Budapest (Figure 7). However, in terms of this indicator, the Western Transdanubia region can be clearly defined as a prosperous area, which may be able to dampen Budapest's hydrocephalus in tourism terms. This process was clearly evident during the crisis periods. Tourism performance in the Western Transdanubian region has increased significantly following the global crisis of 2008 and the pandemic that will unfold in 2020. The stability of the region is due to the relative balance of domestic and foreign tourists.

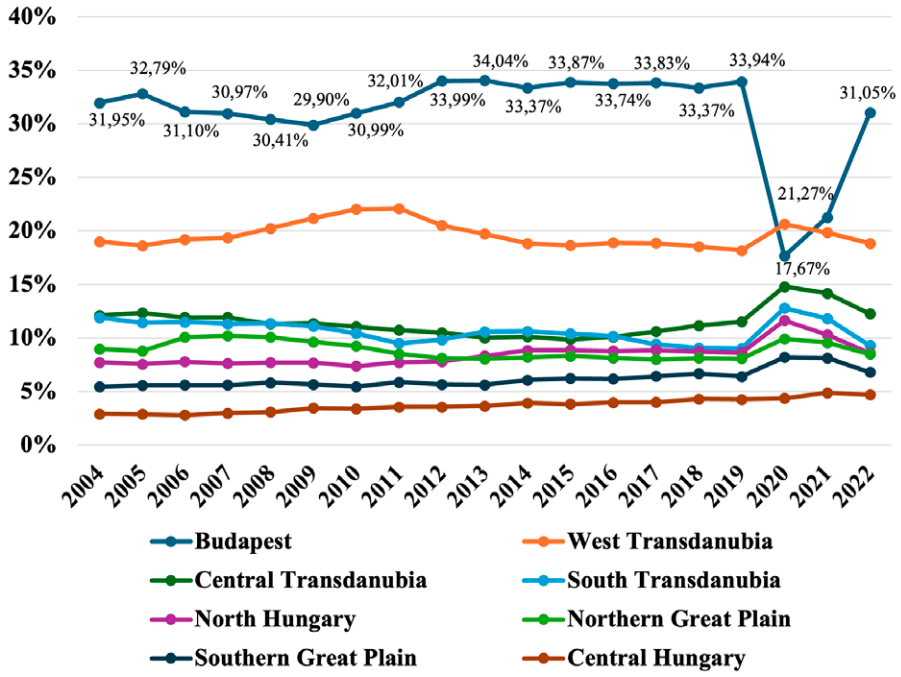

Figure 7. Change in nights spent in commercial accommodation (%) in NUTS2 regions of Hungary between 2004 and 2022
Source: KSH Database, 2023 based on own editing

Discussion

The basic question of the research was: what are the regional differences in economic determination and tourism performance in Hungary? The answer to the basic question can be formulated as follows: there are strong regional differences in economic determination and tourism performance in Hungary. Budapest has an extraordinary economic dominance, which is reflected in almost all socio-economic indicators and influences the direction of national development. Reducing regional disparities is essential to promote economic catching-up and prevent social tensions.

As regards future research directions, further analysis of regional disparities is a priority. The research sheds light on regional disparities in Hungary, but also requires a deeper analysis to identify the factors that exacerbate

disparities and the factors that mitigate them. Future research on the subject should also pay more attention to the economic catching-up of peripheral regions. The study points out that Hungary's peripheral areas have developed serious economic challenges, but the reasons for this are not explored in depth.

Conclusion

The analyses in the study show that there are strong regional differences in economic performance and tourism destinations in Hungary. Budapest stands out in all respects, being the clear economic centre of the country, and is characterised by indicators that are significantly above the national average in almost all socio-economic indicators. The specific weight of the capital city, therefore, fundamentally determines the dynamics and direction of national development. In Hungary, even the EU cohesion development funds, which have been available since 2004, have not been able to mitigate the over-dominance of the capital, which has now led to increasingly serious economic challenges in peripheral regions.

In Hungary, the reduction of regional disparities must be a priority in the coming years, as the lack of dynamic economic development in the peripheral regions could lead to serious social tensions and economic collapse, which in the longer term could lead to the depopulation of rural areas. Continued support for regional development policies and investment is, therefore, vital for Hungary to achieve balanced development in both economic and tourism terms.

The results of the study have clearly shown that the balance between international and domestic tourism is key to the resilience of tourism to the crisis. Multi-directional tourism can reduce exposure to external factors and contribute to the stability of the tourism industry. Another important factor is that a destination should have a diversified tourism product offer, which can also reduce the degree of crisis. In this respect, the example of the Western Transdanubia region illustrates how a stable and diversified tourism industry can be more resilient to crisis situations. Maintaining a balance between domestic and foreign visitors and the diversity of tourist attractions can contribute to the stability of the sector.

Acknowledgements

Supported by the ÚNKP-23-4 New National Excellence Program of the Ministry for Culture and Innovation from the source of the National Research, Development and Innovation Fund.

References

Abbott, P., & Wallace, C. (2014). Rising economic prosperity and social quality the case of New Member States of the European Union. *Social indicators research*, 115(1), 419-439. DOI: https://doi.org/10.1007/s11205-012-9992-0

Antonakakis, N., Dragouni, M., & Filis, G. (2015). How strong is the linkage between tourism and economic growth in Europe? *Economic Modelling*, 44, 142-155 DOI: https://doi.org/10.1016/j.econmod.2014.10.018.

Arbulú, I., Razumova, M., Rey-Maquieira, J., & Sastre, F. (2021): Can domestic tourism relieve the COVID-19 tourist industry crisis? The case of Spain. *Journal of Destination Marketing & Management*, 20(2), 1-12. DOI: https://doi.org/10.1016/j.jdmm.2021.100568

Assadzadeh, A., & Nasab, M. H. N. (2012): Investigating the relationship between tourism industry and GDP in the Islamic Republic of Iran. *International Review of Business Research Papers*, 8(2), 85-95. DOI: https://doi.org/https://doi.org/10.14267/TURBULL.2017v17n1-2.2

Aykac, A. (2010). Tourism employment: Towards an integrated policy approach. *Anatolia*, 21(1), 11-27. DOI: https://doi.org/10.1080/13032917.2010.9687087

Berbekova, A., Uysal, M., & Assaf, A. G. (2021). A thematic analysis of crisis management in tourism: A theoretical perspective. *Tourism Management*, 17(86). DOI: https://doi.org/10.1016/j.tourman.2021.104342

Bohlin, M., Brandt, D., & Elbe, J. (2022). Spatial Concentration of Tourism–a Case of Urban Supremacy. *Tourism Planning and Development*, 19(5), 392–412. DOI: https://doi.org/10.1080/21568316.2020.1855239

Börzel, T. A. (2010). Why you don't always get what you want: EU enlargement and civil society in Central and Eastern Europe. *Acta politica*, 45, 1-10. DOI: https://doi.org/10.1057/ap.2010.1

Bui, PL., & Wickens, E. (2021). Tourism industry resilience issues in urban areas during COVID-19. *International Journal of Tourism Cities*, 7(3), 861-879. DOI: https://doi.org/10.1108/IJTC-12-2020-0289

Çaglayan, E., & Sak, N. (2012). Relationship Between Tourism and Economic Growth: a panel Granger causality approach. *Asian Economic and Financial Review*, 2(5), 591–602.

Cárdenas-García, P. J., Sánchez-Rivero, M., & Pulido-Fernández, J. I. (2015): Does Tourism Growth Influence Economic Development? *Journal of Travel Research*, 54(2), 206-221. DOI: https://doi.org/10.1177/0047287513514297

Christofakis, M., Gaki, E., & Lagos, D. (2019). The impact of economic crisis on the regional disparities and the allocation of economic branches in Greek regions. *Bulletin of Geography. Socio-economic Series*, 44, 7-21. DOI: https://doi.org/10.2478/bog-2019-0011

Cracolici, M.F., Cuffaro, M., & Nijkamp, P. (2010): The Measurement of Economic, Social and Environmental Performance of Countries: A Novel Approach. *Social Indicators Research*, 95(1), 339–356. DOI: https://doi.org/10.1007/s11205-009-9464-3

Csugány, J., & Tánczos, T. (2019). A hazai turizmusban rejlő lehetőségek a negyedik ipari forradalom korszakában [The potential of domestic tourism in the era of the fourth industrial revolution]. In: Gyurkó, Á – Somodi-Tóth, O (eds.): #Turizmus #szálloda #vendéglátás: Jubileumi Kiadvány Az Eszterházy Károly Egyetem Turizmus Tanszék Alapításának 10. Évfordulója Alkalmából. Líceum Kiadó, Eger, 55–65. (in Hungarian with English summary)

Dayananda, K. C (2014): Tourism and employment: Opportunities and challenges in Karnataka-special reference to Kodagu District. *Journal of Humanities and Social Science*, 19(11), 1-11.

Dávid, L., Bujdosó Z., & Patkós, Cs. (2003). *A turizmus hatásai és jelentősége a területfejlesztésben* [The impact and importance of tourism in territorial development]. In: Süli-Zakar, I. (eds.) A terület- és településfejlesztés alapjai [Basics of spatial and urban development]. Dialóg Campus Kiadó, 433-453.

Dávid, L., Tóth, G., Bujdosó, Z., & Herneczky, A. (2007): A turizmus és a regionális versenyképesség kapcsolatának mutatói a Mátravidék példáján keresztül [Indicators of the relationship between tourism and regional competitiveness through the example of the Matravidék]. *Észak-magyarországi Stratégiai Füzetek*, 4(1), 3-20. (in Hungarian with English summary)

Díaz-Padilla, V. T., Travar, I., Acosta-Rubio, Z., & Parra-López, E. (2023). Tourism Competitiveness versus Sustainability: Impact on the World Economic Forum Model Using the Rasch Methodology. *Sustainability*, 15(18). DOI: https://doi.org/10.3390/su151813700

Dobó, R., & Pintér, T. (2023). Regionális különbségek alakulása Magyarországon – kapcsolódási pontok a gazdasági teljesítménnyel és a kereskedelmi tendenciákkal [Regional disparities in Hungary - links with economic performance and trade trends]. *Multidiszciplináris Kihívások, Sokszínű Válaszok – Gazdálkodás – és Szervezéstudományi Folyóirat*, 6(1), 37–54. (in Hungarian with English summary). DOI: https://doi.org/10.33565/MKSV.2023.01.02

Đokić, I., Fröhlich, Z., & Rašić Bakarić, I. (2016). The impact of the economic crisis on regional disparities in Croatia. *Cambridge Journal of Regions, Economy and Society*, 9(1), 179-195. DOI: https://doi.org/10.1093/cjres/rsv030

Fekete, F. Zsófia., & Jánosi, D. (2022). A 2008. és a 2020. évi válság hatása a hazai munkaerőpiacra és turizmusra [Impact of the 2008-2020 crisis on the domestic labour market and tourism]. *Területi Statisztika*, 62(2), 135–165. (in Hungarian with English summary). DOI: https://doi.org/10.15196/TS620201

Giannetti, B. F., Agostinho, F., Almeida, C. M. V. B., & Huisingh, D. (2015): A review of limitations of GDP and alternative indices to monitor human wellbeing and to manage eco-system functionality. *Journal of Cleaner Production*, 87(1), 11-25. DOI: https://doi.org/10.1016/j.jclepro.2014.10.051.

García-Sánchez, A., Siles, D., & de Mar Vázquez-Méndez, M. (2021). Competitiveness and innovation: effects on prosperity. In *Tourism Research in Ibero-America* (pp. 35-48). Routledge.

Gyurkó, Á. (2020). Az európai uniós turisztikai célú források területisége és hatásai az Észak-Magyarország régióban [The territoriality and impact of EU tourism funds in the North-Hungary region]. In: Bujdosó, Z. – Dinya, L. – Csernák, J. (eds.): XVII. Nemzetközi Tudományos Napok: Környezeti, gazdasági és társadalmi kihívások 2020 után. Líceum Kiadó, Gyöngyös, pp. 421–435 (in Hungarian with English summary)

Gyurkó, Á. (2022). Magyarország vendégforgalmának teljesítményértékelése területi és keresleti szempontból 2019 és 2022 között, különös tekintettel Eger városának turisztikai teljesítőképességére [Evaluation of the performance of tourism in Hungary from a territorial and demand perspective between 2019 and 2022, with a special focus on the tourism performance of the city of Eger]. *Turisztikai és Vidékfejlesztési Tanulmányok*, 7(4), 20–32. (in Hungarian with English summary). DOI: https://doi.org/10.15170/tvt.2022.07.04.02

Gwiaździńska-Goraj, M., Jezierska-Thöle, A., & Dudzińska, M. (2022). Assessment of the Living Conditions in Polish and German Transborder Regions in the Context of Strengthening Territorial Cohesion in the European Union: Competitiveness or Complementation? *Social Indicators Research*, 163(1), 29-59. DOI: https://doi.org/10.1007/s11205-022-02889-7

Káposzta, J., & Nagy, H. (2022). The Major Relationships in the Economic Growth of the Rural Space. *European Countryside*, 14(1), 67–86. DOI: https://doi.org/10.2478/euco-2022-0004

Körtvélyesi, K. (2023). Fejlesztéspolitika. Pénzügyi menedzsment a fejlesztéspolitikai programok esetében [Development policy. Financial management of development policy programmes]. Budapest, Nemzeti Közszolgálati Egyetem.

Khan, N., Hassan, A. U., Fahad, S., & Naushad, M. (2020): Factors Affecting Tourism Industry and Its Impacts on Global Economy of the World. *SSRN Electronic Journal*. DOI: http://dx.doi.org/10.2139/ssrn.3559353

Kummu, M., Taka, M., & Guillaume, J. (2018): Gridded global datasets for Gross Domestic Product and Human Development Index over 1990–2015. *Scientific data*, 5(1), 1-15. DOI: https://doi.org/10.1038/sdata.2018.4

Leonard, L. (2015): Mining and/or tourism development for job creation and sustainability in Dullstroom, Mpumalanga. *Local Economy Policy Unit*, 31(1-2), 249-263. DOI: https://doi.org/10.1177/0269094215621875

Litvinova-Kulikova, L., Aliyeva, Z., & David, L. D. (2023). MICE Tourism: How the Pandemic Has Changed It. *Journal of Tourism and Services*, 14(26), 197–218. DOI: https://doi.org/10.29036/jots.v14i26.496

Manzoor, F., Wei, L., Asif, M., Haq, M.Z.u., & Rehman, H.u. (2019). The Contribution of Sustainable Tourism to Economic Growth and Employment in Pakistan. *International Journal of Environmental Research and Public Health*, 16(19). DOI: https://doi.org/10.3390/ijerph16193785

Paramati, S. R., Alam, M. S., & Chen, C.-F. (2017). The Effects of Tourism on Economic Growth and CO2 Emissions: A Comparison between Developed and Developing Economies. *Journal of Travel Research*, 56(6), 712–724. DOI: https://doi.org/10.1177/0047287516667848

Popa, A. M. (2012). The impact of social factors on economic growth: Empirical evidence for Romania and European Union countries. *Romanian Journal of Fiscal Policy (RJFP)*, 3(2), 1-16.

Priatmoko, S., Kabil, M., Vasa, L., Pallás, E.I., & Dávid, L.D. (2021): Reviving an Unpopular Tourism Destination through the Placemaking Approach: Case Study of Ngawen Temple, Indonesia. *Sustainability*, 13(12). DOI: https://doi.org/10.3390/su13126704

Sam, I. E., Akpo, D. M., Asuquo, E. E., & Etefia, T. E. (2014). Socio-economic impact of tourism development in the forest community of Ikpe, Oro, Urue Offong Oruko local government area of Akwa Ibom State. *European Journal of Hospitality and Tourism Research*, 2(1), 15-23.

Scheyvens, R., & Hughes, E. (2021): Can tourism help to end poverty in all its forms everywhere? The challenge of tourism addressing SDG1. *Journal of Sustainable Tourism*, 27(7), 1061-1079. DOI: https://doi.org/10.1080/1331677X.2022.2150871

Schultz, É. – Somodi-Tóth, O. (2021): A magyarországi múzeumok, mint attrakciók a Tripadvisor belföldi látogatói véleményeinek tükrében a koronavírus idején [Museums as attractions in Hungary in the light of Tripadvisor's domestic visitor reviews during the age of the Crown Jewel]. *Turisztikai és Vidékfejlesztési Tanulmányok*, 6(4), 79–100. (in Hungarian with English summary). DOI: https://doi.org/10.15170/TVT.2021.06.04.06

Stec M., & Grzebyk M. (2022): Socio-economic Development and the Level of Tourism Function Development in European Union Countries – a Comparative Approach. *European Review*, 30(2),172-193. DOI: https://doi.org/10.1017/S106279872000099X

Sulhaini, Saufi, A., Herman, L.-E., & Scott, N. (2023). Network behaviour for tourism business resilience. *Tourism and Hospitality Research*. DOI: https://doi.org/10.1177/14673584231151900

Suurna, M., & Kattel, R. (2010). Europeanization of innovation policy in Central and Eastern Europe. *Science and Public Policy*, 37(9), 646-664. DOI: https://doi.org/10.3152/030234210X12778118264459

Tömöri, M., & Staniscia, B. (2023). The impact of the COVID-19 pandemic on cross-border shopping tourism: the case of Hungary. *Hungarian Geographical Bulletin*, 72(2), 147–161. DOI: https://doi.org/10.15201/hungeobull.72.2.4

Varghese, B., & Chennattuserry, J. C. (2023). Community Resilience and Crisis Management: Stakeholders Perspective of the Tourism Industry. In *Tourism and Hospitality in Asia: Crisis, Resilience and Recovery* (pp. 21-33). Singapore: Springer Nature Singapore. DOI: https://doi.org/10.1007/978-981-19-5763-5_2

INTERNATIONAL SCIENTIFIC JOURNAL
GEOGRAPHICA PANNONICA
Volume 28, Issue 1, 34–43 (March 2024)
Contents lists available at ScienceDirect
Journal homepage: http://www.dgt.uns.ac.rs/en/homepage/pannonica/

NDVI and NDBI Indexes as Indicators of the Creation of Urban Heat Islands in the Sarajevo Basin

Nusret Drešković[A], Samir Đug[B], Muniba Osmanović[A*]

[A] *University of Sarajevo – Faculty of Science, Department of Geography, Zmaja od Bosne 33-35, 71 000, Sarajevo; n.dreskovic@pmf.unsa.ba; muniba.osmanovic@pmf.unsa.ba*

[B] *University of Sarajevo – Faculty of Science, Department of Biology, Zmaja od Bosne 33-35, 71 000, Sarajevo; samirdjug@pmf.unsa.ba*

KEYWORDS

Landsat 8
NDVI
NDBI
LST
Sarajevo basin
urban ecology

ABSTRACT

Remote sensing plays a vital role in analyzing urban changes. In this regard, various datasets collected from satellites today serve as a foundation for decision-makers and urban planners. This study compares the Normalized Difference Vegetation Index (NDVI) and the Normalized Difference Built-up Index (NDBI) as indicators for the creation of surface heat islands. Using Landsat 8 OLI/TIRS C2 L2 images, spatial correlations between land surface temperature (LST) were examined for August 2013, 2019 and 2023. Urban heat islands (UHI) are a contemporary phenomenon and increasingly common in large urban areas compared to surrounding, less populated areas. With the advancement in remote sensing, it is possible to adequately determine the spatial differentiation and prevalence of urban heat islands (UHI). The study is based on Landsat 8 satellite image sets for the Sarajevo basin in August 2013, 2019 and 2023, which were used to analyze LST, NDVI, and NDBI indices. This work indicates a relationship between LST and NDVI but varies depending on the analyzed year. Normalized Difference Built-up Index (NDBI) serves as a suitable indicator for surface UHI effects and can be used as an indicator to assess its spatial distribution within a larger urban environment.

Introduction

Urban areas are subjected to continuous surface changes that influence local climatic characteristics. Such areas become warmer compared to the surrounding environment, with temperature differences particularly pronounced at night when vegetated surroundings cool more rapidly than paved urban surfaces. This phenomenon is known in the literature as the Urban Heat Island (UHI) (Voogt & Oke, 2003). The primary factor contributing to the formation of urban heat islands is the increasing replacement of undeveloped or vegetated areas with paved surfaces and buildings. UHI forms in environments with low cloud cover and weak air circulation, specifically in clear-sky and low-wind conditions. Dominantly, the summer months (June, July, August) are periods when the formation of the urban heat island can be observed and its spatial characteristics determined. Numerous scientists and researchers have explored the phenomenon of urban heat islands. Kim (1992) highlighted crucial indicators related to UHI in the capital of the United States based on Landsat TM mission data. He emphasized that temperatures in urban areas during summer can be up to 10°C higher than in nearby forested areas. The entire substrate

* Corresponding author: Muniba Osmanović, email: muniba.osmanovic@pmf.unsa.ba

doi: 10.5937/gp28-48216

Received: December 15, 2023 | Revised: March 04, 2024 | Accepted: March 15, 2024

begins to heat up in the mid-morning, driven by the rapid warming of urban surfaces such as buildings, paved areas, surfaces devoid of vegetation, and low vegetation. The effects of urban heat islands are studied at micro (below the surface and on the surface), local (urban canopy layer), and meso (urban boundary layer) scales due to the urban nature and multilayered structure of the atmosphere (Roth, 2013). UHI at the local level has far-reaching consequences for energy use in buildings, water use for irrigation, air quality, and urban ecology, as well as its impact on the thermal comfort of urban residents (Roth, 2013). The adverse effects of UHI are recognized worldwide, leading to increased demand for cooling, higher energy consumption, water demand, and contributing to elevated rates of diseases and mortality from heat stress or poor air quality (Heaviside et al., 2017; Yao et al., 2022).

In the early years of urban heat island research, the focus was on studying the atmospheric urban heat island (AUHI) based on meteorological data from a network of permanent weather stations. To create an accurate thermal map of the city, it was necessary to provide a large number of evenly distributed weather stations for data collection. However, maintaining these stations was expensive, and the reliability and accuracy of the data were questionable on a long-term scale (Wang, 2015). With the development of remote sensing, the research focus shifted to determining surface urban heat islands (SUHI). This method relies on the use of infrared radiation sensing sensors (TIRS), allowing for significantly greater spatial coverage (Fabrizi et al., 2010). Subsequent research has offered improvements over earlier sensor versions, and data from the thermal infrared sensor of the Landsat 8 satellite are widely used to study the state and dynamics of the urban thermal environment (Wang, 2015). Land Surface Temperature (LST) is defined as the temperature at the boundary between the Earth's surface and its atmosphere (Niclòs et al., 2009). Satellite-derived LST is a crucial parameter in studying the Urban Heat Island (UHI) process as it is used to analyze surface radiation and heat energy flow between the surface and the atmosphere (Mulahusić et al., 2018). LST plays a vital role not only in various surface processes but also in regulating sensible and latent heat flux (Sun et al., 2003). Many areas have recognized the significance of this parameter, and it is widely applied in climate and climate change research, hydrological regimes in specific areas, as well as ecological and vegetation changes. Parks and other green spaces in the city usually have lower temperatures than built-up areas, contributing to lowering air temperatures, while densely populated areas directly impact air warming, thus increasing its temperature (Srivanit & Hokao, 2012).

Improvements in high-resolution sensors have aided in the precise monitoring of Land Surface Temperature (LST) and Urban Heat Island (UHI) on large spatial and temporal scales (Naserikia et al., 2019). Numerous studies have indicated that bare soil and impervious surfaces are crucial factors influencing UHI, while vegetation and water surfaces can mitigate UHI formation (Song et al., 2014). Many researchers have explored the relationship between LST and built-up areas (Normalized Difference Built-up Index - NDBI) and vegetation (The Normalized Difference Vegetation Index - NDVI) indices (Chen et al., 2014; Guha et al., 2017; Değerli & Çetin, 2022; Alademomi et al., 2022; Haji et al., 2023). Research has confirmed the exceptional correlation between NDVI and LST, as well as between LST and NDBI. The results of these studies have robustly explained the relationship between urban development and the expansion of UHI in urban areas. The main objective of this study was to examine the values of NDVI and NDBI indices, representing the two main types of land cover. Additionally, based on Landsat 8 satellite imagery, the study aimed to define zones where UHI formation occurs. The specific goal was to explore the application potential of remote sensing products in studying further urban development in the Sarajevo basin. This study is innovative, considering the limited number of studies addressing the UHI phenomenon in Sarajevo during recent years of intensified urbanization (Mulahusić et al., 2018; Drašković et al., 2020). The study results provide a foundation for urban planners and decision-makers at the entity and cantonal levels to plan future urban development in the basin adequately. In this regard, the study attempted to answer two fundamental research questions related to a) the relationship between NDVI, NDBI, and LST and b) defining spatial zones where the intensity of UHI formation is most pronounced. A limitation of the study was the generalization, i.e., the size of the spatial coverage of Landsat 8 satellite images, which were 30x30 m, and the absence of entirely cloud-free satellite imagery, as the 2019 image was somewhat covered by clouds.

The main aim of this study was to compare two fundamental indices, NDVI and NDBI, from the years 2013, 2019, and 2023. The study sought to identify changes occurring during the analyzed years, utilizing Landsat 8 satellite imagery obtained from the United States Geological Survey (USGS) and focusing on the Sarajevo basin as a case study. The specific objective was to highlight the city's expansion and urban development, monitored through the Landsat 8 OLI/TIRS L2 C2 satellite. In line with these goals, the study aimed to address the fundamental research questions – RQ1: Can the urbanization of the Sarajevo basin be tracked based on NDVI and NDBI? RQ2: Is the spatial distribution of Urban Heat Island (UHI) related to land use and land cover?

Data and methods

Study area

Sarajevo basin is situated within the intermontane depression between the massifs of Bjelašnica and Igman to the southwest and the low mountainous and sub-mountainous terrain to the northeast. Its general orientation is approximately Dinaric (NW-SE). Within the basin lies the source area of the Bosna river with its tributaries: Zujevina with Rakovica, Željeznica with Kasindolka, Dobrinja with Tilava, and Miljacka. Based on its geological composition and geomorphological structure, the Sarajevo basin can be differentiated into two morphological units: the first being the mountainous periphery and the second, the basin floor of the Miljacka river with the Sarajevo field (Fig. 1). The average elevation of the Sarajevo basin is around 515 meters above sea level. The lowest elevation is in the north of the basin (in Reljevo, at 493 meters), while slightly higher points are located within the drainage basins and the extensions of the Željeznica, Kasindolka, Tilava, Miljacka, and Zujevina rivers (Hadžić et al., 2015). The area of the mountainous periphery exhibits rather heterogeneous climatic characteristics significantly influenced by the surrounding high mountains of Bjelašnica, Jahorina, and Treskavica (Hadžić & Drešković, 2014). Geographically, the research area is situated between 43° 47' North latitude and 18° 24' East longitude.

Landsat 8 data

For the purpose of this study, enhanced Landsat 8 OLI/TIRS L2 C2 data/images were utilized to measure various bands across the electromagnetic spectrum. Landsat 8 data comprise several bands depending on the wavelength (blue, green, red, infrared, thermal, and panchromatic). Landsat 8 encompasses 11 bands. Band 4 represents the Near-Infrared (NIR), while Band 6 is thermal, detecting heat and providing information about soil temperature, which typically tends to be warmer than the air (NASA Landsat Science, 2023). The Landsat 8 OLI/TIRS L2 C2 images used in this study were obtained from the United States Geological Survey (USGS). It is noted that the images from the year 2019 have a 30 cloud cover percentage, which had a minor impact on the results.

Table 1. Landsat 8 data

Path	Row	Cell size	Date
187	030	30x30	2013-08-16
187	030	30x30	2019-08-17
187	030	30x30	2023-08-28

Source: Processed by authors according to ArcGIS geo-database of GIS Center of Department of Geography, University of Sarajevo – Faculty of Science, 2023.

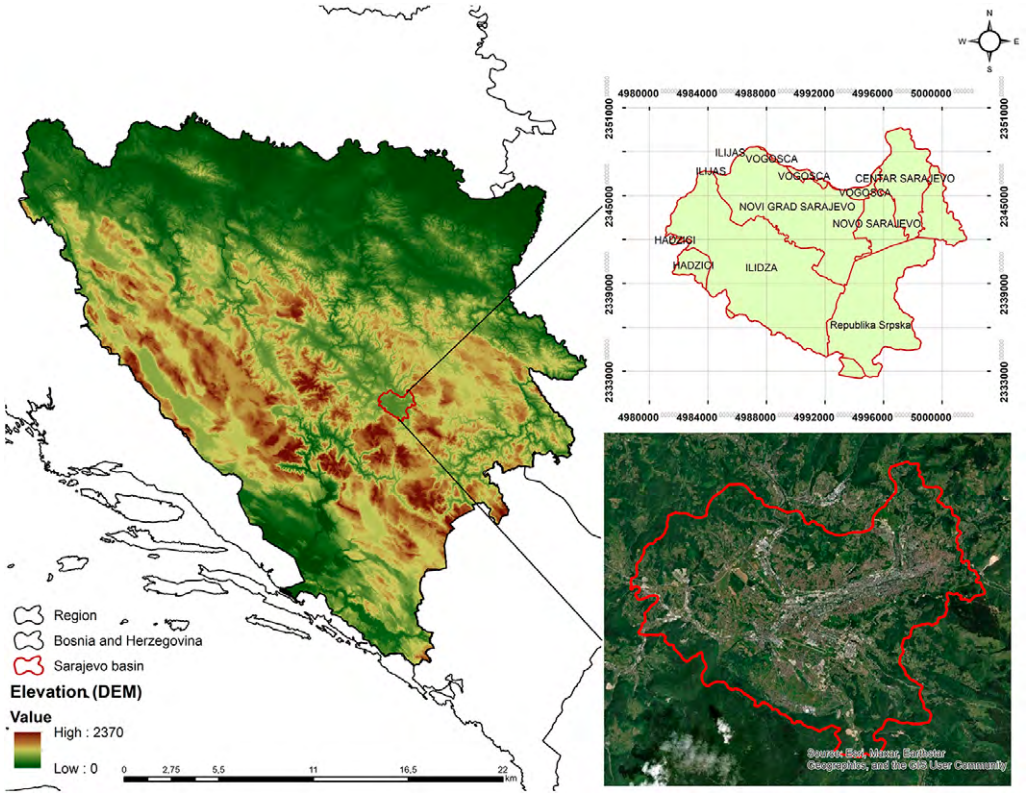

Figure 1. Study area
Source: Geo-database of GIS Center of Department of Geography, University of Sarajevo – Faculty of Science adapted by the authors using ArcGIS [GIS software] Version 10.6.1.

Data processing

The NDVI (Normalized Difference Vegetation Index) is calculated as the ratio between the reflectance of the red band around 0.66 μm and the near-infrared (NIR) band around 0.86 μm. NDVI is most easily calculated as the difference between near-infrared (NIR) and red (RED) reflectance divided by their sum. NDVI is represented by the following formula:

NDVI = (NIR–RED) / (NIR+RED)

In the study, this index was calculated in ArcGIS 10.6.1 software using the Raster Calculator: Float(Band 5 - Band 4) / Float(Band 5 + Band 4). NIR (Near-infrared) corresponds to the near-infrared spectrum of Landsat 8 images, while RED refers to the red band of satellite images. Areas with dense vegetation in satellite images tend to have positive values, while water bodies and built-up areas tend to have negative values.

The Built-up Index is essentially an image indicating the built-up and non-vegetated nature of areas because it is characterized solely by positive values. It represents one of the main types of land cover (Zha, Gao, and Ni, 2005). Built-up areas and non-vegetated areas reflect more SWIR than NIR rays. The formula for calculating this index (NDBI) is as follows:

NDBI = (SWIR – NIR) / (SWIR + NIR)

In the study, this index was calculated using the Raster Calculator as follows: Float(Band 6 - Band 5) / Float (Band 6 + Band 5).

Negative values of the NDBI index indicate water bodies and forests, while higher values (approaching 1) represent built-up areas. The NDBI value for vegetation is low (Macarof, 2017). The month of August was selected as relevant for analysis, considering that the biomass increment is highest during this month. A significant limitation in the research was the use of generalized data obtained from Landsat 8 satellite images with a cell size of 30x30m. Data regarding Land Surface Temperature (LST) were derived from Landsat 8 satellite images and logarithmic operations using ArcGIS tools (Raster Calculator), noting that these data only correspond to the month of August for the observed years.

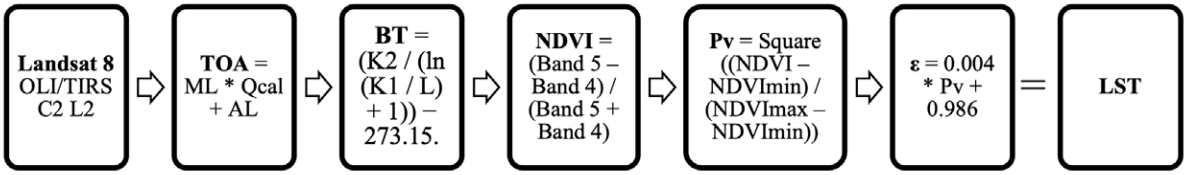

Figure 2. Logarithmic processing of LST data in ArcGIS 10.6 software based on Landsat 8 datasets
Source: Processed by authors, 2023

Results

Landsat 8 OLI/TIRS L2 C2 images were utilized to extract the analyzed parameters in this study. NDVI maps were generated using ArcGIS 10.6.1 software for the years 2013, 2019, and 2023 and are presented in Fig.2. NDVI illustrates significant both temporal and spatial variations between 2013, 2019, and 2023. Green/healthy vegetation absorbs the blue (0.4 - 0.5 μm) and red (0.6 - 0.7 μm) spectra, reflecting the green (0.5 – 0.6 μm) spectrum. Human eyes perceive healthy vegetation as green due to the internal structure of leaves. Healthy plants exhibit high reflectance in the near-infrared radiation (NIR) ranging from 0.7 to 1.3 μm (Fig. 2) (Crippen, 1990). Analyzed statistical parameters (Table 2) demonstrate that the NDVI index mostly varied across the analyzed years. Minimum index values decreased, while maximum values increased. In August 2013, the maximum index value was approximately 0.6, indicating dense vegetation cover, especially in the surrounding mountainous areas. The maximum index value in August 2019 was around 0.7, and in 2023, it increased by 0.01, suggesting a reduced proportion of vegetation cover in favor of built-up areas. NDVI exhibits pronounced annual changes dependent on surface layer temperatures. As expected, a positive correlational relationship (p=0.84) between the NDVI index and LST was confirmed. Statistical analysis of the Pearson linear correlation coefficient affirmed that this correlation (NDVI-LST) lacks statistical significance. In general, changes in surface layer temperatures imply greater plant growth and vice versa. The pronounced annual change in this index is characteristic of densely populated basin centers. Areas with dense vegetation, tending towards positive index values, are mainly at higher altitudes, on the slopes of surrounding mountains and hills (Bjelašnica, Igman, Trebević, Hum, Zuč), which are not under significant anthropogenic pressure. Conversely, areas with negative index values indicate the degree of anthropogenic pressure in the central part of the basin.

To confirm the variations in the indices, an analysis of the NDBI index was conducted for the purposes of this article. The obtained values of the NDBI index, which correlate with the NDVI index (Fig. 2 and 3), confirm a high degree of ur-

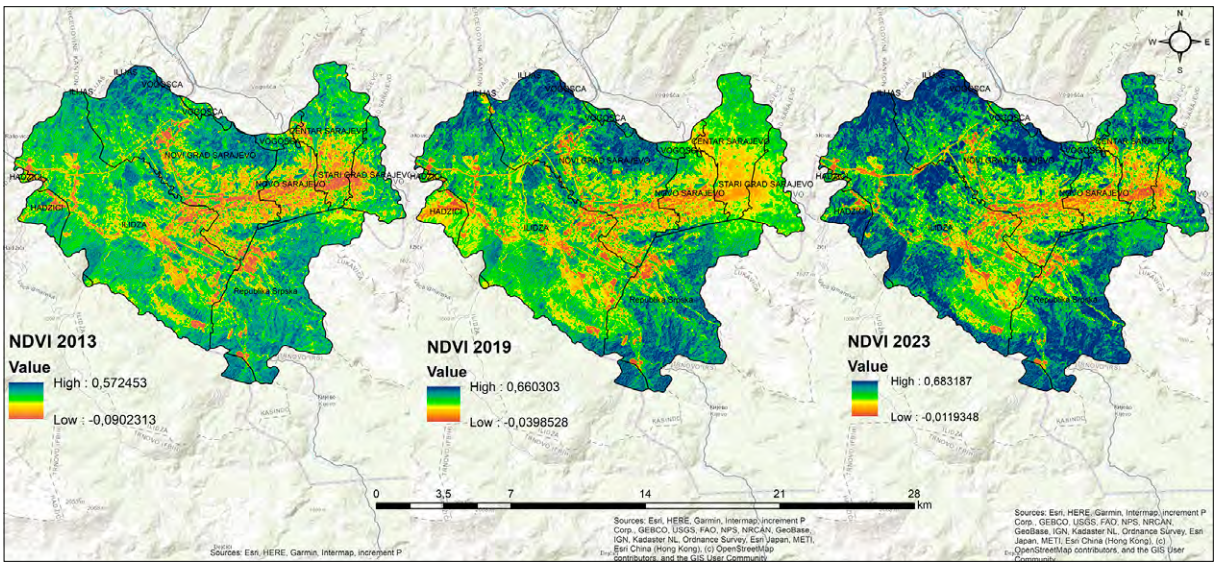

Figure 3. NDVI values for 2013, 2019 and 2023
Source: Geo-database of GIS Center of Department of Geography, University of Sarajevo – Faculty of Science adapted by the authors using ArcGIS [GIS software] Version 10.6.1. and Landsat 8 OLI/TIRS L2 C2 images

Table 2. Statistical Data for NDVI Index by Year

Year	Minimum	Maximum	Mean	Standard Deviation
2013	-0,012	0,683	0,305	0,099
2019	-0,040	0,660	0,320	0,103
2023	-0,090	0,573	0,334	0,099

Source: Processed by the authors using data from ArcGIS geo-database of GIS Center of Department of Geography, University of Sarajevo – Faculty of Science, 2023

banization in the central part of the Sarajevo basin. Positive values of the NDBI index are concentrated in the central part of the basin, which is highly urbanized, while negative values are observed in its peripheral areas, where dense vegetation predominates, in contrast to the NDVI index. This indicates a negative statistical correlation between the analyzed indices. Urbanization in the Sarajevo basin mostly occurs without proper planning. Thousands of structures have been informally built on the slopes surrounding central Sarajevo (Aquilué & Roca, 2016). The response of cantonal authorities to informal construction and the development of numerous settlements resulted in processes of legalizing informally constructed structures. Despite efforts to implement regulatory plans and provide standard infrastructure for all informally built structures, legalization had limited effectiveness (Martín-Díaz et al., 2018). These settlements remained in the realm of "gray areas," even though they eventually moved away from informality (Legrand, 2013).

In line with this, construction intensified in the peripheral southeastern parts of the Sarajevo basin, and significant changes during the analyzed years were experienced by the settlements of Hrasnica, Ilidža, and Istočno Sarajevo (Drešković & Osmanović, 2024). Over the ten-year analyzed period, the percentage of built-up areas increased. Based on the analysis of Corine Land Cover (CLC) images, data indicate that artificial surfaces covered nearly 29% of the total territory in 2012, and by 2018, their percentage had increased by 10% (Drešković & Osmanović, 2024). This increase was caused by the physical-geographical constraints of settlements, infrastructure, and human activities in a very confined space—basin expansions along watercourses (Hrelja et al., 2021). Urbanization, in this sense, harmed dense vegetation in the peripheral parts of the basin due to land conversion, primarily clearing for various commercial purposes. The percentage of built-up areas increased by approximately 10% in the mentioned six-year period, precisely reducing dense vegetation in favor of construction areas, reflecting progressive urban development and, in certain areas of the basin, unplanned construction.

Table 3. Statistical Data of NDBI Index by Years

Year	Minimum	Maximum	Mean	Standard Deviation
2013	-0,318	0,319	-0,140	0,076
2019	-0,039	0,352	-0,023	0,073
2023	-0,320	0,453	-0,099	0,083

Source: Processed by the authors using data from the ArcGIS geo-database of GIS Center of Department of Geography, University of Sarajevo – Faculty of Science, 2023

The surface temperature of built-up layers (LST) was also analyzed to obtain data on areas with the highest heating intensity. The data obtained on the temperature of surface layers indicate the formation of heat islands (UHI) in one of the summer months - August. On the observed

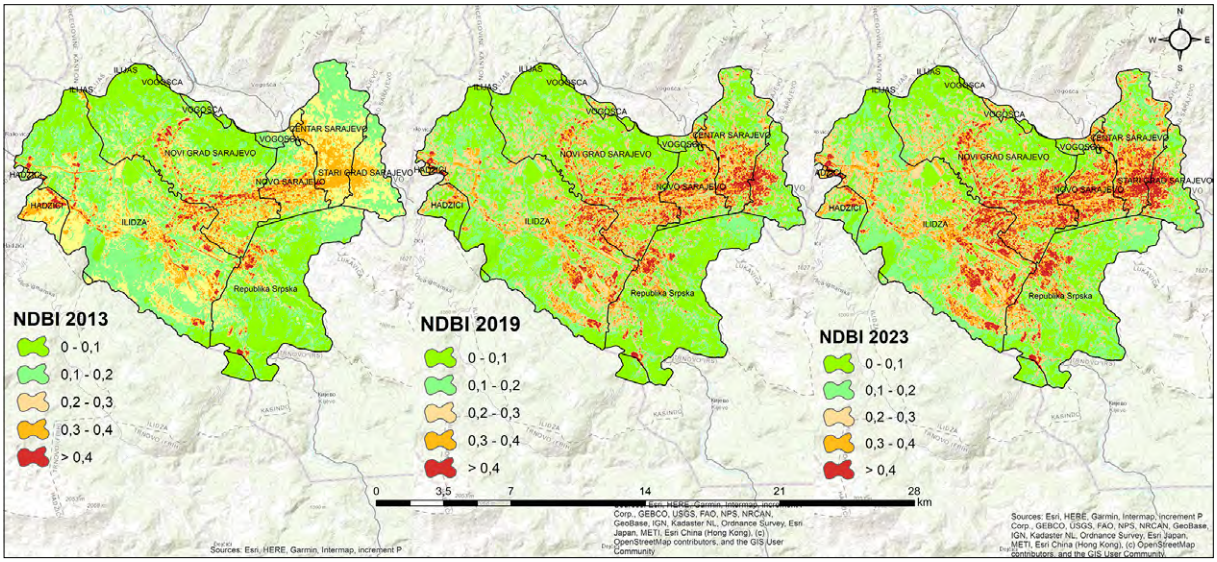

Figure 4. NDBI index for 2013., 2019. and 2023.
Source: Geo-database of GIS Center of Department of Geography, University of Sarajevo – Faculty of Science adapted by the authors using ArcGIS [GIS software] Version 10.6.1. and Landsat 8 OLI/TIRS L2 C2 images

day in August 2013, the average daily air temperature was around 34°C, while in 2023, it was 35.2°C. Correlated with the average daily air temperatures is the emission from asphalted, dark surfaces that heat up more intensely compared to the air. Sarajevo is highly urbanized, with large areas covered in concrete, contributing to the creation of a specific microclimate within certain locations, particularly during the summer months (Fig. 5). It is recommended to mitigate UHI effects in the Sarajevo basin by implementing cool roofs and increasing urban greenery.

The highest degree of surface heating is observed in the old part of Sarajevo, as well as in certain areas of the municipalities of Centar, Novi Grad Sarajevo, Ilidža, Vogošća, and Istočno Sarajevo. These areas, due to unplanned construc-

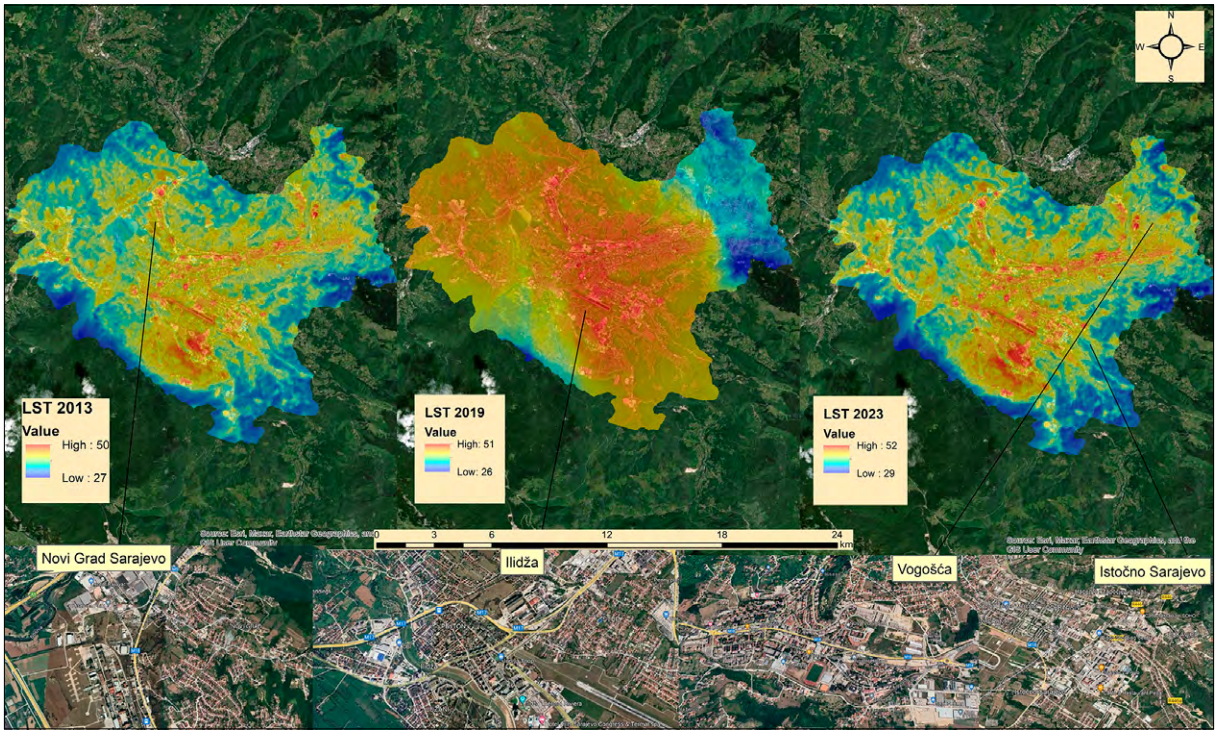

Figure 5. LST in Sarajevo basin in 2013., 2019. and 2023.
Source: Geo-database of GIS Center of Department of Geography, University of Sarajevo – Faculty of Science adapted by the authors using ArcGIS [GIS software] Version 10.6.1. and Landsat 8 OLI/TIRS L2 C2 images

tion and materials used, are predisposed to the formation of urban heat islands (UHI). Extremely high surface layer temperatures in the Sarajevo basin in August during the ten analyzed years (max. 52°C) indicate the predominant spatial representation of concrete and asphalt surfaces that heat up intensively during the summer months, reaching temperatures up to 30°C higher than the surrounding hilly and mountainous areas rich in dense vegetation, which in this case act as cooler air oases. It is essential to note that these areas are mainly residential centers, as well as industrial and commercial areas, predominantly built with materials that have a higher degree of heating and emissions, with sheet metal roofs that intensify heating during the summer months. Mulahusić et al. (2018) found that surface temperatures in 2015 correlated with areas with the highest population density and building density. The images were captured during the hottest summer month because surface heating is most intense during that period, and temperatures remain high for an extended duration. Landsat 8 satellite captures the surface around 10 a.m. local time and only exceptionally at night. Therefore, monitoring urban heat islands during the most intense heat period or analyzing the cooling degree between built-up and non-built-up areas during the night was impossible.

Discussion

Methodology aspect

The widely used methodology has proven successful in identifying the Urban Heat Island (UHI) effect, as numerous studies have established a correlative relationship between NDVI, NDBI, and LST, confirming their significance in monitoring changes and biophysical characteristics of plant communities, as well as the reduction of vegetative cover in favor of built-up areas (Bechtel et al., 2012; Chen et al., 2014; Geletič et al., 2016; Macarof & Statescu, 2017; Guha et al., 2017). Remote sensing products have found broad application in almost all scientific fields and are a good foundation for future studies of these phenomena in the Sarajevo basin, given the limited number of studies on this topic (Mulahusić et al., 2018; Drašković et al., 2020). Typically, only LST has been analyzed as the basic indicator of the spatial distribution of UHI. This study confirms that the degree of urbanization is highest in the city of Sarajevo (municipalities of Stari Grad, Centar, Novo Sarajevo, and Novi Grad), i.e., in the central parts of the basin predisposed to UHI formation due to physical-geographical characteristics and anthropogenic changes. An enhancement of this study could be achieved by investigating the spatial representation and distribution of green areas in the central parts of the basin. The minimum area of urban greenery per capita should be 9 m^2, and the ideal 50 m^2 (World Health Organization, 2012). The number of inhabitants in the Sarajevo Basin according to the last population census from 2013 was 354.030, which means that there should be a minimum of 3.186.000 m^2 of urban greenery in the analyzed area, or 318.6 ha. Of the total area of the city (municipalities of Stari Grad, Centar, Novo Sarajevo, and Novi Grad Sarajevo), which is 14.150 ha, about 25% should be covered by urban greenery, but the Sarajevo basin is far below the average because currently only Veliki Park has an area of about 3 ha and approximately corresponds to the stated criteria. In other areas, green areas were repurposed. This allows urban planners to identify areas with spatial potential for planting trees, which are the best heat absorber (Yaşlı et al., 2023), and find solutions for the future spatial expansion of the basin. A more precise picture could be achieved by selecting and examining specific profiles in different seasons in both central and peripheral parts of the basin to determine temperature differences in micro-locations. Surface temperatures provide important information about the thermal behavior of the annual temperature cycle from thermal infrared images with an accuracy of about 1K. For this reason, urban thermal areas are described by multi-temporal thermal cycles (Bechtel, 2012). A methodological improvement would involve analyzing ASTER satellite images of different spatial resolutions to identify zones with the UHI effect confidently.

Validity of results

One of the main drawbacks is the temporal coverage of Landsat 8 TIRS/OLI L2 C2 satellite images. Landsat 8 captures Earth's surface at 10 AM local solar time, making it impossible to investigate the Urban Heat Island (UHI) effect during the period of most intense surface heating or to determine nighttime temperature differences between built-up and non-built-up areas. This limitation prevents a fully consistent or accurate representation of the actual situation. Satellite image data are processed and validated in ArcGIS software (Imbroane et al., 2014; Gémes et al., 2016) to obtain a more precise depiction of the current state. As remote sensing products are widely applied across scientific disciplines, there is an essential need for an interdisciplinary approach, combining multiple satellite images to detect changes at the local level. Various qualitative approaches, such as Thematic Mapper, Enhanced Thematic Mapper, or Operational Land Imager, could reveal UHI behavior in different parts of the city and establish the interconnection between land cover and surface temperatures in urban and suburban areas. This would provide crucial insights for a more in-depth understanding of the causes and patterns of UHI, as well as in formulating local policies and spatial planning documents.

Conclusion

This study was based on the utilization and processing of multispectral remote sensing products to determine the dynamics of the spatial distribution of NDVI and NDBI indices, as well as their associated Land Surface Temperature (LST) in the urban area of Sarajevo, specifically the Sarajevo basin, during three specific observed years: 2013, 2019, and 2023. The results from the first set of Landsat 8 images indicated significant changes in this area, particularly concerning the NDVI index, whose values varied in August of 2013, 2019, and the same month in 2023. While the urban center itself displayed the highest values across all analyzed parameters, it is notable that even the peripheral parts of the basin experienced significant changes, notably in the clearance of forest communities for land reclamation purposes. Results from the second set of Landsat 8 images confirmed a correlational link between the NDVI and NDBI indices. Specifically, highly urbanized and densely populated areas exhibited predominantly positive NDBI values (up to 1), while areas with various types of vegetation communities and water bodies tended toward negative values. Due to its orographic and topographic position, Sarajevo has historically been densely populated, with intensified urbanization during the post-war period of urban renewal. Novi Grad Sarajevo municipality ranks second in population density in the entire country. Multispectral Landsat 8 imagery and remote sensing, in general, have proven highly effective in studying urban agglomerations and the changes occurring within them. The crucial input parameter for identifying and analyzing urban heat islands in the Sarajevo basin was the data on Land Surface Temperature (LST), specifically the temperature of surface layers in August for 2013, 2019, and 2023. This analysis revealed temperature variations, with extreme values in 2023 representing the highest and lowest values over the analyzed period, attributed partly to increasingly pronounced global climate changes. In the future, more attention should be directed toward urban change patterns, especially urban ecology, through analyzing and comparing satellite imagery from various sources. Such spatial information is invaluable for decision-makers and urban planners to develop appropriate urban and regulatory plans, ensuring sustainable urban expansion.

References

Alademomi, A.S., Okolie, C.J., Daramola, O.E., Akinnusi, S.A., Adediran, E., Olanrewaju, H.O., Alabi, A.O., Salami, T.J. & Odumosu, J. (2022). The interrelationship between LST, NDVI, NDBI, and land cover change in a section of Lagos metropolis, Nigeria. *Applied Geomatics*, 14, 299-314.

Amiri, R., Weng, Q., Alimohammadi, A. & Kazem Alavipanah, S. (2009). Spatial–temporal dynamics of land surface temperature in relation to fractional vegetation cover and land use/cover in the Tabriz urban area, Iran. *Remote Sensing of Environment*, 113(12), 2606-2617. doi: https://doi.org/10.1016/j.rse.2009.07.021

Aquilué, I. & Roca, E. (2016). Urban development after the Bosnian War: The division of Sarajevo's territory and the construction of East Sarajevo. *Cities*, 58, 152-163. doi: https://doi.org/10.1016/j.cities.2016.05.008

Bechtel, B., Zakšek, K. & Hoshyaripour, G. (2012). Downscaling Land Surface Temperature in an Urban Area: A Case Study for Hamburg, Germany. *Remote Sensing*, 4(10), 3184-3200. doi: https://doi.org/10.3390/rs4103184

Bhandari, A.K., Kumar, A. & Singh, G.K. (2012). Feature Extraction using Normalized Difference Vegetation Index (NDVI): A Case Study of Jabalpur City. *Procedia Technology*, 6, 612-621.

Chen, A., Yao, L., Sun, R. & Chen, L. (2014). How many metrics are required to identify the effects of the landscape pattern on land surface temperature? *Ecological Indicators*, 45, 424-433. doi: https://doi.org/10.1016/j.ecolind.2014.05.002

Copernicus Global Land Service (2023). https://land.copernicus.eu/global/index.html (20.09.2023)

Crippen, R.E. (1990). Calculating the vegetation index faster. *Remote sensing of Enviroment*, 34, 71-73.

Cvitanović, M. (2014). Promjene zemljišnog pokrova i načina korištenja zemljišta u Krapinsko-zagorskoj županiji od 1991 do 2011. *Hrvatski geografski glasnik*, 76/1, 41-59.

Değerli, B. Ç. & Çetin, M. (2022). Evaluation from Rural to Urban Scale for the Effect of NDVI-NDBI Indices on Land Surface Temperature, in Samsun, Türkiye. *Turkish Journal of Agriculture -Food Science and Technology*, 10(12), 2446-2452. doi: https://doi.org/10.24925/turjaf.v10i12.2446-2452.5535

Drašković, B., Miletić, B. & Gutalj, M. (2020). Analysis of Land Surface Temperature at Sarajevo Canton using Landsat 8 data, GEA (Geo Eco-Eco Agro) International Conference (2020), *Book of Proceedings II* (pp. 24-35), Montenegro.

Drešković, N. & Osmanović, M. (2024). Changes in land use/land cover in the Sarajevo valley from 2000 to 2018 – CLC based analysis. *Geographical Review*, 49, 31-44.

Fabrizi, R., Bonafoni, S. & Biondi, R. (2010). Satellite and ground-based sensors for the Urban Heat Island analysis in the city of Rome. *Remote Sensing*, 2(5), 1400–1415. doi: https://doi.org/10.3390/rs2051400

Geletič, J., Lehnert, M. & Dobrovolný, P. (2016). Land Surface Temperature Differences within Local Climate Zones, Based on Two Central European Cities. *Remote Sensing*, 8(10), 788. doi: https://doi.org/10.3390/rs8100788

Gémes, O., Tobak, Z. & Van Leeuwen, B. (2016). Satellite Based Analysis of Surface Urban Heat Island Intensity. *Journal of Environmental Geography*, 9(1–2), 23–30. doi: 10.1515/jengeo-2016-0004

Guha, S., Govil, H. & Mukherjee, S. (2017). Dynamic analysis and ecological evaluation of urban heat islands in Raipur city, India. *Journal of Applied Remote Sensing*, 11(3). doi: https://doi.org/10.1117/1.JRS.11.036020

Hadžić, E. & Drešković, N. (2014). Analysis of the impact of temperature and precipitation fluctuations on river flow in the Sarajevo valley. *Vodoprivreda*, 46, 65–75.

Hadžić, E., Lazović, N. & Mulaomerović-Šeta, A. (2015). The Importance of Groundwater Vulnerability Maps in the Protection of Groundwater Sources. Key Study: Sarajevsko Polje. *Procedia Environmental Sciences*, 25, 104-111.

Hafner, J. & Kidder, S.Q. (1999). Urban Heat Island Modeling in Conjunction with Satellite-Derived Surface/Soil Parameters. *Journal of Applied Meteorology and Climatology*, 38(4), 448–465. doi: https://doi.org/10.1175/1520-0450(1999)038<0448:UHIMIC>2.0.CO;2

Haji, G.Y., Hasan, S.K. & Hussein, L.T. (2023). Relationship of LST, NDVI, and NDBI using Landsat-8 data in Duhok city in 2019-2022. *Journal of Planner and development*, 28(1).

Heaviside, C., Macintyre, H. & Vardoulakis, S. (2017). The Urban Heat Island: Implications for Health in a Changing Environment. *Current Environmental Health Reports*, 4, 296–305.

Howard, L. (1833). The Climate of London. *Deduced from Meteorological Observations*. Volume 2.

Hrelja, E., Sivac, A., Korjenić, A. & Banda, A. (2021). Spatial Planning of the Green Infrastructure of the City of Sarajevo. International Conference Making Healthy Cities for People - Education, Research, Practice in Planning, Architecture and Engineering – HURBE, *Conference Proceeding* (pp.37-47), Sarajevo, Bosnia and Herzegovina.

Imbroane, A., Croitoru, A.E., Herbel, I., Rus, I. & Petrea, D. (2014). Urban heat island detection by integrating satellite image data and GIS techniques. Case study: ClujNapoca city, Romania. 14th International Multidisciplinary Scientific GeoConference SGEM, *Book 1* (pp.359-366), Albena, Bulgaria.

Jackson, R.D., Idso, S.B., Reginato, R.J. & Pinter P.J. (1981). Canopy temperature as a crop water stress indicator. *Water Resource Research*, 17(4).

Johnson, G. T., Oke, T. R., Lyons, T. J., Steyn, D. G. & Watson, I. D. (1991). Simulation of Surface Urban Heat Islands Under "Ideal" Conditions at Night Part. 1: Theory and Tests against Field Data. *Boundary-Layer Meteorology*, 56, 275-294.

Kim, H. H. (1992). Urban heat island. *International Journal of Remote Sensing*, 13(12), 2319-2336. doi: https://doi.org/10.1080/01431169208904271

Lambin, E.F., Rounsevell, M.D.A. & Geist, H.J. (2000). Are agricultural land-use models able to predict changes in land-use intensity? *Agriculture, Ecosystems & Environment* 82(1-3), 321-331.

Legrand, O. (2013). Sovereignty, Planning and Gray Space: Illegal construction in Sarajevo, Nicosia and Jerusalem. *Planum The Journal of Urbansim*, 1(23).

Le-Xiang, Q., Hai-Shan, C. & Jie, C. (2006). Impacts of Land Use and Cover Change on Land Surface Temperature in the Zhujiang Delta. *Pedosphere*, 16(3), 681-689. https://doi.org/10.1016/S1002-0160(06)60103-3

Macarof, M. & Statescu, F. (2017). Comparasion of NBI and NDVI as indicators of surface Urban heat island effect in Landsat 8 imagery: a case study of Iasi. *Present Environment and Sustainable Development*, 11(2).

Manley, G. (1958). On the Frequency of Snowfall in Metropolitan England. *Quarterly Journal of the Royal Meteorological Society*, 84, 70-72. doi: https://doi.org/10.1002/qj.49708435910

Martín-Díaz, J., Palma, P., Golijanin, J., Nofre, J., Oliva, M. & Čengić, N. (2018). The urbanisation on the slopes of SARAJEVO and the rise of geomorphological hazards during the post-war period. *Cities*, 72, 60-69. doi: https://doi.org/10.1016/j.cities.2017.07.004

Mulahusić, A., Tuno, N., Topoljak, J., Kolić, T. & Kogoj, D. (2018). Satellite thermography of Sarajevo. *Geodetski vestnik*, 62(2), 173-187. doi: 10.15292//geodetski-vestnik.2018.02.

Myrup, O.L. (1969). A Numerical Model of the Urban Heat Island. *Journal of Applied Meteorology and Climatology*, 8(6), 908–918. https://doi.org/10.1175/1520-0450(1969)008<0908:ANMOTU>2.0.CO;2

Naserikia, M., Shamsabadi, E.A., Rafieian, M. & Filho, W.L. (2019). The Urban Heat Island in an Urban Context: A Case Study of Mashhad, Iran. *International Journal Environmental Research and Public Health*, 16(3), 313. doi: https://doi.org/10.3390/ijerph16030313

Niclòs, R., Valiente, J.A, Barbera, M.J., Estrela, M.J., Galve, J.M. & Caselles, V. (2009). Preliminary Results on the Retrieval of Land Surface Temperature from MSG-SEVIRI Data in Eastern Spain. *Proceedings for the 2018 EUMETSAT Meteorological Satellite Conference*. Tallinn, Estonia.

Oke, T. R., Johnson, G. T., Steyn, D. G. & Watson, I. D. (1991). Simulation of Surface Urban Heat Islands under "Ideal" Conditions at Night Part 2: Diagnosis of Causation. *Boundary-Layer Meteorology*, 56, 339-358.

Prata, A.J., Caselles, V., Coll, C., Sobrino, J.A. & Ottle, C. (1995). Thermal remote sensing of land surface temper-

ature from satellites: current status and future prospects. *Remote Sensing Reviews*, 12(3-4).

Roth, M. (2013). Urban Heat Islands. *Handbook of Environmental Fluid Dynamics*, 2, 143-159. doi: 10.1201/b13691-13

Sherafati, S., Saradjian, M.R. & Rabbani, A. (2018). Assessment of Surface Urban Heat Island in Three Cities Surrounded by Different Types of Land-Cover Using Satellite Images. *Journal of the Indian Society of Remote Sensing*, 46, 1013-1022.

Solecki, W.D., C. Rosenzweig, L. Parshall, G. Pope, M. Clark, J. Cox & Wiencke, M. (2005). Mitigation of the heat island effect in urban New Jersey. *Global Environment Change*, 6, 30-49, doi:10.1016/j.hazards.2004.12.002

Song, B. & Park, K. (2014). Validation of ASTER Surface Temperature Data with In Situ Measurements to Evaluate Heat Islands in Complex Urban Areas. *Advances in Meteorology*, 2014, doi: http://dx.doi.org/10.1155/2014/620410

Srivanit, M. & Hokao, K. (2012). Thermal infrared remote sensing for urban and environmental studies: An application for the city of Bangkok, Thailand. *Journal of Architectural / Planning Research and Studies*, 9(1), 83–100.

Sun, D. & Pinker, R.T. (2003). Estimation of land surface temperature from a Geostationary Operational Environmental Satellite (GOES-8). *Journal of Geophysical Research*, 108(D11), doi:10.1029/2002JD002422.

Voogt, J.A. & Oke, T.R. (2003). Thermal Remote Sensing of Urban Climates. *Remote Sensing of Environment*, 86, 370-384. doi: https://doi.org/10.1016/S0034-4257(03)00079-8

Wang, M. (2015). *Characterization of Surface Urban Heat Island in the Greater Toronto Area Using Thermal Infrared Satellite Imagery.* Master thesis, University of Waterloo, Kanada.

World Health Organisation (2012). Health Indicators of sustainable cities in the Context of the Rio+20 UN Conference on Sustainable Development, available at: https://www.who.int/docs/default-source/environment-climate-change-and-health/sustainable-development-indicator-cities.pdf?sfvrsn=c005156b_2, November 10, 2023.

Yao, X., Yu, K., Zeng, X., Lin, Y., Ye, B., Shen, X., & Liu, J. (2022). How can urban parks be planned to mitigate urban heat island effect in "Furnace cities" ? An accumulation perspective. *Journal of Cleaner Production*, 330. doi: https://doi.org/10.1016/j.jclepro.2021.129852

Yasli, R., Yucedag, C., Ayan, S. & Simovski, B. (2023). The Role of Urban Trees in Reducing Land Surface Temperature. *SilvaWorld*, 2(1), 36–49. doi: https://doi.org/10.29329/silva.2023.518.05

Zha, Y., Gao, J. & Ni, S. (2003). Use of normalized difference built-up index in automatically mapping urban areas from TM imagery. *International Journal of Remote Sensing*, 24(3), 583-594.

URL 1: United States Geological Survey, https://earthexplorer.usgs.gov/, October 09, 2023

URL 2: NASA Landsat Science, https://landsat.gsfc.nasa.gov/, November 23, 2023

INTERNATIONAL SCIENTIFIC JOURNAL
GEOGRAPHICA PANNONICA
Volume 28, Issue 1, 44–52 (March 2024)
Contents lists available at ScienceDirect
Journal homepage: http://www.dgt.uns.ac.rs/en/homepage/pannonica/

Which Psychological Characteristics Make a Good Geography Teacher in High School?

Tamara Jovanović[A], Katarina Otašević[A], Ljubica Ivanović Bibić[A], Jelena Milanković Jovanov[A], Anđelija Ivkov Džigurski[A], Aleksandra Dragin[A,B], Smiljana Đukičin Vučković[A*], Stefan Stajić[A], Aco Lukić[A,C], Lazar Kotorčević[A]

[A] *University of Novi Sad, Faculty of Sciences, Department of Geography, Tourism and Hotel Management, Trg Dositeja Obradovića 3, 21000 Novi Sad, Serbia; katarinaotasevic@yahoo.com; tamara.jovanovic@dgt.uns.ac.rs; ljubica.ivanovic@dgt.uns.ac.rs; jelenamj@dgt.uns.ac.rs; andjelija.ivkov@dgt.uns.ac.rs; aleksandra.dragin@dgt.uns.ac.rs; smiljana.djukicin@dgt.uns.ac.rs; stefan.staic@dgt.uns.ac.rs; acolukic994@gmail.com; lazar0711@gmail.com*

[B] *University of Jaen, Faculty of Law and Social Sciences, Department of Business Organization, Marketing and Sociology and School of Engineering of Jaen, Campus Las Lagunillas, 23071 Jaén, Spain*

[C] *University of J.E. Purkyne, Faculty of Education, Department of Preschool and Primary Education, České mládeže 8, 40001 Usti nad Labem, Czech Republic*

KEYWORDS

geography teaching
teacher's personality
Big Five model
good teacher myths
pupil's perception

ABSTRACT

This study seeks to examine what traits, "myths" and skills pupils will attribute to good geography teachers, and whether their assessments are influenced by gender, age, grade and satisfaction with a teacher. The sample consists of 150 high school pupils in Serbia. The survey consisted of four parts: socio-demographic characteristics, Big Five Inventory, good teacher myths, and good geography teacher skills. The results showed that pupils believe that good geography teachers have to be impartial, friendly and conscientious in the first place. Also, 13 high school teachers were also interviewed. The data are somewhat in line with previous research, but also indicate pupils' specific expectations of their geography teachers and teachers' awareness that they are not just ordinary teachers.

Introduction

Statement of the Problem

Psychological traits of teachers as well as what makes a good teacher represent topics that have been present for a long time among researchers (Genc et al., 2014; Gordon, 2008; Lamke, 1951; Li & Wu, 2011; Radulović et al., 2019; Ryans, 1960; Sakač & Marić, 2018). The students', the parents', the teachers', the teacher students' or the school principals' beliefs are different concerning what makes a good teacher (Arnon & Reichel, 2007; Bullock, 2015, Zagyvane Szucs, 2017;). A teacher's personality is generally claimed to be crucial and the question that is often posed says: "What are desirable traits that a good teacher should possess?" (Grgin, 1997; Korthagen, 2004; Stanojević, 2009). It is desirable for teachers to be emotionally stable, kind and patient in their work, to be cooperative, impartial and democratic (Stojiljković, 2014). Ryans (1960) claims that crucial dimensions of a teacher's personality are warmth, understanding, responsibility, businesslike manner (efficiency), stimulatory behaviour, and enthusiasm. Good teachers are enthusiastic, friendly, easy-going, able to develop rapport with learners, committed to the growth of their students, approachable, interested in learners as people,

* Corresponding author: Smiljana Đukičin Vučković, email: smiljana.djukicin@dgt.uns.ac.rs

doi: 10.5937/gp28-47894

Received: October 28, 2023 | Revised: March 15, 2024 | Accepted: March 15, 2024

and always conscious of their status as role models (Guskey, 2002; Samy, 2005).

If teachers are surveyed, researchers generally observe predictive value of measured personality traits on the professional success of surveyed teachers Comparing successful and unsuccessful beginning teachers in 16 dimensions of Cattell's theory (Cattell & Mead, 2008), Lamke (1951) found that teachers who scored highly in the dimensions F and H (which describe open, friendly, approachable, lively, talkative, cheerful, calm but also socially bold personalities), achieved above-average results. The research conducted by Li and Wu (2011) on 340 university teachers showed no differences between good and bad teacher.

In their research, Genc and his associates (Genc et al., 2014) used the Big Five Model for measuring teachers' personality traits. Their sample were students (N = 443) of the Faculty of Philosophy, Faculty of Sciences and the Academy of Arts, from the University of Novi Sad. First, they estimated their own personalities and then they estimated what are desirable qualities of an university teacher, that is they put themselves in the position of a good teacher and assessed what is, in their opinion, a good university teacher. The results indicate that good teachers are expected to have higher than average scores in all qualities, that is they are expected to be primarily more extraverted, more conscientious, more open to experience, more pleasant and emotionally stable (Genc et al., 2014). The results showed statistically significant gender differences on the scales of agreeableness and extraversion (Genc et al., 2014). It is obvious that female students expect higher agreeableness and extraversion from good university teachers, and the same tendency holds true for openness to experience. In Arnon's and Reichel's study (Arnon & Reichel, 2007), students of education (who work as educators or only study) assessed what is an ideal teacher for them and how they see themselves as future teachers. The results indicate that there are two main categories that shape the image of an ideal teacher – personal traits and the knowledge of the subject they teach. Personal traits of an ideal teacher are sense of humour, kind-heartedness, calmness, fairness, openness, sensitivity towards children, self-discipline, authority, motivation and attentiveness (Arnon & Reichel, 2007). The study of Pavlović and Tošić-Rudić (2009) on primary school pupils, showed that desirable qualities are sense of humour, understanding of pupils, patient explaining and tolerance (Pavlović & Tošić-Rudić, 2009). Undesirable traits that pupils named are strictness, arrogance, excessive seriousness and boringness in giving lectures. There were no age differences, but girls highlighted the importance of fairness while boys gave priority to sense of humour and encouragement.

This research is inspired by the study of Genc and his associates (Genc et al., 2014), except that the focus is on secondary school pupils and a specific profile of a geography teacher. As Genc and colleagues (2014), we also used the BFI (Big Five Inventory – the Big Five model) (Goldberg, 1993; John & Srivastava, 1999). Teaching geography is rather specific because of its task to create a clear picture in students' mind of a place they live in and of the rest of the world as well. Geography also serves to introduce pupils to natural beauties, landscape differences and to develop pupil's criticalness toward economic, social and political issues in the world. Lastly, geography is largely a multidisciplinary science that partially relies on natural sciences (e.g. geology, climatology, hydrology) and partially on social sciences (e.g. population geography, economic geography, settlement geography). Because of all that, it is very important for geography teachers to be objective, creative, innovative and open to new experiences and knowledge (Romelić & Ivanović Bibić, 2015). The field that a teacher teaches largely determines what characteristics that teacher should possess. Characteristics of, for example, a good music teacher (Bogunović, 2006) and a good natural science teacher (Druva & Anderson, 1983) may differ significantly. Therefore, it is assumed that there is a need to examine what teachers' traits from the aspect of separate disciplines are desirable for the main users of their services – students and that examination would provide a profile that is specific for a given field. Besides personality, this study also examined students' attitudes about good geography teachers.

Problem and purpose of the Study

The research included eight ideal conceptions of a good teacher that Thomas Gordon mentioned in his book *Teacher Effectiveness Training* (Gordon, 2008). These ideal conceptions are interesting because they vividly depict high expectations that are set for teachers by students or by teachers themselves. We also used three claims that represent skills that a geography teacher cannot do his job without – using modern technology, environmental awareness and following modern trends in geography. The aim of this research was to determine what traits, "myths/ideal conceptions of good teachers" and skills students will dominantly ascribe to good geography teachers and whether the emphasizing of all these traits is influenced by students' gender, age, grade in geography and satisfaction with geography classes and geography teachers. Five questions were addressed in the study: 1) Is there a difference between boys and girls in their perception of what constitutes a good geography teacher? 2) Is there an effect of students' age on the perception and attitudes about psychological characteristics of a good geography teacher? 3) Does a student's grade affect their perception of what psychological characteristics should a good geography teacher have? 4) Do students evaluations of the subject affect their responses regarding psychological characteristics of a good geography teacher? 5) What do geography teachers highlight as characteristics of a good geography teacher?

Methodology

Research Sample

150 secondary school pupils were surveyed, the majority of which were from Secondary School of Economics – 90 of them, while the other 60 respondents attended Grammar school and Technical School in Gornji Milanovac, Serbia. Respondents were aged between 15 and 19 (M = 16.5) and were predominantly females (64%). Their average mark in geography was 3.4, and their satisfaction with that subject was 4.1. Thirteen high school geography teachers were interviewed in order to get to know what their beliefs are about good geography teachers.

Instrument and Procedures

For the needs of the study of psychological characteristics of a good geography teacher, respondents responded to surveys anonymously. In the survey, respondents first provided data about their age, gender, mark in geography and the degree to which they are satisfied with the subject (geography). Besides socio-demographic characteristics, the authors also used BFI (Big Five Inventory, John et al.,1991), which measures five personality traits (extraversion, neuroticism, agreeableness, openness to experience and conscientiousness) with 44 items on a 5-point Likert scale. Using Cronbach's alpha, the value obtained for survey reliability was 0.82. The initial question "I see Myself as Someone Who..." was replaced with the question "A good geography teacher should be someone who...". Students also estimated on a 5-point Likert scale 11 statements about what a good geography teacher should be like. The statements were taken from Thomas Gordon's book Teacher Effectiveness Training (Gordon, 2008) and adjusted to geography teaching and they embody ideal conceptions about everything that a good teacher has to know and has to do. In the end, students estimated three chosen skills that a good geography teacher should possess: using modern technology, environmental awareness and following modern trends in geography.

The interview questions for the teachers were designed specifically for the purpose of this research. The interview contained questions closely related to the problem what characteristics make a good geography teacher. In order to investigate the attitudes of teachers pertaining to characteristics of a good geography teacher, the interview mostly contained open-ended questions, where teachers had the opportunity to give longer answers and to explain more precisely their ideas. Four questions were related to the personality traits, skills and abilities of a good geography teacher. Teachers were also asked what are the specificities of geography teachers when compared to the other teachers. Through three items, they estimated their satisfaction and abilities as a teacher on the 5-point Likert scale.

Research Methods

The data was collected during regular geography classes and the survey was anonymous and voluntary. Before the researchers handed out questionnaires to students, they gave them all necessary instructions and advice so that they could fill out the questionnaire well and to minimise possible mistakes and misunderstandings. As for geography teachers, they were interviewed online through open-ended questions and were informed that their participation was voluntary and anonymous.

Research results and analysis

The analysis was carried out using the programme for statistical data analysis – SPSS 17.0 (Statistical Package for Social Sciences). Table 1 represents average students' answers to questions about psychological characteristics that a good teacher should possess.

On the basis of the obtained results, we can conclude that for students it is the most important that teachers treat them equally, that is to say that they don't single out favourites or teacher's pets, and then, that they don't treat them unequally because of prejudices, gender differences, or differences in achieved grades. Answers like these are understandable since such teachers' behaviour undoubtedly affects overall classroom climate and overall relationships among pupils. Pupils also emphasised *agreeableness* and cooperativeness as the most important characteristics, which indicates that it is very important to pupils that teachers are attentive, humble, sensitive and open to any kind of cooperation. On the other hand, pupils believe that a teacher doesn't necessarily have to be in united front with other teachers regardless of personal feelings, values and preconceptions. A teacher should cooperate with pupils and openly solve all problems they face instead of separating himself by forming "fronts" with other teachers. Logically, pupils negatively estimated the group of personal traits that depicts *neuroticism*, which shows that pupils believe a good teacher should not be nervous, insecure, sad nor depressed.

Table 2 shows the influence of pupils' gender to their attitudes about psychological characteristics of "a good teacher". On the basis of the results from the table 2 we conclude that boys' answers and girls' answers differ on almost every variable. It is interesting that girls generally had greater arithmetic means (except for *neuroticism* for which the differences were not statistically significant),

Table 1. Average values and standard deviations for all questionnaire items (statements – S and five BFI dimensions)

Items	Arithmetic mean	Standard deviation
S1: Doesn't have favourites nor teacher's pets.	4.53	.880
S2: Doesn't have preconceptions nor prejudices.	4.39	1.067
S3: Provides pleasant work environment.	4.36	.943
S4: Good spatial orientation, skilfulness in using geographic maps and other modern technologies.	4.28	.935
S5: Does not express strong feelings (composed)	4.14	1.017
S6: Has environmental awareness.	4.00	1.030
S7: Keeps abreast with world's geographic current trends.	3.99	1.039
S8: Is consistent, doesn't make mistakes.	3.89	1.031
S9: Hides feelings	3.81	1.097
S10: Is wiser than students	3.79	1.222
S11: Is in united front with other teachers	3.65	1.176
Agreeableness (BFI)	4.15	.701
Conscientiousness (BFI)	4.02	.693
Openness to experience (BFI)	3.84	.529
Extraversion (BFI)	3.83	.559
Neuroticism (BFI)	2.22	.501

that is female pupils gave more significance to all characteristics than the male pupils did.

The correlation between pupils' age and their perceptions of psychological characteristics of a good geography teacher is not statistically significant. That indicates that estimates of what makes a good teacher do not change with age, and that all the researched characteristics were similarly estimated in different forms. Table 3 shows to what degree pupils' answers differ depending on grades they obtained in geography.

On the basis of the results from the Table 3 we conclude that in several cases, there is a significant correlation between grades pupils obtained in geography and their attitudes about characteristics of a good teacher. Pupils who have higher grades think it is less important that good teachers are composed, calm, serene and in a good mood. Likewise, it is less important to them that good teachers are consistent, that they do not make mistakes and that they are superficial. This could be interpreted as a fact that pupils attach the most importance to grades they attained in that teacher's subject, and far less importance to the characteristics of that teacher. This indicates to a certain degree that in our school system still exists the big problem where pupils study solely because of grades and grades are considered to be proper measures of their

Table 2. Significant differences in pupils' answers depending on gender (t-test)

Items	t	p
Doesn't have preconceptions nor prejudices	-2.580	0.011
Doesn't have favourites nor teacher's pets	-2.241	0.027
Provides pleasant work environment	-2.465	0.015
Doesn't show strong feelings (composed)	-2.126	0.035
Consistent, doesn't make mistakes	-2.041	0.043
Is wiser than students	-2.527	0.013
Is in united front with other teachers	-2.240	0.027
Has environmental awareness.	-2.002	0.047
Good spatial orientation, skilfulness in using geographic maps and other modern technologies.	-2.234	0.027
Extraversion	-2.073	0.00
Conscientious	-2.221	0.028

knowledge. Weak significant correlation was also established with the variable extraversion, which means that pupils who have higher grades believe that a good teacher should be sociable, communicative, energetic, optimistic and full of enthusiasm. On the other hand, higher correlation was established with the variable *openness to experience*, which indicates that the higher grades pupils have the more importance they ascribe to teacher's originality, creativity, curiosity and intelligence. It is understandable since pupils who achieve better results are usually more creative, more original and more intelligent than other pupils and for those reasons, it is important to them that teachers possess same those characteristics.

The following table shows the correlation between grades with which pupils assessed their satisfaction with the subject and the given variables.

Table 3. Significant correlations between obtained grade of a pupil and characteristics of a good teacher

Items	Grade	
Doesn't show strong feelings (composed)	r	-.171*
	p	.036
	N	150
Consistent, doesn't make mistakes	r	-.176*
	p	.031
	N	150
Extraversion	r	.172*
	p	.035
	N	150
Openness to experience	r	.244**
	p	.003
	N	150

Looking at Table 4, we can conclude that significant correlations were established for some variables. It is particularly interesting to single out variables that relate to teacher's personal characteristics because that is where we found the strongest correlations between chosen variables. In this case negative correlation was established only with neuroticism, which means that this variable declines with the increase of pupils' satisfaction with the subject.

Table 4. Significant correlations between satisfaction with the subject and characteristics of a good teacher

Items	Satisfaction with the subject	
Doesn't have favourites nor teacher's pets	r	.217**
	p	.008
	N	150
Provides pleasant work environment	r	.227**
	p	.005
	N	150
Wiser than pupils	r	.207*
	p	.011
	N	150
United front with his colleagues	r	.170*
	p	.038
	N	150
Good spatial orientation, skilfulness in using geographic maps and other modern technologies	r	.163*
	p	.046
	N	150
Extraversion	r	.319**
	p	.000
	N	150
Agreeableness	r	.335**
	p	.000
	N	150
Conscientiousness	r	.316**
	p	.000
	N	150
Neuroticism	r	-.422**
	p	.000
	N	150
Openness to experience	r	.403**
	p	.000
	N	150

It should be emphasized that the term "satisfaction with the subject" implies educational content that pupils learn during the school year and the way class teaching is carried out. In that case we could expect high correlation with variables that relate to teachers' skills and abilities. However, we haven't got such results (even though there are significant, but mostly low correlations). This only shows us to what extent teachers' personal characteristics influence pupils' satisfaction with the subject, regardless of the fact that satisfaction should refer to the educational content and teaching methods. It also indicates that students identify teachers' characteristics with subjects they teach and thus they often say that a subject is "good" or "their favourite " if they see their teacher as such.

The interview with the high school geography teachers provided some interesting results. Most of the teachers stated that the main characteristics of a good geography teacher were: excellent professional competences, versatility, tolerance, creativity, patience, determination, empathy. Some of the responses are that high school geography teacher should be adventurous since this trait plays a crucial role in teaching students about places they have never been or about phenomena they have never seen. The respondents provided the authors with a wide variety of answers pertaining to some specific abilities and skills that good geography teacher should possess. Some of the answers were as follows: ability to express geographical content with clarity, good interaction in communication, ability to develop students' skills about applying geographical knowledge in everyday life. Also, they emphasize teachers' skills to develop students' knowledge about modern geographical tools (GPS, GIS), helping students in understanding other cultures, nations and customs and fostering students' habits to learn geography on the field and outside the classroom. When geography teachers were asked to express what distinguished them from other colleagues at school, they stated that they had intimate knowledge of natural and social sciences at the same time. Teachers of other subjects are usually good at natural or social sciences, but geography is an interdisciplinary subject and it requires versatility from the teachers. The possibility of teaching geography outside the classroom and working with students on the field distinguishes geography teacher from others. Having this in mind, it should be stated that most of the respondents don't think that anyone can be a geography teacher. The vast majority of the respondents think that they are good teachers and they are satisfied with their job, which brings them the opportunity to be unique.

Discussion

Considering different theories of personality, it is very difficult to determine what desirable qualities of a geography teacher are. In this case, teachers and pupils of high schools evaluated good geography teachers' characteristics. Because of previous studies, the authors expected that respondents' answers would show that good geography teachers should be, among other things, innovative, creative, objective; that they shouldn't be emotionally unstable and rigid. The authors also wanted to determine if there are significant differences in pupils' answers with respect to gender, age, grade in a given subject and general satisfaction with teaching.

If we observe average scores of *ideal conceptions* and other characteristics of a good teacher, the results show that a good geography teacher above all else, should not treat pupils unequally and should not have prejudices about them. This finding indicates that pupils were the most conscious of this aspect of the pupil-teacher relationship most probably because it is often talked about and possibly because of aversion since such behaviour is often found in practice. There is a multitude of prejudices at schools (racial, sexist, ethnic, class and so on) and they are a big source of conflicts between teachers and pupils as well as between teachers and parents. The fact that pupils put that very characteristic in the first place as important for a good geography teacher is also an indicator that we should put as much effort as possible to get to know mechanisms that cause favouritism and prejudices. Discussing them and educating in them will surely reduce their occurrence in practice. Interestingly, it was not very important to pupils that teachers are a united front, while teachers in their interviews highlighted precisely this facet i.e. team work and cooperation. It seems that pupils are not aware of the significance of cooperation among teachers and of healthy work environment. They emphasize characteristics that relate directly to themselves, that is the way teachers treat them, and what happens "behind the scenes" is irrelevant to them. Even though team work between colleagues is not of great significance to the pupils, it affects the quality of teaching and teachers are aware of this.

As for the three researched skills, pupils emphasize the importance of spatial orientation and as an important aspect of that orientation they emphasise skilfulness in using geographic maps and modern technologies such as GPS. These results are in accordance with the teachers answers and with the other published articles pertaining to using modern technologies in geography. Geography teacher should be ready to teach his students how to use maps or GPS as a tool for orientation (Simon & Budke, 2023). It is a logical finding since it is a crucial skill that differentiates geography teachers from teachers of other fields. Familiarity with modern technology is very important nowadays and is implied for pupils who grow up with it (Olschewski et al., 2023; Wilcke & Budke, 2019). As for the personal traits, it is very important to pupils that geography teachers are attentive, humble, sensitive and open to cooperation and that they are not nervous, insecure, sad or depressed. Since geography teachers teach about other cultures and customs, being openminded and intuitive is crucial. This largely corresponds with findings of previous studies (Arnon & Reichel, 2007; Genc et al., 2014; Stojiljković, 2014). However, it is interesting that pupils give preference to agreeableness and conscientiousness while extraversion is second to last. It seems that it is not so important that geography teachers are talkative and sociable as it is that they are reliable and attentive. The combination of traits might be suitable for teaching geography, where a lot of lessons are shown practically and through student's experience. This was substantiated by teachers in their interviews. If the focus of the study were teaching other subjects, such as languages, that require direct teaching and communication skills, the results would be different. Future research pertaining to this are needed.

This study shows differences in answers of pupils of different *gender*, that is, female pupils have higher arithmetic means for every measured characteristic. The biggest differences were obtained in ideal conceptions of good teachers and skills and in two of five measured personal traits – conscientiousness and extraversion. This also partly corresponds with findings of Genc and his associates (Genc et al., 2014), where it was more important for female pupils that teachers are agreeable, extraverted and open to experience, as well as with findings of Pavlović and Tošić-Rudić (2009), where female pupils claimed that teachers should be fair, and male pupils claimed that teachers should encourage them and have a sense of humour. The information that female pupils in their evaluations generally attached higher value to all characteristics is probably the result of their greater awareness of what makes a good teacher, but it may also mean that they are more demanding and have higher expectations from geography teachers.

Pupils' *age* didn't prove to be an important predictor of differences in the assessment of psychological characteristics of good geography teachers. The study of Pavlović and Tošić-Rudić (2009) showed the same, which means that the assessment of characteristics of good teachers remains stable while pupils mature. However, expansion of the research into primary schools would additionally confirm that statement.

Pupils who receive higher *grades* in geography believe that good teachers should be original, creative and curious. Those with lower grades in geography give more importance to teachers' consistency and composedness. It is generally known that grades are not always the reflection

of knowledge, but it is more probable that those who have higher grades also have higher expectations from teachers in terms of knowledge and creativity (Brooks et al., 2017). Gifted pupils often require richer curriculum to be stimulated and not to get bored. That is particularly important in teaching geography, which gives many opportunities for experiential enrichment of the teaching process. Furthermore, pupils with lower grades are probably more afraid of uncertainty and they rely more on luck, thus it is more important to them that teachers are consistent, not unpredictable, in their relations with pupils.

Satisfaction with teaching affects the degree to which a teacher will be seen as good or favourite and if a teacher has adequate psychological traits, the satisfaction with teaching will increase or decrease. This variable is in the strongest correlation with teachers' personality traits, which indicates that a teacher's personality is crucial for the satisfaction with the given subject. Skills and ideal conceptions did not prove to be very important for determining satisfaction with the subject. To be satisfied with the subject, it is important for pupils that teachers are emotionally stable and open, that they are agreeable, extraverted and conscientious. Research should focus on which aspects of teaching make pupils satisfied or dissatisfied.

Finally, the question remains of how much were the pupils using their current or previous teachers as prototypes. The research involved a large number of pupils, but if their teachers were their starting points, there is a question what would results look like if the number of surveyed pupils was far larger. We suggest a larger sample of pupils from different social settings in the future, in order to increase the number of teachers/benchmarks for identifying individual teachers' characteristics. There is a need to conduct the same or similar study with other geography teachers in order to determine "the ideal type of a teacher", that is the profile that satisfies the needs of society/pupils to the largest degree (Azim & Islam, 2018; Lachmann et al., 2018; Maričić et al., 2020; Milošević et al., 2016; Price et al., 2018; Ramli et al., 2018).

Conclusions and implications

It is very difficult to determine the exact profile of a teacher for a given area – subject, but considering the really large number of desirable personality traits of a teacher, obtained results largely match previous studies (Arnon & Reichel, 2007; Genc et al., 2014; Stojiljković, 2014), but there are also certain specific qualities. Agreeableness, cooperativeness and composedness are undoubtedly characteristics that every good teacher should possess, regardless of what subject they teach. Teachers themselves state that it is important to collaborate with other colleagues, to be openminded and creative and to be versatile.

From the aspect of geography as a subject, we can conclude that the skill that differentiates geography teachers from other teachers is good spatial orientation, and an important segment of it is the usage of modern technology in orientation (GPS and GIS – Geographic Information System). Using modern technologies, a geography teacher can depict and demonstrate some phenomena and processes that pupils haven't had opportunity to encounter with, that they haven't experienced and which contents are abstract and difficult to understand. Because of all those, pupils consider this skill of geography teachers to be very important and useful. Additionally, teachers believe that their specificity is being knowledgeable about both social and natural sciences and being capable of teaching outside the classroom.

Secondary school pupils emphasize the importance of sensitivity, agreeableness, and conscientiousness as personal characteristics of a geography teacher. This has to do with the fact that geography is a subject in which many things could be demonstrated and explained experientially, through sensory perception, and that requires the above mentioned characteristics from a geography teacher. Conscientiousness as a personal characteristic of a geography teacher is desirable in pupils' opinion and it could be connected with conscientiousness and responsibility towards the preservation of nature and natural resources and of historical and cultural heritage. Geography is a subject that synthesizes these spatial components and that is why this personal characteristic of a geography teacher is considered desirable. It is very important to remember the fact that the study was conducted among secondary school pupils who are supposed to already have well-developed consciousness of the importance of protection of natural and social specific qualities and of treating them with care. Since teachers also recognised these qualities, it is believed that they comprise the good geography teacher profile.

Finally, the estimates of a good geography teacher do not change with pupils' age, but there are gender differences in attitudes about desirable characteristics of a geography teacher.

Acknowledgement

This research was supported by the Ministry of Education, Science and Technological Development of the Republic of Serbia (Grant No. 451-03-68/2020-14/ 200125), Slovak Research and Development Agency (project No. SK-SRB-21-0025 Mentor´s Vademecum), and Erasmus+ Project "Mentor Training" No. 2020-1-SK01-KA201-078250. This research is a part of the project approved by the Autonomous Province of Vojvodina, Provincial Secretariat for Higher Education and Scientific-Research Activity, Program 0201, with the project title "Research of the entrepreneurial potentials among the local population for using the thermo-mineral water resources of Vojvodina", registration number: 142-451-3467/2023-02 (2021–2024). The authors also gratefully acknowledge the financial support of the Ministry of Science, Technological Development and Innovation of the Republic of Serbia (Grants No. 451-03-66/2024-03/ 200125 &451-03-65/2024-03/200125).

References

Arnon, S., & Reichel, N. (2007). Who is the ideal teacher? Am I? Similarity and difference in perception of students of education regarding the qualities of a good teacher and of their own qualities as teachers. *Teachers and Teaching*, 13(5), 441-464. https://doi.org/10.1080/13540600701561653

Azim, M. T., & Islam, M. M. (2018). Social Support, Religious Endorsement, and Career Commitment: A Study on Saudi Nurses. *Behavioral Sciences*, 8(1), 8. doi: 10.3390/bs8010008

Bogunović, B. (2006). Svojstva ličnosti nastavnika muzike. [Personality traits of music teachers]. *Zbornik Instituta Za Pedagoška Istraživanja*, 38(1), 247–263.

Brooks, C.; Butt, G.; Fargher, M. (Eds.) (2017). *The Power of Geographical Thinking*. Cham, Switzerland: Springer International Publishing.

Bullock, M. (2015). What makes a good teacher? Exploring Student and Teacher Beliefs on Good Teaching, *Rising Tide*, 7, 1-30.

Cattell, H. E. P., & Mead, A. D. (2008). The Sixteen Personality Factor Questionnaire (16PF). In G. J. Boyle, G. Matthews, & D. H. Saklofske (Eds.), *The SAGE handbook of personality theory and assessment. Vol. 2. Personality measurement and testing*. Sage Publications, Inc. https://doi.org/10.4135/9781849200479.n7

Druva, C. A., & Anderson, R. D. (1983). Science teacher characteristics by teacher behavior and by student outcome: A meta-analysis of research. *Journal of Research in Science Teaching*, 20(5), 467–479. https://doi.org/10.1002/tea.3660200509

Genc, L., Pekić, J., & Genc, A. (2014). The structure of personality of a good teacher from students perspective according to the Big-Five model. *Psihologija*, 47(1), 49–63. https://doi.org/10.2298/PSI1401049G

Goldberg, L. R. (1993). The structure of phenotypic personality traits. *American Psychologist*, 48(1), 26–34. https://doi.org/10.1037/0003-066X.48.1.26

Gordon, T. (2008). *Kako biti uspešan nastavnik*. [How to be a successful teacher]. Beograd: Kreativni centar.

Grgin, T. (1997). *Edukacijska psihologija*. [Educational psychology]. Jastrebarsko: Naklada Slap.

Guskey, T. (2002). Professional development and teacher change. *Teachers and Teaching: Theory and Practice*, 8, 381–391. https://doi.org/10.1080/135406002100000512

John, O. P., Donahue, E. M., & Kentle, R. L. (1991). *The Big-Five Inventory*. Berkeley, CA: University of California, Berkeley Institute of Personality and Social Research.

John, O. P., & Srivastava, S. (1999). The Big Five Trait taxonomy: History, measurement, and theoretical perspectives. *In Handbook of personality: Theory and research, 2nd ed* (pp. 102–138). New York, NY, US: Guilford Press.

Korthagen, F. (2004). In search of the essence of a good teacher: towards a more holistic approach in teacher education. *Teaching and Teacher Education*, 20(1), 77–97. https://doi.org/10.1016/j.tate.2003.10.002

Lachmann, B., Sariyska, R., Kannen, C., Błaszkiewicz, K., Trendafilov, B., Andone, I., Eibes, M., Markowetz, A., Li, M., Kendrick, K.M., et al. (2018). Contributing to Overall Life Satisfaction: Personality Traits Versus Life Satisfaction Variables Revisited—Is Replication Impossible? *Behavioral Sciences*, 8(1), 1. https://doi.org/10.3390/bs8010001

Lamke, T. A. (1951). Personality and Teaching Success. *The Journal of Experimental Education*, 20(2), 217–259. https://doi.org/10.1080/00220973.1951.11010441

Li, H. Q., & Wu, Y. Z. (2011). *Comparative Study on the Personality Patterns of "Good Teacher" and "Bad Teacher" as Perceived by College Students. Advanced materials research - ZUG*, 271/273, 760–763. Durnten-Zurich: Trans Tech.

Maričić, O., Ivkov-Džigurski, A., Stojšić, I., Cvjetićanin, S. & Ivanović Bibić, Lj. (2020). Multimedia Teaching Effectiveness in Natural Science Teaching. *Geographica Pannonica*, 24(2), 147-156. doi: https://doi.org/10.5937/gp24-23357

Milošević, D., Ivanović Bibić, Lj., Đukičin, S., Ivkov-Džigurski, A., & Ristanović, B. (2016). The possibilities of application of programmed instruction in the sixth grade of the second cycle of education in accordance with

standards. *Geographica Pannonica*, 20(2), 96-104. https://doi: 10.18421/GP20.02-01

Olschewski, P., Herzmann, P., & Schlüter, K. (2023). Group Work during Inquiry-Based Learning in Biology Teacher Education: A Praxeological Perspective on the Task of (Collaborative) Protocol Generation. *Education Sciences*, 13, 401. https://doi.org/10.3390/educsci13040401

Pavlović, J., & Tošić-Rudić, M. (2009). Mišljenje učenika o osobinama nastavnika. [Students' opinion about teacher's characteristics]. *Nastava i Vaspitanje*, 58(3), 458–468.

Price, J. A., Morris, Z. A., & Costello, S. (2018). The Application of Adaptive Behaviour Models: A Systematic Review. *Behavioral Sciences*, 8(1), 11. https://doi.org/10.3390/bs8010011

Radulović, B., Gajić, O., Španović, S., & Lungulov, B. (2019). Challenges of initial teacher education in the context of higher education reform in Serbia. *Образование и саморазвитие*, 14(3), 34-39.

Ramli, N. H. H., Alavi, M., Mehrinezhad, S. A., & Ahmadi, A. (2018). Academic Stress and Self-Regulation among University Students in Malaysia: Mediator Role of Mindfulness. *Behavioral Sciences*, 8(1), 12. https://doi.org/10.3390/bs8010012

Romelić, J., & Ivanović Bibić, Lj. (2015). *Metodika nastave geografije*. [Methodology of teaching geography]. Novi Sad, Srbija: Univerzitet u Novom Sadu, Prirodno-matematički fakultet.

Ryans, D. G. (1960). *Characteristics of teachers: Their description, comparison, and appraisal*. Washington D. C.: American Council on Education.

Samy, A. (2005). The qualities of a good teacher: how can they be acquired and sustained? *Journal of the Royal Society of Medicine*, 98(2), 67-69. https://doi.org/10.1177/014107680509800211

Sakač, M., & Marić, M. (2018). Psychological characteristics as the predictors of subjective well-being in future class and preschool teachers. *Zbornik Instituta za pedagoska istrazivanja*, 50(1), 93–112. https://doi.org/10.2298/ZIPI1801093S

Simon, M., & Budke, A. (2023). German and French Students' Strategies While Performing Geographical Comparisons in a Group Task Setting. *Education Sciences*, 13(8), 849.

Stanojević, D. (2009). Kako biti uspešan nastavnik geografije. [How to be a successful geography teacher]. *Globus*, 34, 145–150.

Stojiljković, S. (2014). *Psihološke karakteristike nastavnika*. [Psychological characteristics of teachers]. Niš, Srbija: Univerzitet u Nišu, Filozofski fakultet Univerziteta u Nišu.

Wilcke, H., & Budke, A. (2019). Comparison as a Method for Geography Education. *Education Sciences*, 9(3), 225. https://doi.org/10.3390/educsci9030225

Zagyvane Szucs, I (2017). What makes a Good Teacher? *Universal Journal of Educational Research*, 5(1), 141-147. https://doi.org/10.13189/ujer.2017.050118

INTERNATIONAL SCIENTIFIC JOURNAL
GEOGRAPHICA PANNONICA
Volume 28, Issue 1, 53–70 (March 2024)
Contents lists available at ScienceDirect
Journal homepage: http://www.dgt.uns.ac.rs/en/homepage/pannonica/

Evaluation and Correction Analysis of the Regional Rainfall Simulation by CMIP6 over Sudan

Waleed Babiker[A, B, C], Guirong Tan[A*], Mohamed Abdallah Ahmed Alriah[C, D, E], Ayman M. Elameen[E,F]

[A] *School of Atmospheric Sciences, Nanjing University of Information Science and Technology, Nanjing 210044, China; waleedbab200@gmail.com, tanguirong@nuist.edu.cn*
[B] *Environmental Protection Department, Air Quality and Meteorology, Aramco Saudi Arabia, P.O. Box 5000, Dhahran 31311, Kingdom of Saudi Arabia*
[C] *Sudan Meteorological Authority, Khartoum - P.O. Box 574, Sudan; mabdallah318@yahoo.com*
[D] *School of Geographical Sciences, Nanjing University of Information Science and Technology, Nanjing 210044, China*
[E] *Organization of African Academic Doctors (OAAD), Nairobi, Kenya; aymanmohamed1991@outlook.com*
[F] *School of Remote Sensing and Geomatics Engineering, Nanjing University of Information Science and Technology, Nanjing 210044, China*

KEYWORDS

Sudan
CMIP6
rainfall
GCM evaluation
bias correction

ABSTRACT

This study utilizes satellite-based rainfall CHIRPS to evaluate GCMs-CMIP6 models over Sudan from 1985 to 2014. Overall, the GCMs of BCC-CSM2-MR, CAMS-CSM1-0, CESM2, EC-Earth3-Veg, GFDL-ESM4, MIROC-ES2L, and NorESM2-MM are well reproduced in the unimodal pattern of June to September (JJAS), and hence employed to calculate Multi-Model Ensemble (MME). Then, we examine the capability of the GCMs and MME in replicating the precipitation patterns on annual and seasonal scales over Sudan using numerous ranking metrics, including Pearson Correlation Coefficient (CC), Standard Deviation (SD), Taylor Skill Score (TSS), Mean Absolute Error (MAE), absolute bias (BIAS), and, normalized mean root square error (RMSD). The results show that the MME has the lowest bias and slightly overestimates rainfall over most parts of our study domain, whilst, others (ACCESS-CM2, BCC-CSM2-MR, CAMS-CSM1-0, CESM2, CNRM-CM6-1, CNRM-CM6-1-HR, CNRM-ESM2-1, FGOALS-f3-L, FGOALS-g3) consistently overestimate rainfall in referring to CHIRPS data, respectively, but FIO-ESM-2-0 underestimates bias value. Moreover, MIROC-ES2L and NorESM2-MM demonstrate better performance than the other models. Finally, we employed a bias correction (BC) technique, namely Delta BC, to adjust the GCMs model products through the annual and monsoon seasons. The applied bias correction technique revealed remarkable improvement in the GCMs against the observations, with an improvement of 0 – 18% over the original. However, MME and MIROC-ES2L show better performance after correction than other models.

[*] Corresponding author: Guirong Tan: tanguirong@nuist.edu.cn

doi: 10.5937/gp28-46565

Received: September 15, 2023 | Revised: February 14, 2024 | Accepted: March 21, 2024

Introduction

Africa is the second-populated continent in the world, with a population of 1.2 billion and an area of about 30 million km² (11.6 million mi²), and one of the most vulnerable to climate change due to its high exposure to droughts, floods, rising temperatures with little ability to adapt (Almazroui et al., 2020). However, Sudan, which lies in the eastern part of the continent, is considered one of the most vulnerable countries to the risks of climate change, especially flood and drought (Alhuseen, 2014), and has experienced several environmental changes in the past, and more are projected to occur in the future (Walthall, 2012). The implementation of the United Nations Framework Convention on Climate Change (UNFCCC), with several studies, shows that the development process will be greatly impacted by climate change, especially in fields like water, agriculture, and health (Alhuseen, 2014).

To investigate the present and future of Earth's climate system, many global climate models have been developed (Kumar et al., 2013). Furthermore, future changes in rainfall across this region must be detected and understood by stakeholders in resource management and planning, as the variability of the future climate is a major concern (Rajbhandari, et al., 2018). Since the primary tools of the analyses and determining what climate we are likely to have in the near and not-so-near future use dynamical downscaling with regional climate models (RCMs) and global climate models (GCMs) (Maroneze et al., 2014), the evaluation of climate models is considered as essential for providing model-based climate data (Babaousmail et al., 2022). Several climate modeling organizations have run climate simulations for the future using various IPCC emission scenarios (Rajbhandari et al., 2018). Global climate models (GCMs), which are mostly used for continental and hemispherical climate research, have proven to be a useful tool for analyzing the changes that could have an impact on these systems in the future. However, due to their typical spatial resolutions, which are on the order of hundreds of kilometers (Expósito et al., 2015), furthermore, often, the availability of numerous GCMs is seen as the main cause of uncertainty in precipitation projections (Tegegne & Mellesse, 2022). So, it is critical to evaluate the fundamental uncertainty. The interior variability of the climate system, model error, and uncertainty in the greenhouse emission scenario are three potential causes of uncertainty in climate projections (Ishida et al., 2020). Therefore, our results should be reduced to a more accurate resolution to reliably evaluate the regional effects of climate change (Ishida et al., 2020). The model evaluation for this study was based on a range of statistical measurements and visual graphical comparisons for the same aggregation periods to postulate potential changes in precipitation (Akurut et al., 2014). These are generally three-dimensional dynamic and physical models of the atmosphere, ocean, Earth's surface, and cryosphere that are coupled and run on supercomputers at full power. Around the world, there are many models of this type, all with varying formulations, strengths, and weaknesses, leading to one of the main uncertainties in climate change projections (Collins & Senior, 2002).

This insight is particularly important in climate research on Sudan's complex orography, where regional models should be able to resolve a few kilometers. The attribution of uncertainties in the projection study brings to light some factors, such as systematic and non-systematic biases in the model datasets or methods that take into account the natural variability of the climate, such as the El Nino-Southern oscillation or warming of the tropical oceans (Ngoma et al., 2021). Hence, from the perspective of climate dynamics, the spatial and temporal variability of precipitation poses a variety of difficulties for process comprehension, event prediction, and climate change projection, and the urgency of the issue is increased by the fact that many communities in Africa are particularly vulnerable to climate change (Badr et al., 2016). Also, the rainy season for this study, which spans from June to September over the entire region, was linked to the annual migration of the intertropical convergence zone (ITCZ), where the Atlantic Ocean, Red Sea, Mediterranean, and Indian Ocean are the major main sources of water vapor (Salih et al., 2015). The variability of rainfall in various locations in Sudan is significantly influenced by sea surface temperature (SST) in the Indian and Pacific Oceans, and the Atlantic Multidecadal Oscillation (AMO) is brought on by modifications in essence.

Based on the aforementioned studies, and to address the gap in existing research in this area, as far as we know, we seek to conduct such a study. This study aims to evaluate the performance of a general circulation model (GCM) in simulating regional rainfall and to correct any potential biases through data assimilation techniques. The study aims to assess the accuracy of the GCM simulations by comparing them against the Climate Hazard Group Infrared Precipitation with Station (CHIRPS) dataset over Sudan and to identify any discrepancies or biases in the model.

Materials and Methods

Study area

Sudan is situated in Eastern Africa within [8.4 and 23.3° N] and [21.5 and 39.0° E] as in (Figure 1). Its total area is 1,886,068 km², with adjoint borders with South Sudan from the South, Ethiopia and Eretria in the East, Libya Northwest, Chad and Central Africa in the West, and Egypt in the North (Elramlawi et al., 2018).

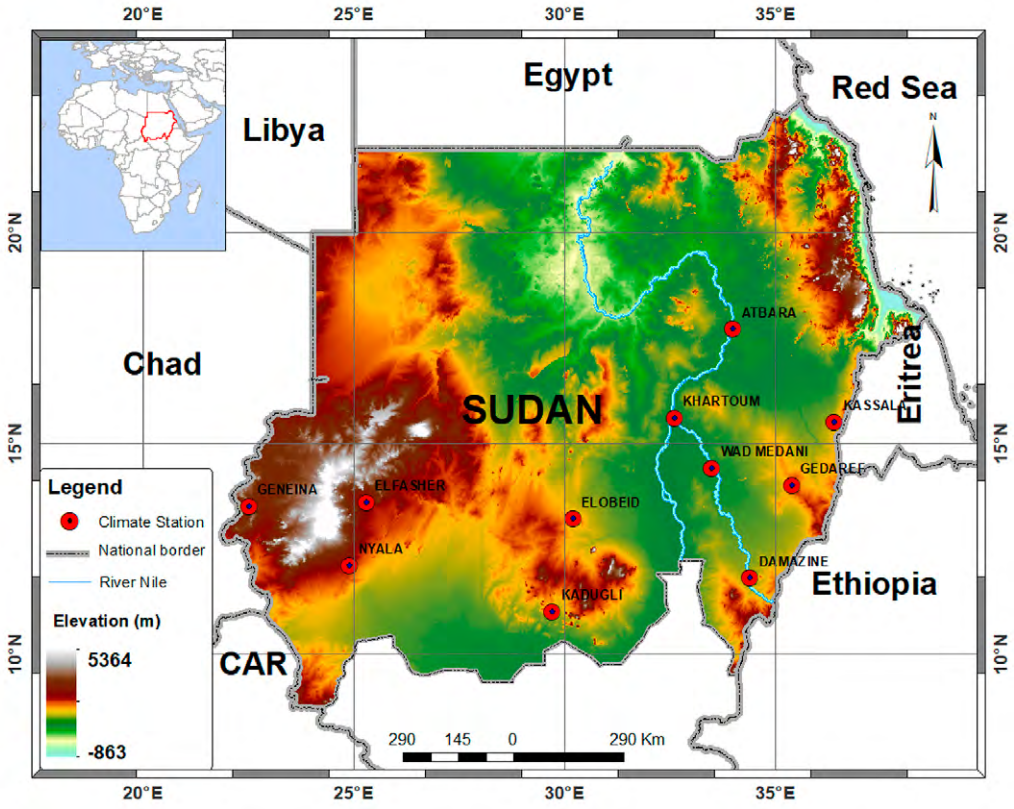

Figure 1. The study area location and its topographical features

Rainfed agriculture inhabits more than 90% of the cultivated land, producing agricultural products and the related means of subsistence for the Sudanese people (Siddig et al., 2020). The country is characterized by several topographic features such as the valleys of the Blue and White Nile Rivers, and the elevated eastern and southern boundaries, as well as the main Nile River and its tributaries, besides some isolated uplands (Williams & Nottage, 2006). The dry season in the country spans from October to March, followed by a hot season from April to June, and a wet season from June to September. However, the environment and social circumstances in Sudan are significantly influenced by rainfall (Gamri, et al., 2009). The rainy season (June to September) across Sudan has been linked to the annual migration of the Intertropical Convergence Zone (ITCZ) (Salih et al., 2015). During the boreal summer, this rainfall was brought on by winds from the Arabian Peninsula that were blowing North and adverting moisture from the Red Sea. August, is the wettest month of the year in much of Sudan, with up to 100 mm/month (Alriah et al., 2021). However, there is a humid area on the Red Sea coast, where the rains fall during the winter with a sporadic distribution with a peak quantity in November, and also fall during the summer when the temperature is moderate. In other locations, August is typically the month with the most rainfall, but July can also be rainy in some places, from one region to another, there is a significant difference in the quantity of rainfall and the length of the rainy season (Ahmed & Elhag, 2011).

Data

This study used Climate Hazard Group Infrared Precipitation with Station monthly precipitation datasets (CHIRPS. v2), with a spatial resolution 0.05° × 0.05° (5.55 x 5.55 km²) (https://data.chc.ucsb.edu/products/CHIRPS-2.0/), was obtained from (1985-2014), it is blending station data and reduce any uncertainties that may lack rain gauge, therefore, it has a better performance among east Africa and recently evaluated over the study domain (Alriah et al., 2022).

Also, the initial realizations (r1i1p1f1), for all CMIP6 models were downloaded from the website (https://

Table 1. The GCMs-CMIP6 information and their spatial coverage

№	Model ID	Country	resolution	Reference
1	ACCESS-CM2	Australia	1.9° × 1.3°	(Mkala et al., 2023)
2	BCC-CSM2-MR	China	1.1° × 1.1°	(Wu et al., 2021)
3	CAMS-CSM1-0	China	1.1° × 1.1°	(S & L, 2023)
4	CESM2	USA	1.3° × 0.9°	(Meehl et al., 2020)
5	CNRM-CM6-1	France	1.4° × 1.4°	(Voldoire et al., 2019)
6	CNRM-CM6-1-HR	France	0.5° × 0.5°	(Weijer et al., 2020)
7	CNRM-ESM2-1	France	1.4° × 1.4°	(Séférian et al., 2019)
8	EC-Earth3-Veg	Europe	0.7° × 0.7°	(Babaousmail et al., 2021)
9	FGOALS-f3-L	China	1.3° × 1°	(Klutse et al., 2021)
10	FGOALS-g3	China	2° × 2.3°	(Wang et al., 2022)
11	FIO-ESM-2-0	China	1.3° × 0.9°	(Bao et al., 2020)
12	GFDL-ESM4	USA	1.3° × 1°	(Zheng et al., 2022)
13	MIROC-ES2L	Japan	2.8° × 2.8	(Hajima et al., 2020)
14	MRI-ESM2-0	Japan	1.1° × 1.1°	(Kawai et al., 2019)
15	NorCPM1	Norway	1.9° ×2.5°	(Bethke et al., 2021)
16	NorESM2-MM	Norway	1.3° × 0.9°	(Seland et al., 2020)

cds.climate.copernicus.eu/cdsapp#!/dataset/projections-cmip6). Climate models' information and details of the 16 historical GCM models utilized in this study are obtained in Table 1.

Methodology

The evaluation of climate models is a critical step in assessing the accuracy and reliability of their outputs. Hence, the best correlated methods are selected based on statistical and error measures like the Pearson Correlation Coefficient (CC), Standard Deviation (SD), Taylor Skill Score, Mean Absolute Error (MAE), and absolute bias (BIAS). Many scholars, (Alriah et al., 2022; Karim et al., 2023), use it for comparing the performance of the climate data simulation against the observed data using the climatology of annual and intra-annual time scales. Here, we used a multi-Models ensemble for the best selected GCM models, after unifying (Bilinear-interpolation) their resolution into the same resolution of reference data (CHIRPS), followed by averaging the CHIRPS dataset within the region, as shown in the equations below.

$$M\overline{x} = \frac{1}{n}\sum_{i=1}^{n} x_i \tag{1}$$

The variability is calculated using the Square Root of Variance (standard deviation), represented as σ,

$$\sigma_x = \sqrt{\frac{1}{n}\sum_{1}^{n}\left(x_i - \overline{x}\right)^2} \tag{2}$$

Where x_i is the monthly rainfall, x is the mean of the entire series, and σ_x is the standard deviation for the models, with respect to data used to rate the evaluation. Furthermore, the measure of statistical error validation of model-based versus observed-based precipitation.

$$CC = \frac{\sum_{n=1}^{n}\left(G_l - \overline{G}\right)\left(S_l - \overline{S}\right)}{\sum_{n=1}^{n}\left(G_1 - \overline{G}\right)^2 \sum_{n=1}^{1}\left(S_i - \overline{S}\right)^2} \tag{3}$$

It was used to evaluate the observation data and dataset of the gridded simulation model, when the *CC* is close or equal to 1, it means that there is a correlate high, the negative bias expresses the area where the model is higher than the reference data, and positive bias expresses the area the model is lower than the observation data.

$$TSS = \frac{4\left(1+R_m\right)^2}{\left(\frac{\sigma_m}{\sigma_o} + \frac{\sigma_o}{\sigma_m}\right)^2 \left(1+R_o\right)^2} \tag{4}$$

For both models and observation patterns, Rm is the correlation coefficient, and R_o is the maximum possible correlation coefficient (i.e., 0.999), whereas m and o are the standard discrepancies from the simulation and reference precipitation patterns, respectively. Between 0 and 1, the *TSS* value is measured, with values closer to 1 indicating higher model performance.

$$BIAS = \frac{\sum_{n=i}^{n} Gi - Si}{\sum_{n=1}^{n} Gi} \quad (5)$$

In order to evaluate the model, we calculate the Mean Bias of GCM- The difference between the observed and modeled rainfall is calculated to determine the mean bias. The mean bias is calculated for monthly rainfall based on the CHIRPS dataset, the GCM and the observations to obtain a spatial distribution of the mean bias, Overall, spatial distribution of mean bias GCM of rainfall is a crucial step to determine the accuracy and reliability of GCM simulations, and it helps to suggest improvements in the GCM models it helps to suggest improvements in the GCM models. Climate Index: In order to evaluate the climate model with reference data (CHIRPS) the large-scale effects of atmospheric circulation on rainfall. This bias can be due to a variety of factors, such as inaccuracies in the models' physical processes, limitations in the models' spatial or temporal resolution, or errors in the input data used to initialize and run the models. The framework process of this study is illustrated in the flowchart (Figure 2).

For precipitation variables, the bias in a geographical location x is given by the difference between observed and simulated precipitation, Bias-corrected precipitation in x at some time t in the past was estimated as below (Mendez et al., 2020).

$$P_{ass}^{BC} = \frac{Pass(d) \cdot \left[\frac{\mu_m\left(P_{obs(t)}\right)}{\mu_m\left(P_{ass(t)}\right)} \right]}{30} \quad (6)$$

Where a simulation historical of precipitation GCM to be corrected, reference observation precipitation CHIRPS dataset, a simulation historical of precipitation GCM.

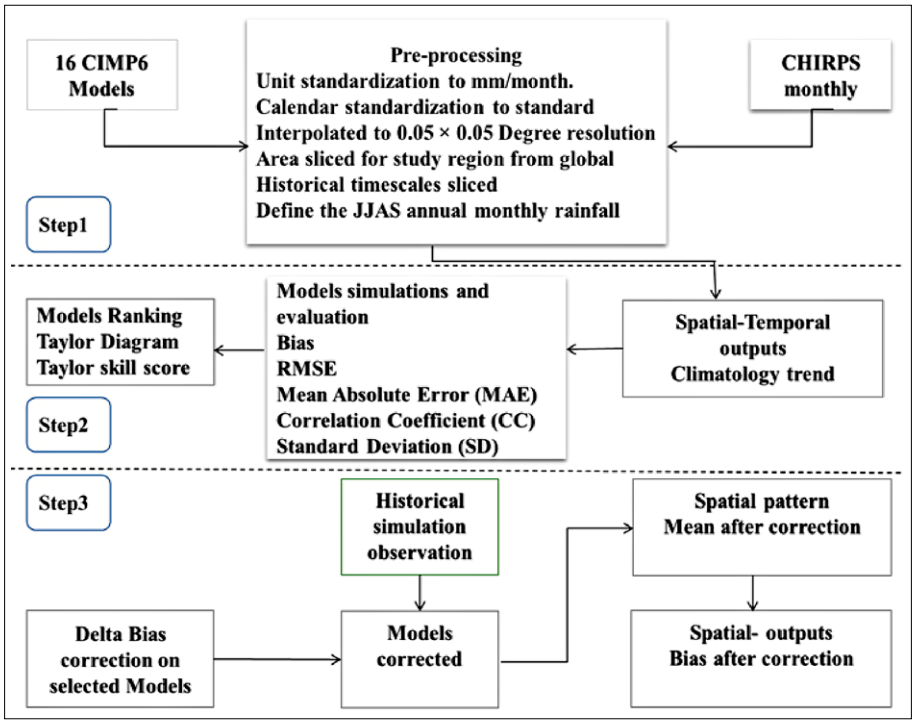

Figure 2. The framework of this study is presented in a flow-chart format for historical data processing, evaluation, and Bias correction, of rainfall variables over the study Domain

Results

Climatology of Rainfall

The rainfall of Sudan is heavily influenced by the Inter-Tropical Convergence Zone (ITCZ). Hence, the country experiences a variety of summer rainy seasons from June to September. The region's diverse topography also affects where and how much rainfalls, with the Southeast and Southwest zones receiving more rain than the Northern zone. Figure 3 shows the monthly mean rainfall time series of CHIRPS and 16 GCMs over Sudan during 1985 - 2014. We compare the GCMs products against the reference data (CHIRPS) based on the annual cycle to see how well the models could represent the observed pre-

cipitation pattern. The degree to which a model can properly mimic precipitation is what determines how accurate it is. The GCMs' monthly precipitation trends demonstrate distinct patterns that represent the annual mean precipitation cycle in our domain. Most of the models exhibit a unimodal peak in August; however, few models show a bimodal peak in June and September. The rainfall amounts vary from 0 to 105 mm/month across the models, with relatively higher rainfall amounts during the peak months. The following models: BCC-CSM2-MR, CAMS-CSM1-0, CESM2, EC-Earth3-Veg, GFDL-ESM4, MIROC-ES2L, and NorESM2-MM robustly replicate the peak rainfall while reproducing different rainfall amounts. They also have a shallow bias, which means that they simulate a lower range of precipitation values than the reference data. However, it might suggest that averaging a group of different GCMs that perform well may result in better rainfall simulation than using a single GCM. Therefore, these seven advantageous GGMs were averaged as mean ensemble model (MME) and examined alongside the other 16 GGMs in the following analyses. The obtained results further revealed that the ACCESS-CM2, FGOALS-f3-L, FGOALS-g3, CNRM-CM6-1, CNRM-CM6-1-HR, and CNRM-ESM2-1 are notably underestimating the mean rainfall.

Specifically, the CNRM-CM6-1, CNRM-CM6-1-HR, and CNRM-ESM2-1 are found to be strongly underestimating the precipitation than other GCMs. The models observed to underestimate precipitation may have insufficient representation of the atmospheric and oceanic processes that contribute to our study domain. On the other hand, FIO-ESM-2-0 was detected to be significantly overestimating the mean of precipitation. Overall, the models that significantly underestimate or overestimate precipitation may have inaccurate parameterizations, which could lead to erroneous projections of future water availability, and thus, have serious consequences for the country's agricultural and economic sectors. In conclusion, the GCMs showed varying levels of skill in simulating the Sudan rainfall regime. The accuracy of the GCMs in simulating precipitation over Sudan has significant implications for climate change projections and regional water resource management; therefore, further investigation and improvement are required.

Model performance evaluation

Here, the performance of the considered CIMP6 models for this study is evaluated against the CHIRPS dataset to assess their capabilities in simulating annual and seasonal (JJAS) rainfall over Sudan from 1985-2014. Numerous validation metrics including Pearson's correlation coefficient (CC), standard deviation (SD), Taylor Skill Score (TSS), Mean Absolute Error (MAE), and absolute bias (BIAS) are employed to evaluate and test the model's performance versus CHIRPS observation. Taylor diagrams for annu-

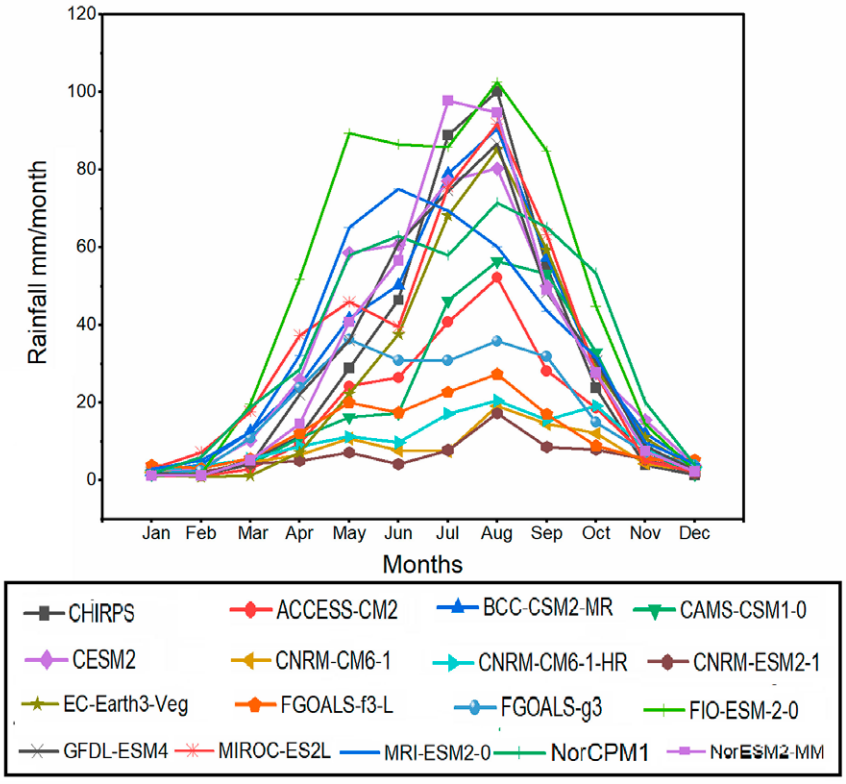

Figure 3. Monthly mean rainfall of CHIRPS and 16 multi-model ensembles (mm/month), the black line is the reference dataset (CHIRPS)

al and seasonal comparison are shown in Figures 4 and 5, whilst the values of TSS and BIAS are illustrated in Figures 6 and 7, respectively. Tables 2 and 3 summarize the outcomes of the previous statistical metrics during the annual and seasonal (JJAS) comparisons. It found that all GCMs produced higher scores in terms of TSS, CC, MAE, RMSD, and BIAS during annual comparisons than seasonal (JJAS) comparisons. This result indicates that those models simulate the rainfall over Sudan during the annual phase more accurately than the seasonal (JJAS) phase. Moreover, through the annual comparison, the MME captured the largest score in terms of TSS, CC, MAE, RMSD, and BIAS with values of 93%, 96%, 6.76, 10.37, and 0.42, respectively. On the other side, CESM2 captured the highest score in terms of TSS, MAE, and RMSE during the seasonal (JJAS) comparison and showed reads of 50%, 8.8, and 10.5, respectively, while CAMS-CSM1-0 demonstrated the highest CC (41%) and NorESM2-MM showed the lowest bias (-0.42).

Our results further showed that the following models: NorESM2-MM, EC-Earth3-Veg, GFDL-ESM4, BCC-CSM2-MR, MIROC-ES2L, and CESM2 outperform the

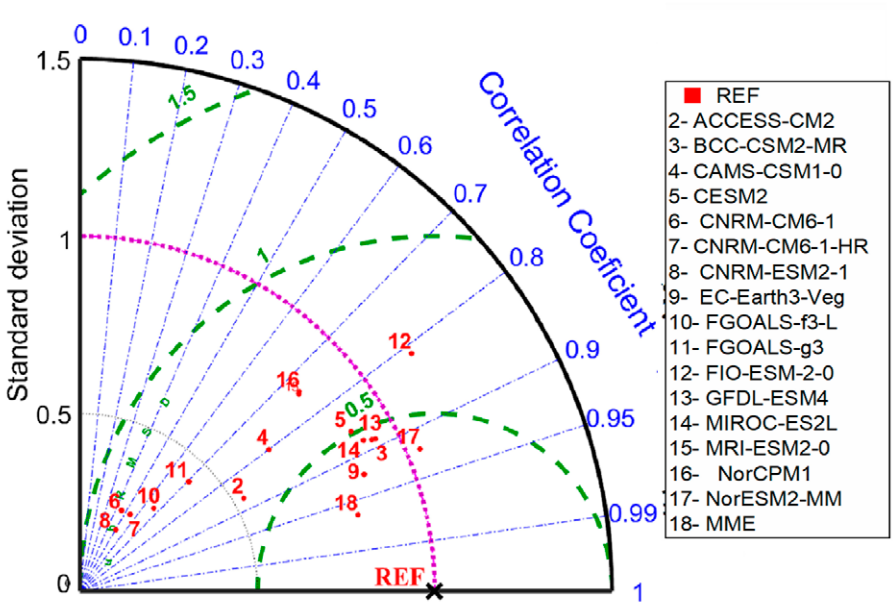

Figure 4. Comparison of annual GCMs-CMIP6 models against satellite-based rainfall CHIRPS from 1985 to 2014

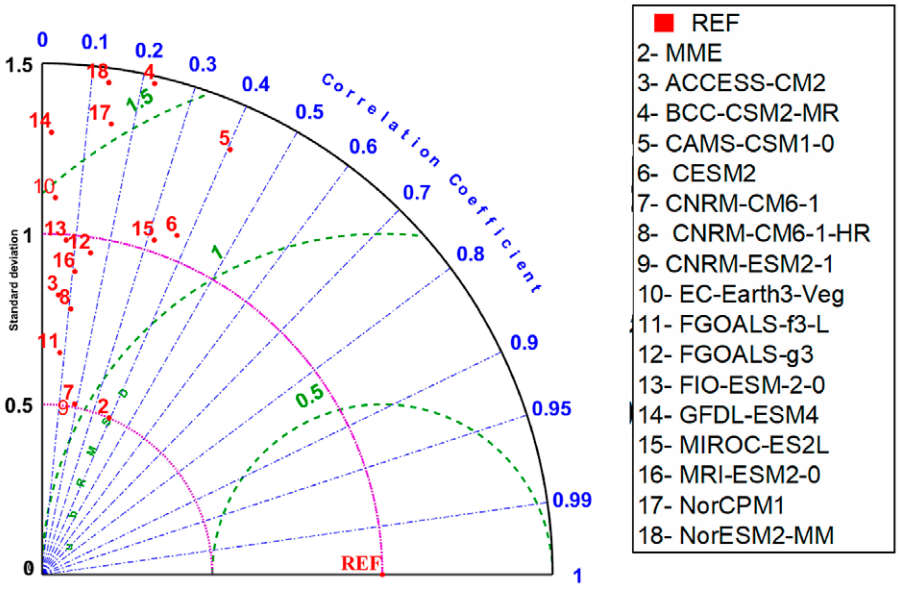

Figure 5. Comparison of GCMs-CMIP6 summer monsoon rain against CHIRPS from 1985 to 2014.

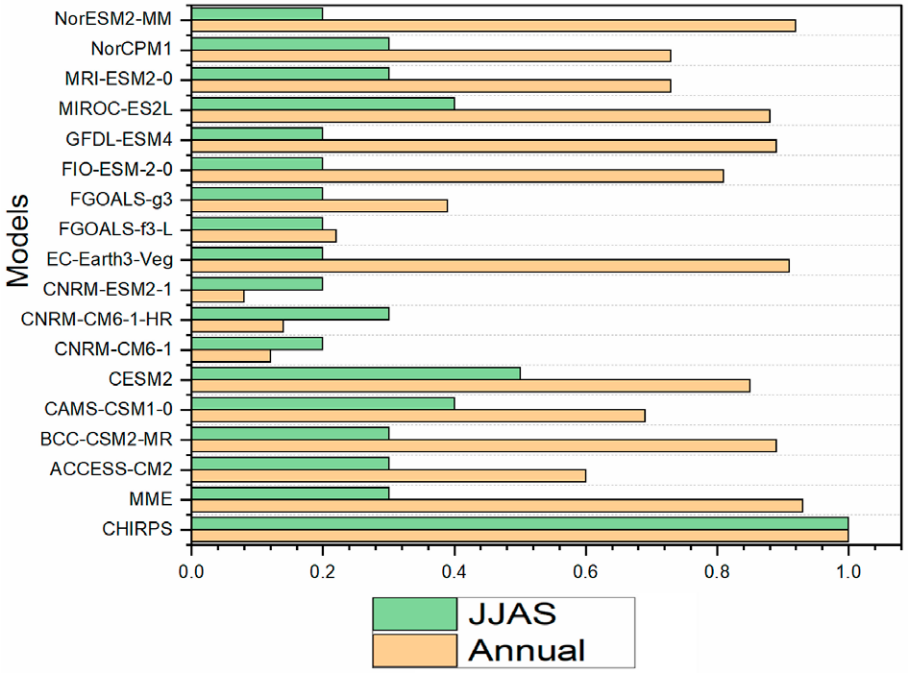

Figure 6. Summarizing Taylor Skill Score (TSS) of Annual

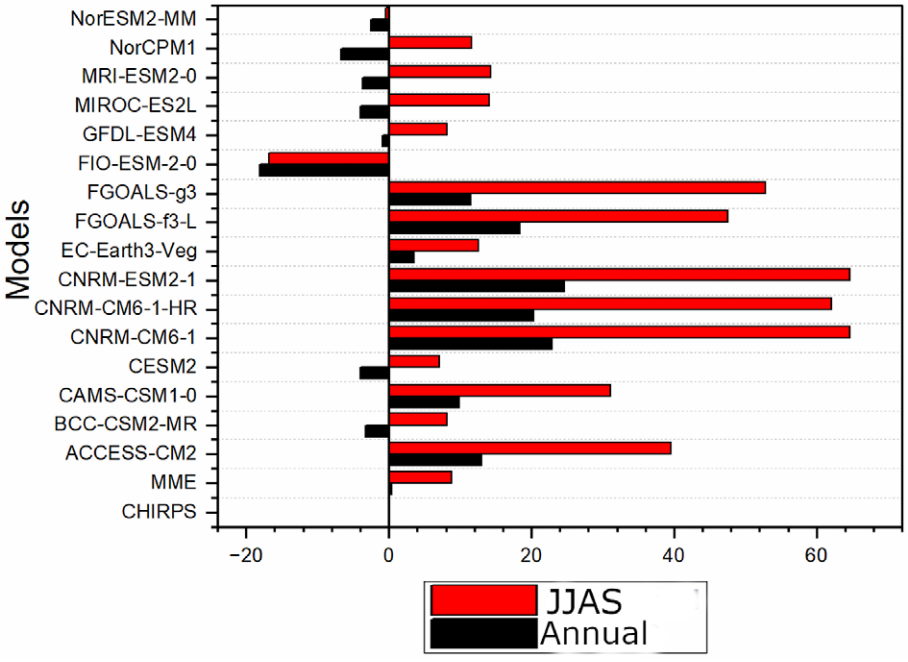

Figure 7. Bias for annual and JJAS multi-model ensemble and CHIRPS

other CIMP6 models in all statistical tests during the annual comparison. More so, NorESM2-MM demonstrated the highest CC with reference data, the largest TSS and SDV, and the lowest MAE and BIAS amongst the different CIMP6 models. As a result, it might be concluded that the six aforementioned models are more efficient than the other 16 GCMs in simulating annual rainfall across Sudan. It also found that the CNRM-ESM2-1, CNRM-CM6-1, CNRM-CM6-1-HR, and FGOALS-f3-L produced a much larger bias and significantly lower TSS and CC than other GCMs. In particular, CNRM-ESM2-1 exhibited the lowest CC (0.08), the largest bias of 24.65 annually, and 64.66 in JJAS. Consequently, these four models are considered incapable of simulating rainfall over Sudan since they have produced statistically insignificant results. Other remaining models (including FIO-ESM-2-0, MRI-ESM2-0, ACCESS-CM2, and FGOALS-g3) displayed varied scores among different statistical tests.

Table 2. Summary of statistical that presents the findings of comparisons among annual using CHIRPS Rainfall data and historical simulation multi-Model data

Models	TSS	CC	SDV	BIAS	MAE	RMSD
CHIRPS	1.00	1.00	1.00	0.00	0.00	0.00
MME	0.93	0.96	0.81	0.42	6.76	10.37
ACCESS-CM2	0.60	0.87	0.53	12.96	14.90	24.13
BCC-CSM2-MR	0.89	0.89	0.94	-3.24	11.01	15.98
CAMS-CSM1-0	0.69	0.80	0.66	9.86	14.53	23.11
CESM2	0.85	0.86	0.89	-3.95	11.81	17.72
CNRM-CM6-1	0.12	0.46	0.26	22.93	24.69	38.57
CNRM-CM6-1-HR	0.14	0.55	0.26	20.28	23.01	36.31
CNRM-ESM2-1	0.08	0.50	0.20	24.65	25.92	39.71
EC-Earth3-Veg	0.91	0.93	0.87	3.54	9.06	13.53
FGOALS-f3-L	0.22	0.66	0.31	18.35	21.37	33.54
FGOALS-g3	0.39	0.71	0.43	11.49	17.65	28.24
FIO-ESM-2-0	0.81	0.81	1.15	-18.12	20.77	29.18
GFDL-ESM4	0.89	0.89	0.93	-0.85	9.82	15.73
MIROC-ES2L	0.88	0.88	0.91	-4.00	11.45	16.48
MRI-ESM2-0	0.73	0.74	0.83	-3.64	16.69	23.24
NorCPM1	0.73	0.74	0.84	-6.66	17.74	24.05
NorESM2-MM	0.92	0.92	1.04	-2.54	8.58	13.91

Table 3. Summary of statistical that presents the findings of comparisons among JJAS using CHIRPS Rainfall data and historical simulation multi-model data

Models	TSS	CC	SDV	BIAS	MAE	RMSD
CHIRPS	1.0	1.00	1	0.00	0.00	0.00
MME	0.3	0.39	0.50	8.80	9.16	10.78
ACCESS-CM2	0.3	0.06	0.82	39.55	39.55	40.45
BCC-CSM2-MR	0.3	0.22	1.48	8.16	11.18	13.45
CAMS-CSM1-0	0.4	0.41	1.36	31.06	31.06	32.31
CESM2	0.5	0.37	1.07	7.04	8.88	10.53
CNRM-CM6-1	0.2	0.19	0.51	64.66	64.66	65.04
CNRM-CM6-1-HR	0.3	0.11	0.78	62.11	62.11	62.63
CNRM-ESM2-1	0.2	0.19	0.51	64.66	64.66	65.04
EC-Earth3-Veg	0.2	-0.04	1.11	12.53	13.06	16.17
FGOALS-f3-L	0.2	0.08	0.65	47.51	47.51	48.14
FGOALS-g3	0.2	-0.15	0.95	52.78	52.78	53.71
FIO-ESM-2-0	0.2	-0.07	0.98	-16.79	17.49	19.43
GFDL-ESM4	0.2	0.02	1.30	8.11	10.93	13.60
MIROC-ES2L	0.4	0.32	1.03	14.04	14.19	16.16
MRI-ESM2-0	0.3	0.11	0.89	14.30	14.54	16.66
NorCPM1	0.3	0.15	1.34	11.60	13.11	15.58
NorESM2-MM	0.2	-0.13	1.46	-0.42	10.09	12.63

Spatial annual and JJAS mean evaluation of rainfall simulations

Sudan has a wide variety of rainfall variations. Hence, it is necessary to understand the fluctuations of rainfall across the entire parts of our study area. In this section, the spatial distribution of simulated precipitation from 16 GCMs as well as MME was assessed versus the CHIRPS dataset on the annual and seasonal (JJAS) cycle during 1985-2014, as illustrated in Figures 8 and 9. Our initial focus was on how well the GCMs could recreate the observed spatial variability of precipitation along the study domain. Both annual and intra-annual results show that most of the CMIP6 models can replicate the orographic precipitation pattern concerning the CHIRPS dataset. Moreover, the behavior of all CMIP6 models runs against the reference dataset demonstrating that rainfall increases towards the South. Nevertheless, some discrepancies exist among the different GCMs from 1985 to 2014. The average maximum and lowest annual precipitation were between (5-120 mm), respectively, and JJAS's mean maximum was more than 120mm and the lowest was greater than 5 mm. The mean maximum value was observed over the south to the south-east zones across all models, whilst the mean lowest value was detected over the Northern parts. The results in Figures 8 and 9 further revealed that the MME model tends to follow the reference data; however, certain variations in the amount of precipitation were observed in comparison to the CHIRPS dataset. The following eight products: BCC-CSM2-MR, CAMS-CSM1-0, CESM2, EC-Earth3-Veg, GFDL-ESM4, MIROC-ES2L, MRI-ESM2-0, and NorESM2-MM were shown to be efficient in simulating the spatial change of precipitation based on the reference dataset. However, they have slight overestimate or underestimate spatial mean distribution (2-120mm/month) relative to the other models. In particular, NorESM2-MM performs better than other GGMs and exhibits lesser bias through the annual and seasonal phases.

On the other hand, other superior seven GGMs exhibited slight variations of distribution rainfall in comparison to the reference dataset. For example, CAMS-CSM1-0

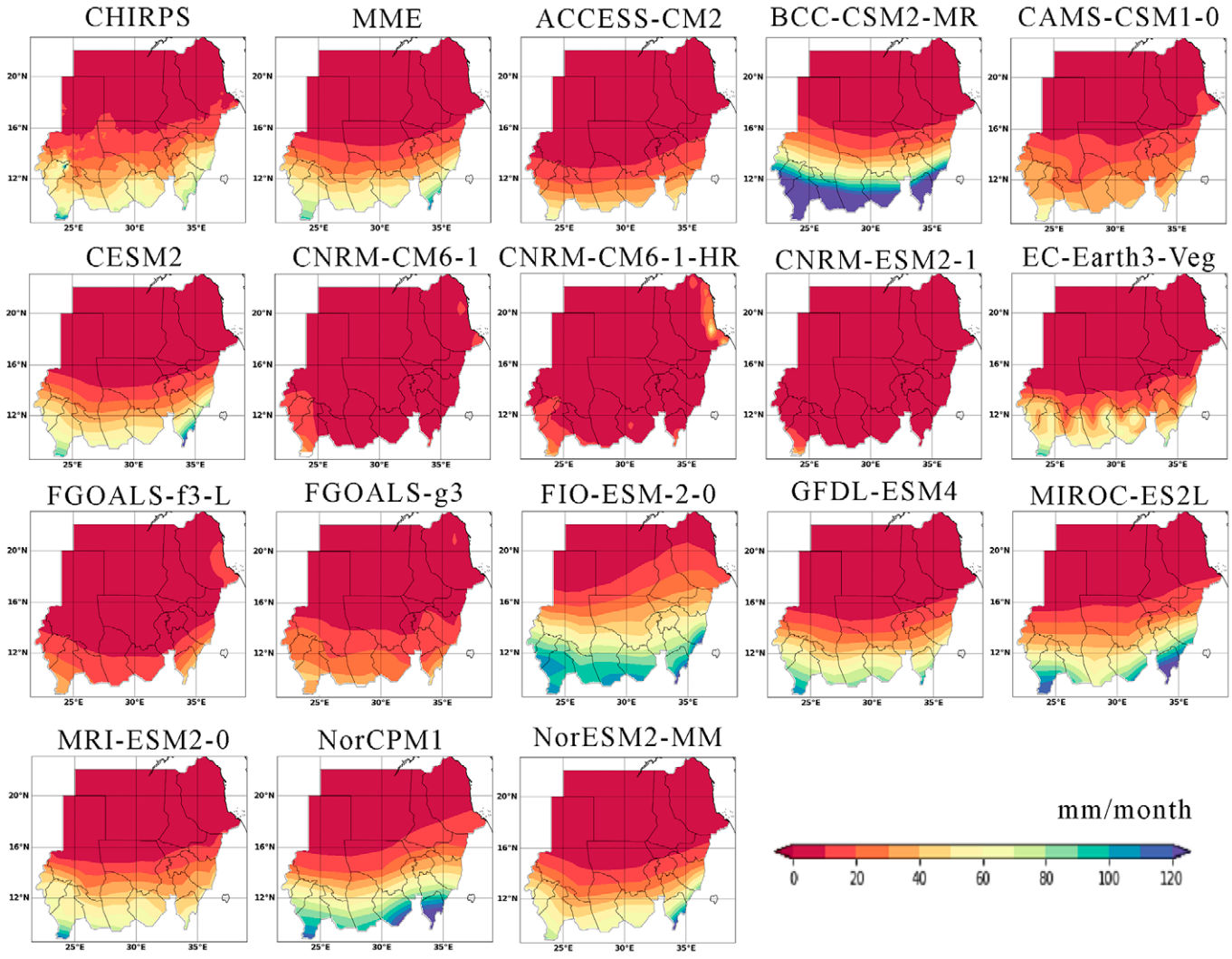

Figure 8. Spatial patterns of annual mean rainfall observation dataset and data simulation from (1985-2014)

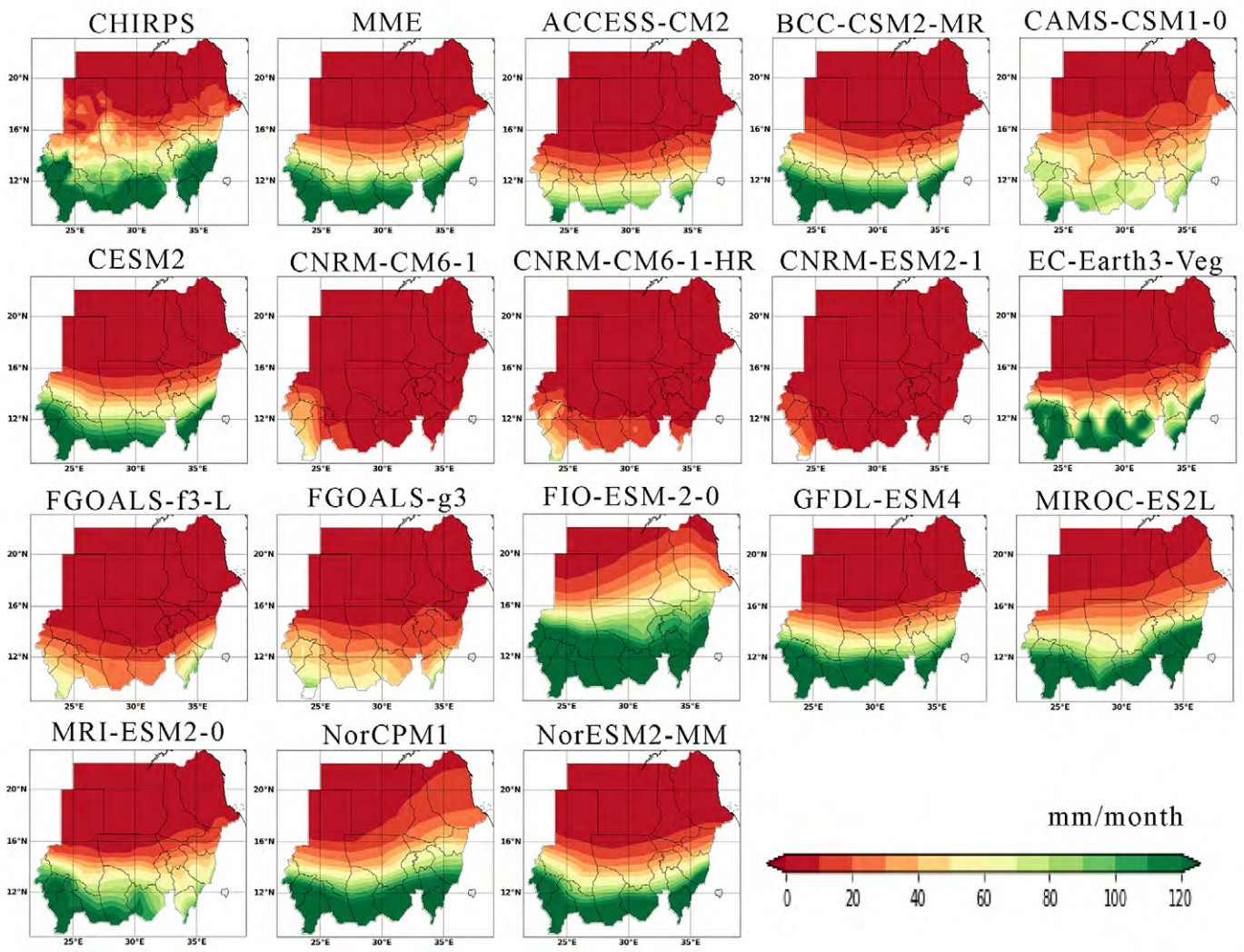

Figure 9. Spatial patterns of JJAS mean rainfall observation and data simulation from (1985-2014)

reveals a shallow decrease in the precipitation magnitude over the Southern parts and a slight increase across the far Northeast parts; MIROC-ES2L and GFDL-ESM4, and BCC-CSM2-MR showed a certain increase in the rainfall along the Southern zones through the annual phase; EC-Earth3-Veg has a slight variation over the Southern, Southeasterly, and Western borders; and MRI-ESM2-0 shows a decrease in the precipitation over the Southeast areas. It also observed that the subsequent products (including CNRM-CM6-1, CNRM-CM6-1-HR, CNRM-ESM2-1, FGOALS-f3-L) substantially underestimate the values of annual and seasonal rainfall over the majority of our study domain. Besides, FIO-ESM-2-0 and NorCPM1 appear to overestimate the rainfall over the far Northeast borders, as seen in Figures 8 and 9.

Spatial Distribution of the Bias

Analyzing the bias of GCMs products is crucial to determine the performance of GCMs simulations. In this part, we analyzed the spatial bias of 16 GCMs models and MME at JJAS and yearly scale for the period of 1985-2014 over Sudan. However, such analysis will demonstrate how well the GCM can simulate the precipitation patterns over Sudan during the analyzed period. The spatial biases of the GCMs were determined as mean differences between those models' outputs and the respective CHIRPS precipitation during the annual and seasonal phases (see Figures 10 and 11). It found that, during the annual and seasonal (JJAS) phase, the bias over most areas for different models was between (+40) and (-40) mm (see Figures 10 and 11). Furthermore, MME exhibited the lowest amount of bias amongst all models, however, it slightly overestimated bias across the study area. The subsequent GGMs: MIROC-ES2L, NorESM2-MM, EC-Earth3-Veg, and GFDL-ESM4 showed analogous bias distribution with a relatively little bias (i.e. the amount of bias positive or negative is little than other models) over most areas in the country. Other models (including ACCESS-CM2, BCC-CSM2-MR, CAMS-CSM1-0, CESM2, CNRM-CM6-1, CNRM-CM6-1-HR, CNRM-ESM2-1, FGOALS-f3-L, FGOALS-g3) are con-

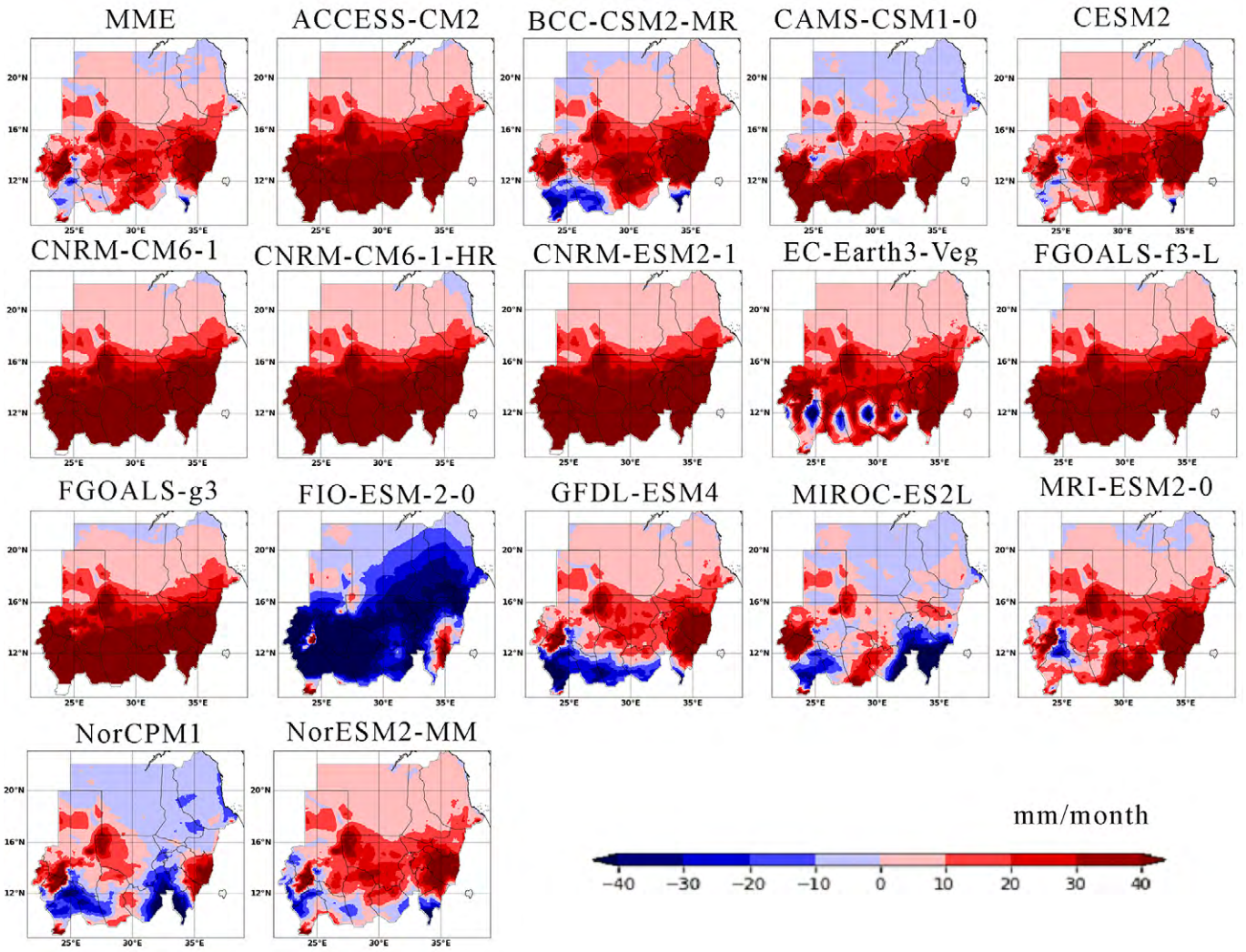

Figure 10. Bias of mean JJAS rainfall(mm/month) over Sudan based on CHIRPS Dataset 1985-2014

sistently overestimated bias based on CHIRPS data. Overall, MIROC-ES2L and NorESM2-MM displayed the lowest biases and showed better performance than other individual GCMs during the annual and JJAS rainfall. Based on the achieved results from Figures 10 and 11 it can be concluded that the considered CIMP6 GCMs for this study are not able to simulate precipitation patterns accurately over the region. The findings of this analysis could be of great use in identifying potential improvements in the GCMs and optimizing the model's parameters for future predictions.

Delta Bias Correction

We conducted a more in-depth analysis in this study to determine the extent to which the correction algorithm enhances the accuracy of the simulation models. The GCMs models are complex systems that simulate the Earth's climate system by solving a set of mathematical equations. It provides a representation of how the climate system might change due to natural variability, human activity, or a combination of both. These models simulate the complex interactions of different elements of the climate system and land-sea-atmosphere-cryosphere interaction. However, these models are not perfect and can contain errors or biases. Therefore, corrections are necessary to improve the accuracy of the simulations, as these errors can lead to inaccurate projections of future weather conditions. In this work, to improve the accuracy of GCM simulations, we used the Delta method to correct the models.

Spatial bias distributions after correction of eight GCM models, in addition to MME, are shown in Figures 12 and 13. The correction is applied at each grid point across the spatial domain. After the correction, these models were evaluated against CHIRPS datasets as a reference from 1985 to 2014, on a seasonal (JJAS) and annual basis. The GCMs rainfall estimates are expected to be closer to the observed rainfall values after applying the correction. The obtained results in Figures 12 and 13 indicate that the spatial mean bias of GCMs precipitation has significantly (i.e. 0.2-6 mm/month overestimate or underestimate) re-

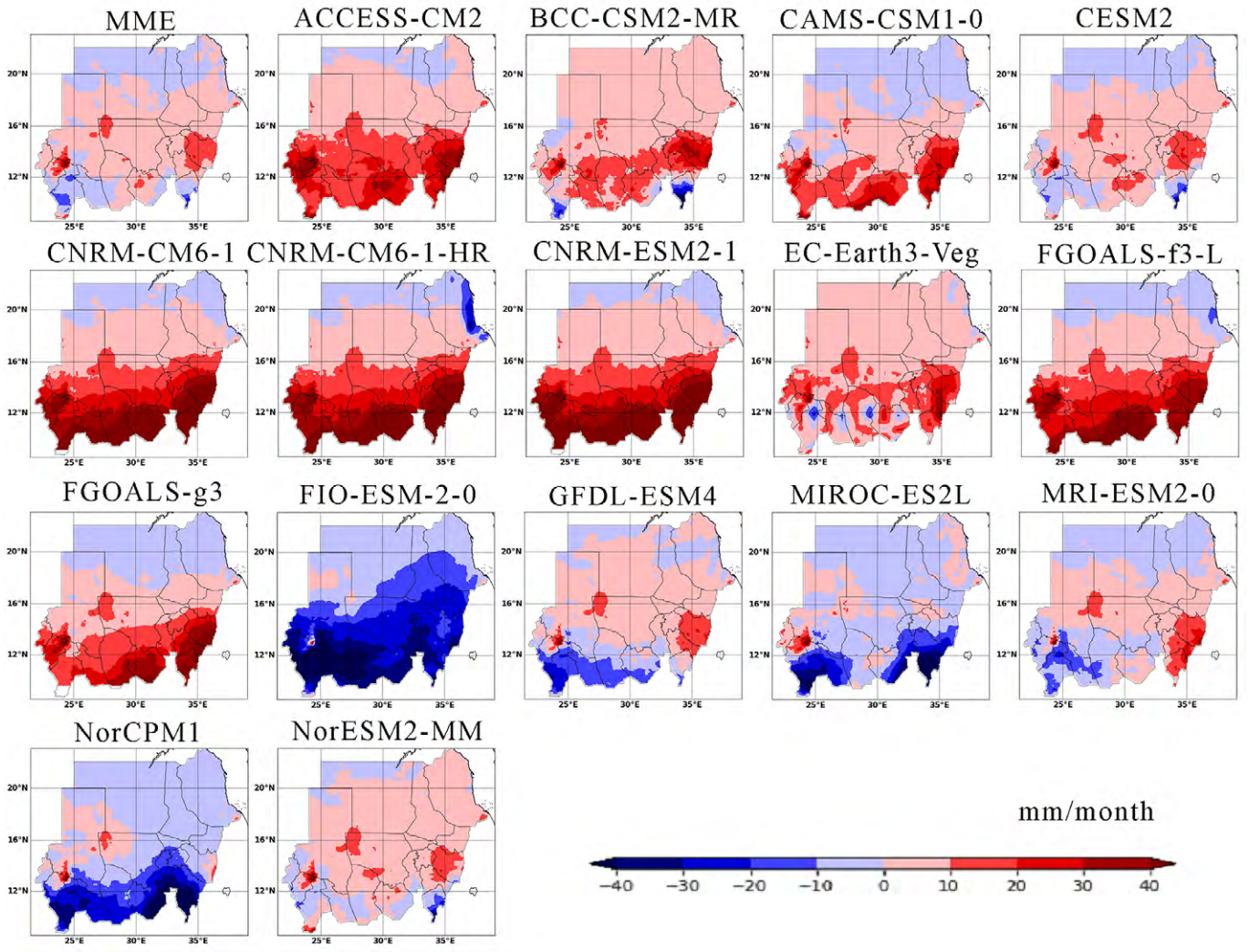

Figure 11. Bias of mean annual rainfall (mm/month) over Sudan based on CHIRPS Dataset 1985-2014

duced after applying the correction in comparison to the CHIRPS dataset. In addition, the reduction in the positive bias of the GCM estimates was more noticeable than the negative bias. MME and MIROC-ES2L demonstrate the lowest bias amount based on CHIRPS data, more so, they show better performance on the annual and seasonal (JJAS) scale after applying the correction in comparison to other GCMs. For most GCMs, greater improvement in the model's performance was observed through the annual rainfall than the seasonal (JJAS) rainfall; however, only EC-Earth3-Veg showed a poor improvement of 3% over the original. Although BCC-CSM2-MR has reduced the bias amount after applying the correction; nerveless, it enlarged the bias domain over the study area, which cannot be ignored and might result in more uncertainties in the future projection. The model's ensemble mean has proved its ability to be trusted for any further analysis regarding future projections among the annual and seasonal phases, according to their shown performance against the observations. Overall, the spatial mean bias correction of GCMs rainfall distribution using the CHIRPS dataset is an effective method for improving the accuracy of GCM precipitation estimates. However, it is important to note that the correction is not perfect and should be used with caution, especially in regions with complex precipitation patterns.

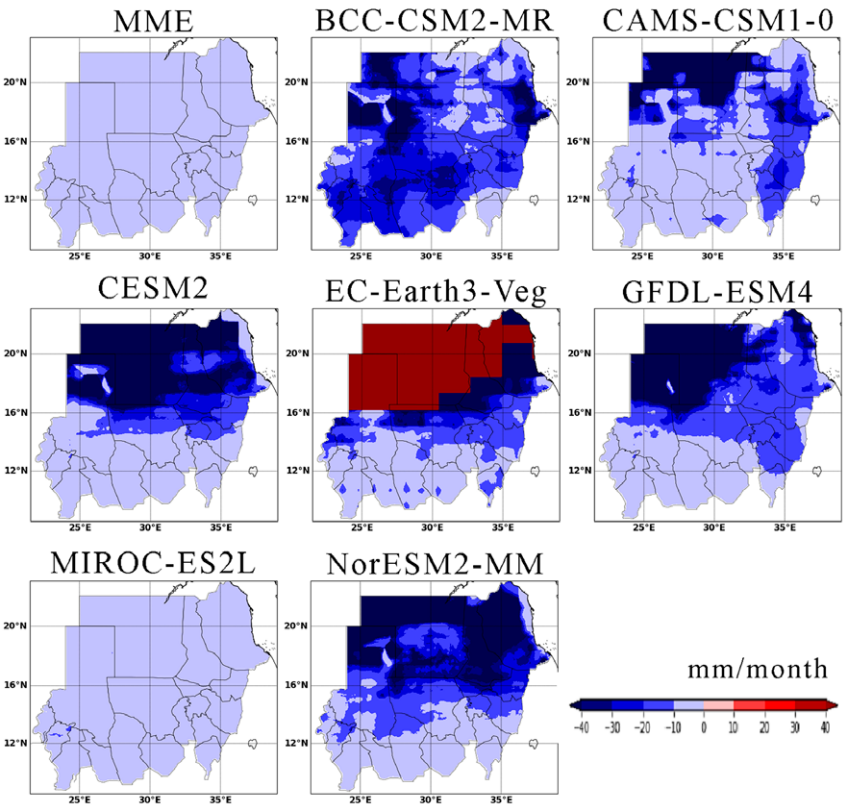

Figure 12. Spatial pattern of Bias after correction JJAS Rainfall period 1985–2014 based on CHIRPS dataset

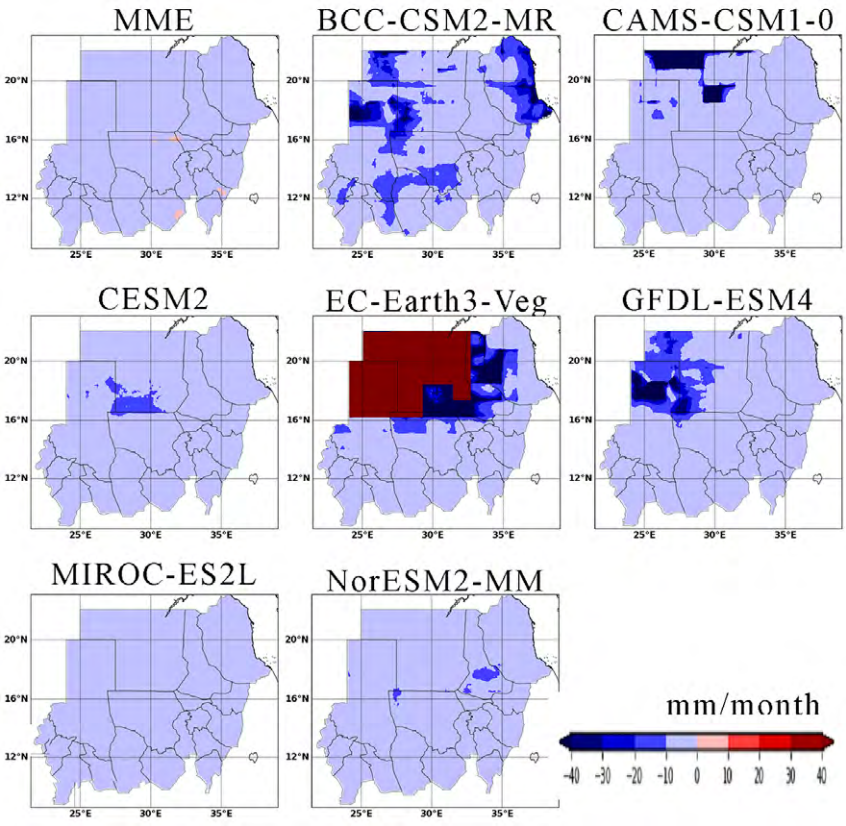

Figure 13. Spatial pattern of Bias after correction of annual rainfall from 1985–2014 based on the CHIRPS dataset

Discussion

Climate models, such as those included in the Coupled Model Intercomparison Project Phase 6 (CMIP6), are critical tools in understanding and projecting future climate change. These models simulate the most complex aspects of the climate system, including rainfall, sea level, temperature, and ocean circulation, and are used to inform policymakers, as well as businesses and individuals, about the expected impacts of climate change. One of crucial regions that requires accurate evaluation of climate models is the study domain, is the study domain highly vulnerable to the impacts of climate change. Climate models need to simulate rainfall patterns correctly to aid decision-makers in developing strategies to mitigate the effects of climate change on agriculture and other activities. This study used high-resolution satellite-based precipitation with Station (CHIRPS.v2) monthly precipitation datasets with a 0.05° × 0.05° spatial resolution (Babaousmail et al., 2019; Ngoma et al., 2021). While previous studies on this domain, used source observation data over Sudan and employed CRU TS as reference data, they examine the changes in monsoon's (June–September) future precipitation over three zones distributed through Sudan based on GCMs from CMIP5 and (CMIP6). The models are GISS-E2-H, IPSL- CM5A-MR, and MPI-ESM-LR (BCC-CSM2-MR, INM-CM4-9 MPI-ESM1-2-LR) in addition to the ensemble mean of each group Given systematic errors in the GCMs simulations (Hamadalnel et al., 2022). Therefore, in this study, we focused on the evaluation and correction analysis of the regional rainfall simulation of the CMIP6 model over Sudan, considering the rainfall pattern, evaluation of the rainfall simulation, spatial distribution of bias, and bias correction. Before evaluating rainfall simulations, it is essential first to understand the observed rainfall pattern to ensure the accuracy of the results. Sudan's rainfall pattern is primarily influenced by the African monsoon system, which is responsible for most of the country's annual precipitation and seasonal (JJAS) from June to September. Observations of rainfall patterns in Sudan showed that the distribution of rainfall varies significantly across the region. The Southern region received the highest amount of rainfall of 120 mm (Figures 8 and 9), while the Northern part received the least.

Sudan also experiences rainfall variability, which is attributed to the large-scale circulation patterns, such as the Inter-Tropical Convergence Zone (ITCZ) and the El-Nino Southern Oscillation (ENSO) (Alriah et al., 2021). In this study, the evaluation was conducted based on metrics such as the correlation coefficient (R), RMSE, and the Taylor diagram, which provides a graphical representation of the accuracy of the simulated rainfall pattern. The results of the evaluation showed that most of the employed CMIP6 models for this study accurately simulated the rainfall pattern over Sudan in annual and seasonal, but with a positive bias in most parts of Sudan, particularly in the Northwestern part of the country.

The Coupled Model Intercomparing Project (CMIP), which is at the cutting edge of exploring the depth of the planet's past, present, and future climate, has emerged as a key tool in climate science, providing the scientific communities with crucial data for research that informs important assessment activities like the ongoing IPCC process and other fields (Taylor et al., 2012). An assessment of the simulated findings of these GCMs versus the observation must be completed before taking a prospective look at potential future changes, particularly on a regional scale. In most cases, this process is carried out by comparing the simulations to the observations (Trigo & Palutikof, 2001), since it guarantees that the models can accurately represent some aspects of the climate system while employing model performance indicators to assess their potential and limitations (Gleckler et al., 2008). Consequently, the projection process is possible. The results of this study highlight the importance of evaluating and correcting biases in climate models to provide accurate information for future studies of climate change projection.

Conclusion

The study presents the evaluation and performance of 16 GCMs-CMIP6 models and compares their ability to accurately replicate observational satellite-based data over Sudan between 1985 and 2014. After conducting comprehensive statistical error measurements of the GCMs models' products over Sudan including Pearson Correlation Coefficient, Standard Deviation, Taylor Skill Score, Mean Absolute Error, absolute bias (BIAS), and, normalized mean root square error, we found that:

1. MME, which averaged the better GCMs models, demonstrated the strongest overall performance. Additionally, three individual models – NorESM2-MM, MIROC-ES2L, and BCC-CSM2-MR – proved relative accuracy (-12 to 12 mm of mean bias before correction) in reproducing both annual and seasonal patterns. However, several models, including ACCESS-CM2, FGOALS-f3-L, FGOALS-g3, CNRM-CM6-1, CNRM-CM6-1-HR, CNRM-ESM2-1, and CNRM-ESM2-1, performed poorly in simulating the observed data.
2. The models improved by 0-18% over the origin progress after applying bias correction (Delta method),

especially the ensemble mean (MME). In contrast, some CMIP6 models had slight deviations from the observations.

Generally, the study suggests that the MME and the three individual models offer the most promising options for future modeling efforts and have a satisfactory performance after correction.

Author declaration: *All authors declare that: there is no conflict of interest.*

Reference

Ahmed, N., & Elhag, M. M. (2011). Major climate indicators of ongoing drought in Sudan. *Journal of Hydrology*, 409(3–4), 612–625. https://doi.org/10.1016/j.jhydrol.2011.08.047

Akurut, M., Willems, P., & Niwagaba, C. B. (2014). Potential impacts of climate change on precipitation over lake Victoria, East Africa, in the 21st century. *Water*, 6(9), 2634–2659. https://doi.org/10.3390/w6092634

Alhuseen, A. (2014). *Analysis of policy network of adapting to climate change in Sudan*. 4(11), 1–4. https://www.ijsrp.org/research-paper-1114.php?rp=P353366

Almazroui, M., Saeed, F., Saeed, S., Nazrul Islam, M., Ismail, M., Klutse, N. A. B., & Siddiqui, M. H. (2020). Projected Change in Temperature and Precipitation Over Africa from CMIP6. *Earth Systems and Environment*, 4(3), 455–475. https://doi.org/10.1007/s41748-020-00161-x

Alriah, M. A. A., Bi, S., Nkunzimana, A., Elameen, A. M., Sarfo, I., & Ayugi, B. (2022). Multiple gridded-based precipitation products' performance in Sudan's different topographical features and the influence of the Atlantic Multidecadal Oscillation on rainfall variability in recent decades. *International Journal of Climatology*, 1–28. https://doi.org/10.1002/joc.7845

Alriah, M. A. A., Bi, S., Shahid, S., Nkunzimana, A., Ayugi, B., Ali, A., Bilal, M., Teshome, A., Sarfo, I., & Elameen, A. M. (2021). Summer monsoon rainfall variations and its association with atmospheric circulations over Sudan. *Journal of Atmospheric and Solar-Terrestrial Physics*, 225, 105751. https://doi.org/10.1016/j.jastp.2021.105751

Babaousmail, H., Hou, R., Ayugi, B., & Gnitou, G. T. (2019). Evaluation of satellite-based precipitation estimates over Algeria during 1998–2016. *Journal of Atmospheric and Solar-Terrestrial Physics*, 195, 105139. https://doi.org/10.1016/j.jastp.2019.105139

Babaousmail, H., Hou, R., Ayugi, B., Ojara, M., Ngoma, H., Karim, R., Rajasekar, A., & Ongoma, V. (2021). Evaluation of the performance of cmip6 models in reproducing rainfall patterns over north africa. *Atmosphere*, 12(4), 1–25. https://doi.org/10.3390/atmos12040475

Babaousmail, H., Hou, R., Ayugi, B., Sian, K. T. C. L. K., Ojara, M., Mumo, R., Chehbouni, A., & Ongoma, V. (2022). Future changes in mean and extreme precipitation over the Mediterranean and Sahara regions using bias-corrected CMIP6 models. *International Journal of Climatology*, 42(14), 7280–7297. https://doi.org/10.1002/joc.7644

Badr, H. S., Dezfuli, A. K., Zaitchik, B. F., & Peters-Lidard, C. D. (2016). Regionalizing Africa: Patterns of precipitation variability in observations and global climate models. *Journal of Climate*, 29(24), 9027–9043. https://doi.org/10.1175/JCLI-D-16-0182.1

Bao, Y., Song, Z., & Qiao, F. (2020). FIO-ESM Version 2.0: Model Description and Evaluation. *Journal of Geophysical Research: Oceans*, 125(6), 1–21. https://doi.org/10.1029/2019JC016036

Bethke, I., Wang, Y., Counillon, F., Keenlyside, N., Kimmritz, M., Fransner, F., Samuelsen, A., Langehaug, H., Svendsen, L., Chiu, P. G., Passos, L., Bentsen, M., Guo, C., Gupta, A., Tjiputra, J., Kirkeväg, A., Olivié, Di., Seland, Ø., Solsvik Vägane, J., Fan, Y., & Eldevik, T. (2021). NorCPM1 and its contribution to CMIP6 DCPP. *Geoscientific Model Development*, 14(11), 7073–7116. https://doi.org/10.5194/gmd-14-7073-2021

Collins, M., & Senior, C. A. (2002). Projections of future climate change. *Weather*, 57(8), 283-287. https://doi.org/10.1256/004316502320517371

El Gamri, T., Saeed, A. B., & Abdalla, A. (2021). Rainfall of the Sudan: Characteristics and Prediction. *Journal of Faculty of Arts, University of Khartoum*, 27. https://doi.org/10.53332/jfa.v27i.624

Elramlawi, H. R., Mohammed, H. I., Elamin, A. W., Abdallah, O. A., & Taha, A. A. A. M. (2019). Adaptation of sorghum (Sorghum bicolor L. Moench) crop yield to climate change in eastern dryland of Sudan. *Handbook of Climate Change Resilience; Springer: Cham, Switzerland*, 2549-2573. https://doi.org/10.1007/978-3-319-71025-9

Expósito, F. J., González, A., Pérez, J. C., Díaz, J. P., & Taima, D. (2015). High-resolution future projections of temperature and precipitation in the Canary Islands. *Journal of Climate*, 28(19), 7846-7856.

Gleckler, P. J., Taylor, K. E., & Doutriaux, C. (2008). Performance metrics for climate models. *Journal of Geophysical Research Atmospheres*, 113(6), 1–20. https://doi.org/10.1029/2007JD008972

Hajima, T., Watanabe, M., Yamamoto, A., Tatebe, H., Noguchi, M. A., Abe, M., Ohgaito, R., Ito, A., Yamazaki, D., Okajima, H., Ito, A., Takata, K., Ogochi, K., Watanabe, S., & Kawamiya, M. (2020). Development of

the MIROC-ES2L Earth system model and the evaluation of biogeochemical processes and feedbacks. *Geoscientific Model Development*, 13(5), 2197–2244. https://doi.org/10.5194/gmd-13-2197-2020

Hamadalnel, M., Zhu, Z., Gaber, A., Iyakaremye, V., & Ayugi, B. (2022). Possible changes in Sudan's future precipitation under the high and medium emission scenarios based on bias adjusted GCMs. *Atmospheric Research*, 269, 106036. https://doi.org/10.1016/j.atmosres.2022.106036

Hemanandhini, S., & Vignesh, R. L. (2023). Performance evaluation of CMIP6 climate models for selecting a suitable GCM for future precipitation at different places of Tamil Nadu. *Environmental Monitoring and Assessment*, 195(8), 928-928. https://doi.org/10.1007/s10661-023-11454-9

Ishida, K., Ercan, A., Trinh, T., Jang, S., Kavvas, M. L., Ohara, N., Chen, Z. Q., Kure, S., & Dib, A. (2020). Trend analysis of watershed-scale annual and seasonal precipitation in Northern California based on dynamically downscaled future climate projections. *Journal of Water and Climate Change*, 11(1), 86–105. https://doi.org/10.2166/wcc.2018.241

Karim, R., Tan, G., Ayugi, B., Shahzaman, M., Babaousmail, H., Ngoma, H., & Ongoma, V. (2023). Projected changes in surface air temperature over Pakistan under bias-constrained CMIP6 models. *Arabian Journal of Geosciences*, 16(3), 205. https://doi.org/10.1007/s12517-023-11243-1

Kawai, H., Yukimoto, S., Koshiro, T., Oshima, N., Tanaka, T., Yoshimura, H., & Nagasawa, R. (2019). Significant improvement of cloud representation in the global climate model MRI-ESM2. *Geoscientific Model Development*, 12(7), 2875–2897. https://doi.org/10.5194/gmd-12-2875-2019

Klutse, N. A. B., Quagraine, K. A., Nkrumah, F., Quagraine, K. T., Berkoh-Oforiwaa, R., Dzrobi, J. F., & Sylla, M. B. (2021). The Climatic Analysis of Summer Monsoon Extreme Precipitation Events over West Africa in CMIP6 Simulations. *Earth Systems and Environment*, 5(1), 25–41. https://doi.org/10.1007/s41748-021-00203-y

Kumar, P., Wiltshire, A., Mathison, C., Asharaf, S., Ahrens, B., Lucas-Picher, P., Christensen, J. H., Gobiet, A., Saeed, F., Hagemann, S., & Jacob, D. (2013). Downscaled climate change projections with uncertainty assessment over India using a high resolution multi-model approach. *Science of the Total Environment*, 468, S18-S30. https://doi.org/10.1016/j.scitotenv.2013.01.051

Maroneze, M. M., Zepka, L. Q., Vieira, J. G., Queiroz, M. I., & Jacob-Lopes, E. (2014). The primary tools of the analyses targeted at determining what climate we are likely to have in the near and not-so-near future use dynamical downscaling with Regional Climate Models (RCMs) and Global Climate Models (GCMs). *Revista Ambiente e Agua*, 9(3), 445–458. https://doi.org/10.4136/1980-993X

Meehl, G. A., Arblaster, J. M., Bates, S., Richter, J. H., Tebaldi, C., Gettelman, A., Medeiros, B., Bacmeister, J., DeRepentigny, P., Rosenbloom, N., Shields, C., Hu, A., Teng, H., Mills, M. J., & Strand, G. (2020). Characteristics of Future Warmer Base States in CESM2. *Earth and Space Science*, 7(9). https://doi.org/10.1029/2020EA001296

Mendez, M., Maathuis, B., Hein-Griggs, D., & Alvarado-Gamboa, L. F. (2020). Performance evaluation of bias correction methods for climate change monthly precipitation projections over Costa Rica. *Water*, 12(2). https://doi.org/10.3390/w12020482

Mkala, E. M., Mwanzia, V., Nzei, J., Oluoch, W. A., Ngarega, B. K., Wanga, V. O., Oulo, M. A., Munyao, F., Kilingo, F. M., Rono, P., Waswa, E. N., Mutinda, E. S., Ochieng, C. O., Mwachala, G., Hu, G. W., Wang, Q. F., Katunge, J. K., & Victoire, C. I. (2023). Predicting the potential impacts of climate change on the endangered endemic annonaceae species in east africa. *Heliyon*, 9(6), e17405. https://doi.org/10.1016/j.heliyon.2023.e17405

Ngoma, H., Wen, W., Ojara, M., & Ayugi, B. (2021). Assessing current and future spatiotemporal precipitation variability and trends over Uganda, East Africa, based on CHIRPS and regional climate model datasets. *Meteorology and Atmospheric Physics*, 133(3), 823–843. https://doi.org/10.1007/s00703-021-00784-3

Rajbhandari, R., Shrestha, A. B., Nepal, S., & Wahid, S. (2018). Projection of Future Precipitation and Temperature Change over the Transboundary Koshi River Basin Using Regional Climate Model PRECIS. *Atmospheric and Climate Sciences*, 08(02), 163–191. https://doi.org/10.4236/acs.2018.82012

Rajbhandari, R., Shrestha, A. B., Nepal, S., & Wahid, S. (2018). Projection of future precipitation and temperature change over the transboundary Koshi River basin using regional climate model PRECIS. *Atmospheric and Climate Sciences*, 8(2), 163-191. https://doi.org/10.4236/acs.2018.82012

Salih, A. A. M., Zhang, Q., & Tjernström, M. (2015). Lagrangian tracing of Sahelian Sudan moisture sources. *Journal of Geophysical Research*, 120(14), 6793–6808. https://doi.org/10.1002/2015JD023238

Séférian, R., Nabat, P., Michou, M., Saint-Martin, D., Voldoire, A., Colin, J., Decharme, B., Delire, C., Berthet, S., Chevallier, M., Sénési, S., Franchisteguy, L., Vial, J., Mallet, M., Joetzjer, E., Geoffroy, O., Guérémy, J. F., Moine, M. P., Msadek, R., Ribes, A., Rocher, M., Roehrig, R., Salas-y-Mélia, D., Sanchez, E., Terray, L., Valcke, S., Waldman, R., Aumont, O., Bopp, L., Deshayes, J., Éthé, C., & Madec, G. (2019). Evaluation of CNRM Earth System Model, CNRM-ESM2-1: Role of Earth System Processes in Present-Day and Future Climate. *Journal of Advances in Modeling Earth Systems*, 11(12), 4182–4227. https://doi.org/10.1029/2019MS001791

Seland, Ø., Bentsen, M., Seland Graff, L., Olivié, D., Toniazzo, T., Gjermundsen, A., Debernard, J. B., Gupta, A. K., He, Y., Kirkevåg, A., Schwinger, J., Tjiputra, J., Schancke Aas, K., Bethke, I., Fan, Y., Griesfeller, J., Grini, A., Guo, C., Ilicak, M., … Schulz, M. (2020). The Norwegian Earth System Model, NorESM2 – Evaluation of theCMIP6 DECK and historical simulations. *Geoscientific Model Development Discussions*, *February*, 1–68. https://doi.org/10.5194/gmd-13-6165-2020

Siddig, K., Stepanyan, D., Wiebelt, M., Grethe, H., & Zhu, T. (2020). Climate change and agriculture in the Sudan: Impact pathways beyond changes in mean rainfall and temperature. *Ecological Economics*, 169, 106566. https://doi.org/10.1016/j.ecolecon.2019.106566

Taylor, K. E., Stouffer, R. J., & Meehl, G. A. (2012). An overview of CMIP5 and the experiment design. *Bulletin of the American Meteorological Society*, 93(4), 485–498. https://doi.org/10.1175/BAMS-D-11-00094.1

Tegegne, G., & Mellesse, A. M. (2022). Multimodel ensemble projection of precipitation over South Korea using the reliability ensemble averaging. *Theoretical and Applied Climatology*, 1205–1214. https://doi.org/10.1007/s00704-022-04350-8

Trigo, R. M., & Palutikof, J. P. (2001). Precipitation scenarios over Iberia: A comparison between direct GCM output and different downscaling techniques. *Journal of Climate*, 14(23), 4422–4446. https://doi.org/10.1175/1520-0442(2001)014<4422:PSOIAC>2.0.CO;2

Voldoire, A., Saint-Martin, D., Sénési, S., Decharme, B., Alias, A., Chevallier, M., Colin, J., Guérémy, J. F., Michou, M., Moine, M. P., Nabat, P., Roehrig, R., Salas y Mélia, D., Séférian, R., Valcke, S., Beau, I., Belamari, S., Berthet, S., Cassou, C., … Waldman, R. (2019). Evaluation of CMIP6 DECK Experiments With CNRM-CM6-1. *Journal of Advances in Modeling Earth Systems*, 11(7), 2177–2213. https://doi.org/10.1029/2019MS001683

Walthall, C. L. . (2012). Climate Change and Agriculture in the US. *USDA Technical Bulletin 1935*, 186. https://doi.org/10.1016/j.ecolecon.2019.106566

Wang, H., Li, L., Chen, X., & Wang, B. (2022). Evaluating the Nature and Extent of Changes to Climate Sensitivity Between FGOALS-g2 and FGOALS-g3. *Journal of Geophysical Research: Atmospheres*, 127(3), 1–19. https://doi.org/10.1029/2021JD035852

Weijer, W., Cheng, W., Garuba, O. A., Hu, A., & Nadiga, B. T. (2020). CMIP6 Models Predict Significant 21st Century Decline of the Atlantic Meridional Overturning Circulation. *Geophysical Research Letters*, 47(12). https://doi.org/10.1029/2019GL086075

Williams, M., & Nottage, J. (2006). Impact of extreme rainfall in the central Sudan during 1999 as a partial analogue for reconstructing early Holocene prehistoric environments. *Quaternary International*, 150(1), 82-94. https://doi.org/10.1016/j.quaint.2006.01.009

Wu, T., Yu, R., Lu, Y., Jie, W., Fang, Y., Zhang, J., Zhang, L., Xin, X., Li, L., Wang, Z., Liu, Y., Zhang, F., Wu, F., Chu, M., Li, J., Li, W., Zhang, Y., Shi, X., Zhou, W., Yao, J., Liu, X., Zhao, H., Yan, J., Wei, M., Xue, W., Huang, A., Zhang, Y., Zhang, Y., Shu, Q., & Hu, A. (2021). BCC-CSM2-HR: A high-resolution version of the Beijing Climate Center Climate System Model. *Geoscientific Model Development*, 14(5), 2977–3006. https://doi.org/10.5194/gmd-14-2977-2021

Zheng, X., Li, Q., Zhou, T., Tang, Q., Van Roekel, L. P., Golaz, J. C., Wang, H., & Cameron-Smith, P. (2022). Description of historical and future projection simulations by the global coupled E3SMv1.0 model as used in CMIP6. *Geoscientific Model Development*, 15(9), 3941–3967. https://doi.org/10.5194/gmd-15-3941-2022

INTERNATIONAL SCIENTIFIC JOURNAL
GEOGRAPHICA PANNONICA
Volume 28, Issue 1, 71–84 (March 2024)
Contents lists available at ScienceDirect
Journal homepage: http://www.dgt.uns.ac.rs/en/homepage/pannonica/

Assessing Pedestrian Thermal Comfort to Improve Walkability in the Urban Tropical Environment of Nagpur City

Shivanjali Mohite[A*], Meenal Surawar[A]

[A] *Department of Architecture and Planning, Visvesvaraya National Institute of Technology (VNIT) Nagpur, Maharashtra, India; shivanjali.mohite@students.vnit.ac.in, meenalms28oct@gmail.com*

KEYWORDS

Walkability
Sustainable Transportation
Microclimate
Pedestrian Thermal Comfort

ABSTRACT

Walking can be an efficient and sustainable mode of transportation for "last mile" connectivity. However, the willingness to walk largely depends on the availability of infrastructure, safety, and comfort. Improving thermal comfort on streets connected to transit stations is crucial for encouraging walking and public transit use. This study assesses seasonal and spatiotemporal variations in pedestrian thermal comfort (PTC) on an N-S-oriented street in Nagpur (India). Thermal walk surveys simultaneously monitored environmental conditions and human thermal perception (thermal sensation vote- TSV). The findings revealed that urban geometry significantly influences PTC and TSV, and the level of influence varied spatiotemporally in both seasons. This study shows the relationship between urban street geometry, microclimate, and PTC, emphasizing the necessity of a multidimensional assessment approach.

Introduction

In recent years, urbanization has resulted in significant changes in land use, characterized by dense built-up areas, extensive pavement, and less vegetation (Zhou & Chen, 2018). These changes have led to adverse environmental and local microclimate consequences, such as the Urban Heat Island effect (UHI), which increases heat stress (Kotharkar et al., 2018; Oke, 1988). The increasing heat stress significantly impacts the quality of outdoor places by decreasing comfort (Nikolopoulou & Lykoudis, 2006; Yahia et al., 2018). The uncomfortable outdoor conditions discourage people from choosing sustainable last-mile connectivity options such as walking and cycling (Arif & Yola, 2020). Instead, many choose motorized vehicles, which increase carbon emissions, air pollution, and traffic congestion. Improving walkability to address these issues and promoting sustainable transportation options is crucial (Chidambara, 2019; Shamsuddin et al., 2012). There are several barriers to walkability, such as the availability of pedestrian infrastructure, accessibility, connectivity, safety, and comfort. Pedestrians in tropical climates face challenges due to extreme heat, humidity, and prolonged sun exposure, which makes walking less feasible (Deevi & Chundeli, 2020). Improving the thermal comfort on streets that connect to transit stations is essential to promote walking and public transit use.

* Corresponding author: Shivanjali Mohite; email: shivanjali.mohite@students.vnit.ac.in, shivanjalimasad12@gmail.com

doi: 10.5937/gp28-48166

Received: December 12, 2023 | Revised: March 05, 2023 | Accepted: March 22, 2023

Literature Review

Thermal comfort refers to the degree of satisfaction and well-being experienced by individuals while walking or moving through outdoor spaces (ASHRAE, 2023; Vasilikou & Nikolopoulou, 2020). The thermal environment influences how individuals perceive and experience outdoor space (Nikolopoulou et al., 2001). It encompasses various physical, psychological, and environmental factors that influence a person's comfort (Chen et al., 2012; Lau et al., 2019; Nikolopoulou & Lykoudis, 2006; Vasilikou & Nikolopoulou, 2013).

Pedestrian thermal comfort (PTC) is influenced by microclimatic parameters such as air temperature, humidity, and wind speed, etc. The microclimate at the street level is influenced by urban geometry, which includes factors such as aspect ratio, sky view factor, and street orientation (Ahmadi Venhari et al., 2019; Jamei & Rajagopalan, 2015; Krüger, 2011). The street orientation and aspect ratio of buildings determine solar exposure and shadow patterns, affecting surface and air temperature variations throughout the day (Baghaeipoor & Nasrollahi, 2019; Cliff Moughtin, 2003; Svensson, 2004). In additional, the density of buildings can influence wind speed, leading to changes in thermal conditions. The presence of trees helps regulate temperature by providing shade and transpiration (Kim & Brown, 2022; Kotharkar et al., 2023; Mahmoud et al., 2021).

Previous studies have shown that a comprehensive understanding of PTC requires an assessment of the thermal environment both objectively and subjectively (Deevi & Chundeli, 2020; Lau et al., 2019; Peng et al., 2022; Vasilikou & Nikolopoulou, 2013). The objective assessment of the thermal environment involves quantifying thermal comfort based on the heat balance of the human body and its heat exchange with the surrounding environment. Various methods and indices have been developed to evaluate PTC. These indices include the predicted mean vote (PMV) (Van Hoof, 2008), the universal thermal climate index (UTCI) (Błazejczyk et al., 2013), and physiologically equivalent temperature (PET) (Mayer & Höppe, 1987). The PMV index evaluates the thermal sensation of people considering microclimatic parameters. The index is widely accepted but can be overly sensitive to wind speed variations, limiting its suitability for tropical hot and dry climates. The UTCI index is a widely known index that uses a simple equation to evaluate thermal comfort based on microclimatic variables. However, it does not consider the physiological aspects of humans, such as metabolic rate and clothing. The current study uses the modified Physiologically Equivalent Temperature Index (mPET) (Chen et al., 2018), which is a modified version of the PET index. The PET is the physiologically equivalent temperature at any given place (outdoors or indoors). It is equivalent to the air temperature at which the human body's heat balance is maintained, with core and skin temperatures equal to those under the assessed conditions. The mPET enhances accuracy by considering thermo-physiological parameters of the human body and climatic factors. Unlike other indices, mPET incorporates a multi-node heat transport model and a self-adapting multi-layer clothing model, providing a more realistic analysis of the impact of climate on humans (Chen et al., 2020; Pecelj et al., 2021).

Subjective assessment of the thermal environment involves the analysis of thermal sensation through people's perception. Thermal sensation is a specific aspect of PTC; it pertains to individuals' immediate perception of the microclimate in their surroundings (Nikolopoulou & Lykoudis, 2006). The "thermal walk" method helps analyze the thermal sensation (Vasilikou & Nikolopoulou, 2013). Thermal walks help to understand how people perceive outdoor environmental conditions in urban settings. During a thermal walk, participants walk through various locations within a specific area, carefully evaluating the thermal conditions at each location. This requires close observation and analysis of the unique thermal attributes that characterize different urban environments.

Research Gap

In India, walkability studies have been conducted by several researchers and authorities, such as the Evangelical Social Action Forum conducted a walkability survey in Nagpur and Kochi (ESAF, 2017), while the Clean air initiative organization conducted surveys in Pune, Bangalore, Bhubaneshwar, Chennai, Rajkot, Surat, Kota, and Indore (Clean air initiative for Asian cities center, 2011). The survey used the Global Walkability Index methodology from the World Bank, involving field surveys, pedestrian preferences, and government policy assessments. These studies focused on walkability from the infrastructure and safety perspective and did not include thermal comfort.

Several studies have been conducted in different cities in India that assess outdoor thermal comfort and the impact of heat stress on people using outdoor environments. Most studies have focused on a neighborhood scale, public parks, etc. (Anupriya & Rubeena, 2023; Kotharkar et al., 2024; Kumar et al., 2022; Salal et al., 2021). Some studies have considered assessing thermal comfort on the street level. However, in these studies, the streets are analyzed as singular locations rather than on the microscale of individual streets (Banerjee et al., 2022; Kotharkar et al., 2019; Manavvi & Rajasekar, 2020). Very few studies have assessed PTC on sidewalks and the impact of urban geometry and microclimate on pedestrians while walking (Chidambaranath & Bitossi, 2018; Deevi & Chundeli, 2020).

Aim and Objective

This study aims to assess and enhance pedestrian walkability on the street level by evaluating PTC on the street that fulfills walkability parameters, using objective (mPET index) and subjective (TSV) methods. The study aims to

achieve three objectives: 1) compare dynamic changes in pedestrians' thermal sensation and comfort concerning variations in urban geometry, 2) identify significant variations in thermal stress with microclimatic factors, and 3) determine the neutral value of mPET, serving as a benchmark for thermal stress in Nagpur city. This pilot study introduces a methodological framework that can be employed in future studies.

Research Area

The study was conducted in Nagpur, Maharashtra, India (21.1458° N and 79.0882° E) (Fig.1). Nagpur has a tropical savanna climate (Aw), with hot and dry summers and cool and dry winters, as per the Köppen-Geiger classification (Kottek et al., 2006). The city is developing as a fast-growing metro city and has a status as a smart city under the Smart City Mission India (India Smart City Mission, 2015). The Nagpur Metro Rail Project comprises two corridors, North–South measuring 19.6 km in length with 17 stations, and East–West measuring 18.5 km in length with 19 stations (Nagpur Metro Rail Corporation, 2023). The city's public transportation connectivity highlights the need to improve walkability around transportation hubs. As per the MOUD walkability index, the city has a walkability index of 0.65, which is above the national minimum average (Ministry of Urban Development, 2008). However, the city's tropical climate encounters significant temperature variations throughout the year, with winters bringing minimum temperatures of 12°C and summers seeing temperatures soaring up to 48°C, often accompanied by heatwaves (Katpatal et al., 2008; Laskar et al., 2016; Surawar & Kotharkar, 2017). This can result in uncomfortable outdoor environments and potential discomfort for pedestrians during summer and heatwave conditions.

The street was selected based on walkability parameters such as mixed land use typology, connectivity to the metro, and availability of pedestrian sidewalks on both sides of the streets. The New Shukrawari Road (Fig 2) is located at one of the prominent CBDs in Nagpur. The nearest metro station to this street is the Agrasen Square metro station, located on the north side of the street. The selected stretch of the street is approximately 1 km long and runs north-south. It is lined with buildings of varying heights, ranging from 1 to 5 floors, with various stores, restaurants, bars, shopping centers, offices, and residential spaces. The street is designed with distinct zones for vehicles and pedestrians. The vehicular zone comprises four lanes, and 1.5 mt wide sidewalks are on both sides of the street, designated as the Eastern and Western Sidewalks.

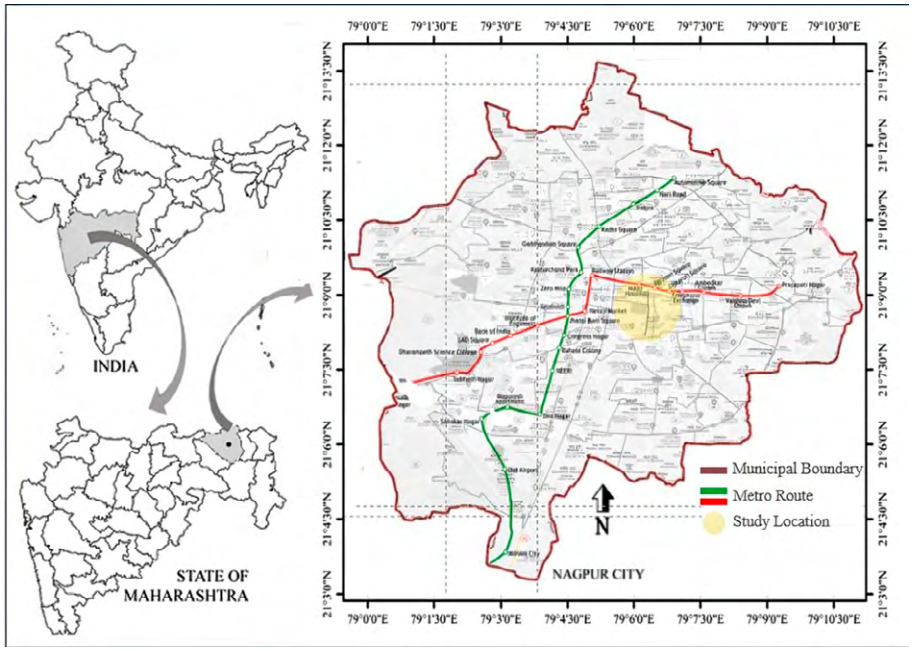

Figure 1. Location of Nagpur City and the study area

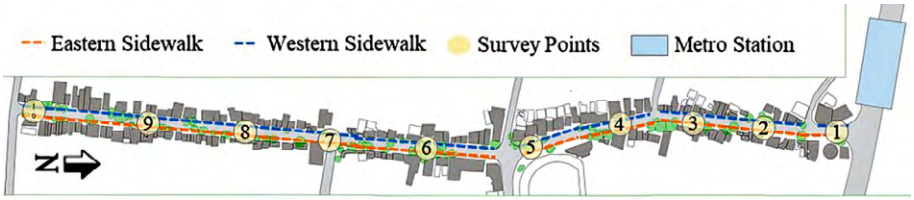

Figure 2. Digitized image of the New Sukrawari Road

Methodology

The study methodology is divided in 4 phases (Fig.3). In the first phase, the selected street was digitized using Arc-GIS software through satellite overviewing to map buildings, streets, vegetation, and sidewalks (Fig.2). The building and vegetation characteristics of the street are evaluated in Arc-GIS by calculating the Building Surface Area Fraction (BSF) (Eq.1), which shows a portion of the ground surface covered with a building footprint, and the Vegetation Density ratio (VDR) (Eq.2), which shows a portion of the ground surface covered with vegetation. These parameters range from 0 to 1. It provides the urban geometry characteristics of the entire street. The calculated BSF for this street is 0.65, and the VDR is 0.40.

$$BSF = L_B / L_s \quad (1)$$

$$VDR = A_V / A_s \quad (2)$$

Where,

- L_B =Total length of building surface facing the street
- L_s = Total length of the sidewalk
- A_V = Total area of vegetation
- A_s = Total area of the street

In second phase, a longitudinal thermal walk survey was conducted to collect microclimate, urban geometry, and pedestrian perception data. The street was divided into the 100m grid; thus, 10 survey points were studied (Fig.2). These points exhibit unequal building heights with varied aspect ratios and SVF to assess different scenarios of thermal conditions. The points on the east side of the street are named East 1, East 2, etc, whereas the points on the west side are West 1, West 2, etc. The survey campaign was conducted in the summer of 2022 (May 22, 2022) and winter 2023 (February 19, 2023) to understand seasonal variations in PTC. In each season, the microclimate and perception data were collected at three different times: 9:00 am -10:00 am, 11:30 am – 12:30 pm, and 5:00 pm – 6:00 pm. These particular time durations were studied because the maximum pedestrian movement around metro stations was observed during morning and evening hours. In contrast, the afternoon hours were studied to understand pedestrian behavior during peak solar radiation and higher radiant heat exposure. To eliminate temporal variations in background meteorological conditions, a survey route was followed to collect data on the same side first and then move to the opposite side (Fig. 3- Representative longitudinal survey route).

The initial data collection process encompassed conducting on-site observations at every survey point to document the urban geometry parameters of the location and measure climatic parameters along with the thermal perception of the participants (Fig.3). The climatic parameters include air temperature (Ta), surface temperature (Ts), relative humidity (RH), and wind speed (Ws). Following the ASHRAE-55 protocol, measurements were taken at a height of 1.2 m from the ground (ASHRAE, 2023; ASHRAE, 2013), using the MS 6252B Digital Anemometer for Ta, RH, and Ws measurements, while the surface temperature was measured using a Laser IR Thermometer-thermal gun. These

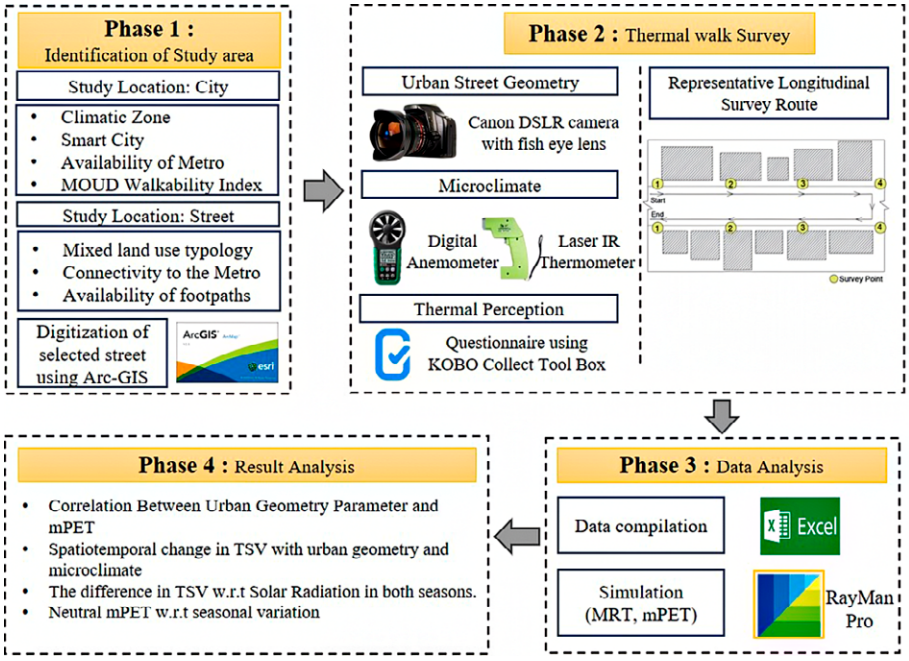

Figure 3. Methodology flow chart

instruments were calibrated and tested in the outdoor environment for their sensitivity before being used for field surveys. The response time of these instruments is 1 sec. The urban geometry parameters include the aspect ratio (AR) and sky view factor (SVF). AR was calculated by measuring street width and building height using Google Earth and Street View, respectively, and a Nikon DSLR camera with a fisheye lens was employed to capture SVF images.

For the perception survey, the questionnaire followed the ASHRAE outdoor thermal comfort protocol. The questionnaire was divided into two parts, first about personal information and second about thermal sensation. The second part of the questionnaire included three questions, and the options were given on a Likert scale. The first set of questions concerns the thermal perception of microclimatic parameters (5-point scale). The second set of questions includes thermal preference for microclimatic parameters (3-point scale); in microclimatic conditions, people would prefer to walk for maximum duration without feeling discomfort. The third set of questions includes the thermal sensation vote (ASHRAE 9-point scale) (Fig.4).

Perception survey data were collected using the KOBO Collect App. It is an Android-based app that helps to record the data initially in the app and then on a cloud server, which makes it easy to process and analyze the recorded data. The perception survey was conducted through a closed group survey during both seasons to capture the two climatic conditions. Six males and nine females aged between 19-31 years participated in the survey. The same people were asked to participate in both seasons to avoid disparity.

For every walk, the participants were asked to be present at the survey location and stand under shade for 15 minutes before the survey time to acclimatize to the microclimate. Each side of the street (approximately 1 km) The thermal walks were conducted in a guided survey manner; thus, all participants walked with a researcher who guided them to the location. The participants were asked to stand for 2 minutes at every location to record their responses. The researcher simultaneously recorded the microclimate and urban geometry data. It took approximately 30 minutes to complete a survey on one side of the street. 90 forms were collected for both sides of the street in a day, leading to a total data sample of 900 for each season, as there were ten survey points on either side of the street.

In the third phase, microclimate data collected were analyzed using the RayMan Pro tool to evaluate the mean radiant temperature (MRT) and the thermal comfort in-

Part 1: Personal Information and Thermal History

Gender: Male Female Other
Age: ≥20 20-30 30-40 40-50 50 and above
Height: __cm Weight: __kg
Clothing:

Part 2: Thermal sensation

1. **Standing in at this moment**

Under sunlight Building shade canopy shade Tree shade

2. **At This precise moment, do you find the following**

Humidity:	Dry	Slightly Dry	Neutral	Slightly Humid	Humid
Wind speed:	Less Windy	Slightly Less Windy	Neutral	Slightly Windy	Windy
Sunlight:	Soothing	Slightly Soothing	Neutral	Slightly Harsh	Harsh

3. **How would you prefer the following?**

Humidity:	Less Humid	Neutral	More Humid
Wind speed:	Less Wind	Neutral	More Wind
Sunlight:	Lower	Neutral	Higher

4. **How do you feel at this precise moment?**

Very Cold	Cold	Cool	Slightly Cool	Neutral	Slightly Warm	Warm	Hot	Very Hot
(-4)	(-3)	(-2)	(-1)	(0)	(1)	(2)	(3)	(4)

Figure 4. Thermal walk questionnaire

Figure 5. Thermal walk survey during winter and summer

dex, mPET. The RayMan Pro tool was also used to evaluate the actual solar radiations, considering the SVF, day, time, and geographical location for calculation. The perception data was compiled and evaluated in Microsoft Excel. In the fourth phase, Pearson's correlation was used to understand the impact of urban geometry parameters on the thermal comfort index. For this purpose, the SVF values were correlated with the mPET values, as the SVF represents all the features of urban geometry, including buildings, vegetation, and other built-up structures. The neutral value of mPET was derived using a regression equation between TSV and mPET values. A one-way ANOVA test was used to check the variation in TSV concerning microclimatic parameters.

Results

Urban Geometry and Microclimate Measurements

The field data observations show that the urban geometry of the studied locations is distinct (fig. 6), and there are considerable spatiotemporal variations in meteorological conditions along the walking routes on both sides of the road in two different seasons. As per urban geometry observations, for the eastern side, the ARmax observed is 1.3 at East 1 because there is a multistory building adjacent to the road, and the ARmin is 0 at East 5 because there is no building adjacent to the road. The SVF varied between the maximum value of 0.78 at East 5 due to the absence of a tree and minimum obstruction from built forms; the minimum value of SVF was 0.25 at East 6 due to a wide canopy tree. On the western side of the street, ARmax is observed at 0.80 at West1 as a multistory building adjacent to the road, and ARmin at 0.20 at West 2 and 3 as a single-story building. The SVF varied between the maximum value of 0.66 at west 3,4 due to the absence of a tree and minimum obstruction from built forms; the minimum value of SVF was 0.18 at west 6 due to a wide canopy tree.

On the N– S orientation street, the variation pattern of microclimatic parameters was observed to be similar in both seasons (fig. 7 and 8). On the eastern side, in the morning duration of 9:00–10:00 am, due to low solar radiation, Ta, Ts, and MRT were observed to be minimum, and RH was maximum. At 11:30 a.m.–12:30 p.m., the duration of RH was observed to decrease, and temperature values were increasing. The temperature values decrease in the evening, 5:00–6:00 p.m., and the RH increases. On the west side of the street, in the morning of 9:00–10:00 a.m., the Ta, Ts, and MRT were observed to be higher than those on the eastern side as this side receives direct solar radiation, and the temperature values were observed to be maximum during the afternoon period of 11:30–12:30 pm. The minimum temperature values were recorded in the evening from 5:00 to 6:00 p.m. The Ws were observed to be dynamic irrespective of the street side throughout the day. In the winter season (Fig. 7), the maximum and minimum solar radiation on the eastern sidewalk was 933.8 W/m² and 22.5 W/m², respectively. On the western sidewalk, it was 938.2 W/m² and 21 W/m². The maximum and minimum Ta values on the eastern sidewalk were 34°C and 26°C, respectively, and on the western sidewalk, the Ta values were 33°C and 25.6°C, respectively. The maximum and minimum RH on the eastern sidewalk was 47.6% and 25%, respectively, and on the western sidewalk, the RH was 46.3% and 26%, respectively. In the summer

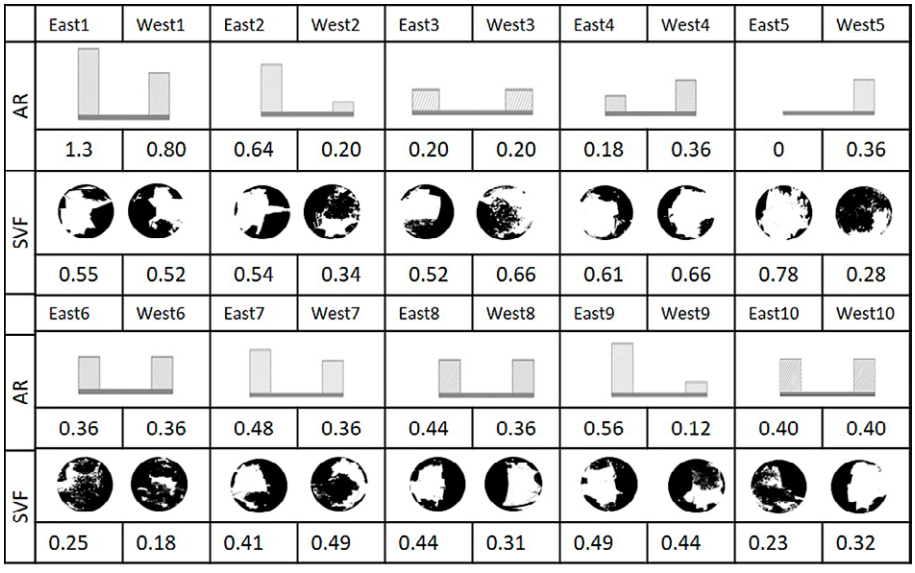

Figure 6. Survey locations with their respective aspect ratios and sky view factors

season (Fig.8), the maximum and minimum solar radiation on the eastern sidewalk was 1012 W/m² and 64.9 W/m², respectively. On the western sidewalk, it was 1015.3 W/m² and 44.7 W/m². The maximum and minimum Ta on the eastern sidewalk were 43.5°C and 36.7°C, respectively, and on the western sidewalk, Ta was 43.5°C and 37.5°C, respectively. The maximum and minimum RHs on the eastern sidewalk were 33.6% and 24%, respectively; on the western sidewalk, the RHs were 34.5% and 23.8%, respectively.

Thermal walks

From the responses of people's perception of individual microclimatic factors, it was observed that most of the participants preferred to walk on sidewalks shaded by buildings and vegetation irrespective of the season. The level of solar radiation and Ws largely influenced thermal perception (TSV). From simultaneous wind perception and Ws measurement, it was observed that participants voted Ws of more than 1m/s as neutral to windy. In winter, the mean TSV (mTSV) was between cool (-2) and slight-

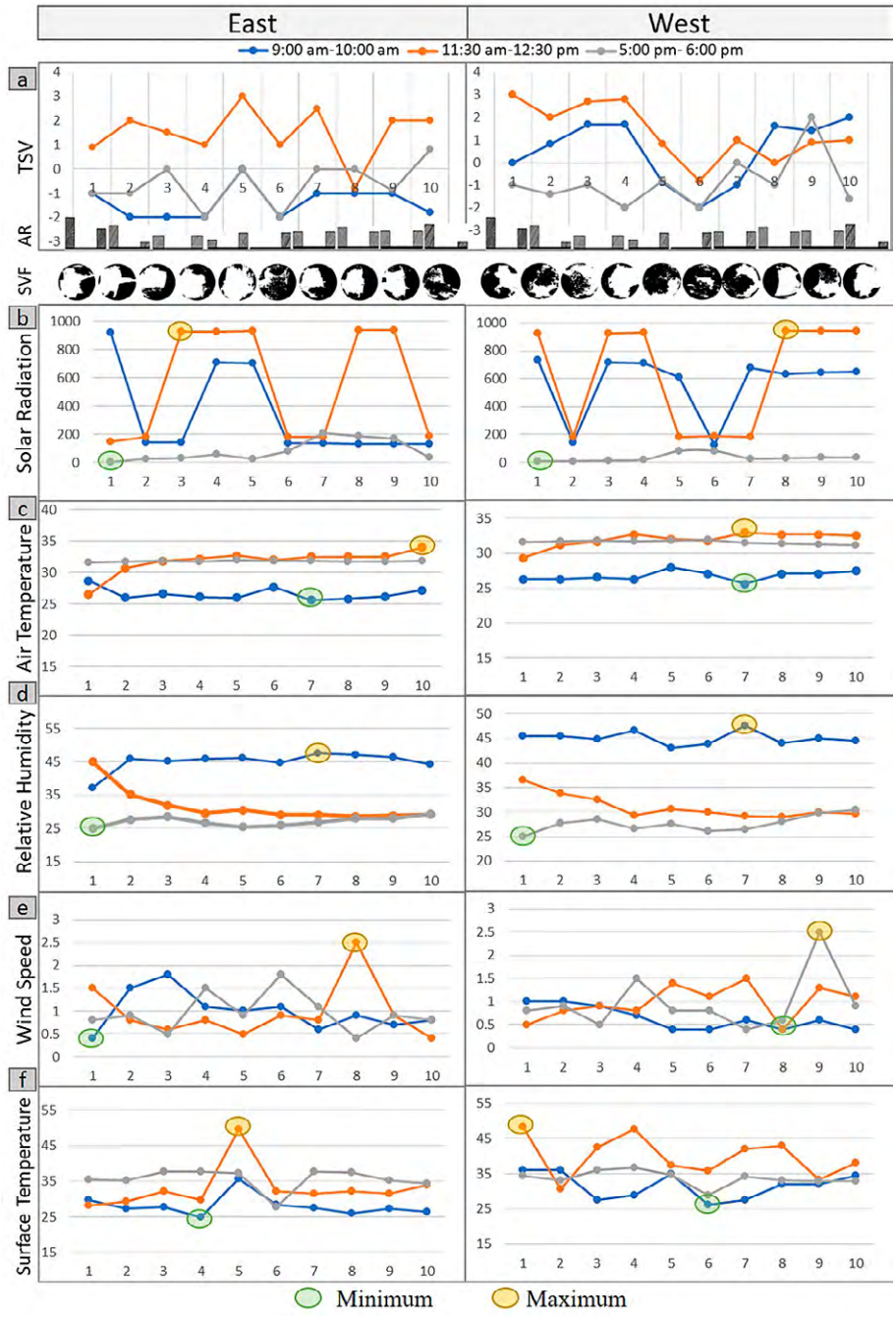

Figure 7. Diagram of factors connecting TSV, urban geometry, and microclimatic factors in Winter. Graph (a) shows variation in TSV at the studied time durations with AR and SVF; graphs (b),(c),(d), and (f) show the variation in microclimatic parameters

ly cool (-1) under shade, whereas slightly warm (2) under sunlight (Fig.7). Participants' Ws perception was between neutral to slightly windy in the morning (9:00 am – 10:00 am) and evening (5:00 pm – 6:00 pm). They preferred slightly less Ws as it made them feel a cool thermal sensation. In the afternoon (11:30 am - 12:30 pm), wind speed perception was between slightly less wind and neutral, and Ws preference was between neutral and more wind as thermal sensation improved with the wind. In Summer, the mTSV was between neutral and warm (2) under shade. In contrast, under sunlight, it was between warm (2) and very hot (4) (Fig.8). In the morning (9:00 am - 10:00 am) and evening (5:00 pm - 6:00 pm), the TSV was between neutral (0) under shade and warm (2) under direct sunlight. Participants' wind preference was neutral to more wind. In the afternoon (11:30 am - 12:30 pm), the TSV was between warm (2) and very hot(4), and participants' Ws preference was between less wind and neutral; the TSV in the afternoon increased because of low RH.

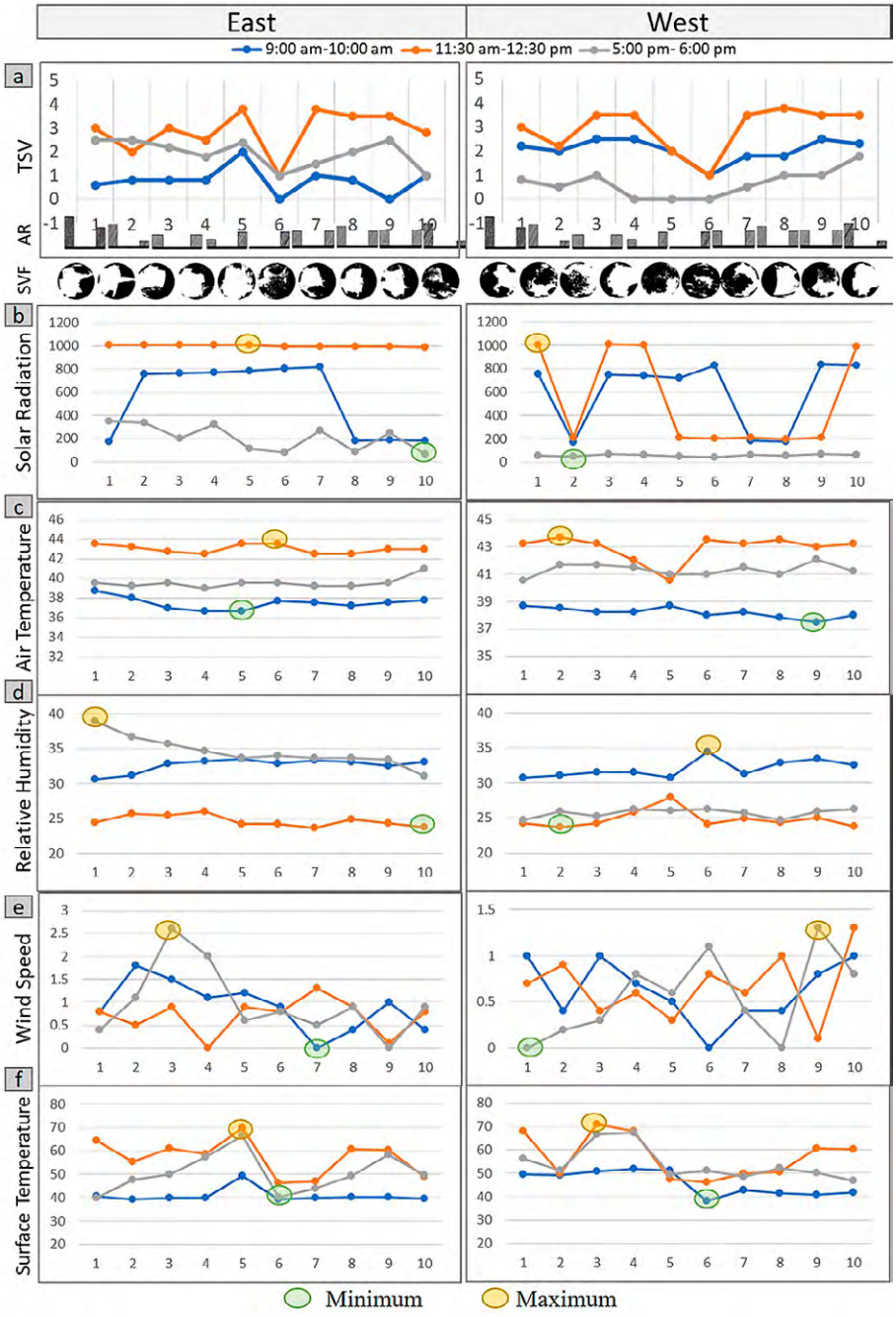

Figure 8. Diagram of factors connecting TSV, urban geometry, and microclimatic factors in Summer. Graph (a) shows variation in TSV at the studied time durations with AR and SVF; graphs (b),(c),(d), and (f) show the variation in microclimatic parameters

Change in TSV with Microclimate and Urban Geometry

Microclimate parameters play an essential role in outdoor thermal sensation. As discussed in thermal walk observations, the increase in Ta and solar radiation, outdoor thermal sensation increases, whereas it decreases with Ws and RH. The changes in TSV with respect to urban geometry and microclimatic parameters throughout the day are represented in Fig (7) for winter and Fig (8) for summer. This representation approach allows to compare the participants' thermal experiences with the measured environmental conditions.

In both the seasons, the TSV on eastern sidewalk in morning was low compared to the western sidewalk due to availability of shade on eastern sidewalk. In the afternoon the points with minimum SVF have low TSV. Whereas in the evening, during winter season, both sidewalks have almost similar TSV, due to low intensity of solar radiation and wind speed. The point 6 on both sidewalks have wide canopy tree thus the TSV at this point is low throughout the day, whereas the location East 5 has maximum SVF thus the TSV is high throughout the day in both seasons. The overall observations show that individuals exposed to direct sunlight tend to overestimate their thermal comfort, irrespective of the season, whereas those in shaded areas often underestimate it.

tion (Table 1). The difference between the F-value and the F-crit value in summer is greater than that in winter, indicating that people prefer to walk under shade for a in summer to feel comfortable. This indicates the importance of shading in the PTC.

Effect of Urban Geometry on mPET

The correlation analysis of urban geometry parameters, SVF, and mPET showed that during both seasons, the influence of urban geometry on thermal comfort varied with time and for the side of the street. During morning hours (9:00 am - 10:00 am) in both seasons, the east side of the street with buildings adjacent to it is not exposed to solar radiation. As a result, the MRT and mPET are at a minimum on this side. Conversely, most of the survey points expose the west side of the street to solar radiation, leading to maximum MRT and mPET values. Thus, the correlation between SVF and mPET is strong on the east side (R^2 value: 0.80 for summer and 0.65 for winter), whereas it is weak on the west side (R^2 value: 0.23 for summer and 0.24 for winter) (Fig 9,10).

In the afternoon (11:30 am - 12:30 pm), during both seasons, both sides of the street with high SVF are exposed to solar radiation, resulting in similar microclimates. Points with the presence of a tree or any other artificial shading

Table 1. Results of ANOVA using TSV as a covariate

One - way ANOVA							
	Source of variation	SS	df	MS	F	P-value	F crit
Summer	Between Groups	22139294	1	22139294	288.35	1.55E-49	3.86
	Within Groups	32016044	410	76777.08			
Winter	Between Groups	3026638	1	3026638	43.38	1.38E-10	3.86
	Within Groups	28603493	410	69764.62			

A one-way ANOVA test was performed to check if the TSV varies equally with solar radiation in both seasons. In this test, solar radiation is considered the independent variable, and TSV is the dependent variable. The level of impact of solar radiation on TSV is determined by comparing the F-value, F-crit value, and P-value. The results of the one-way ANOVA test showed that in both seasons, the TSV varies significantly with the level of solar radiation result in comparatively minimum MRT and mPET. Survey point East 5 has the maximum SVF value, leading to the maximum MRT and mPET values. On the other hand, survey points East 6 and West 6 have the minimum SVF, resulting in minimum MRT and mPET throughout the day. On the studied street, the east side has the presence of trees at multiple survey points; thus, the correlation on the east side is strong (R^2 value: 0.90 for summer and 0.92 for

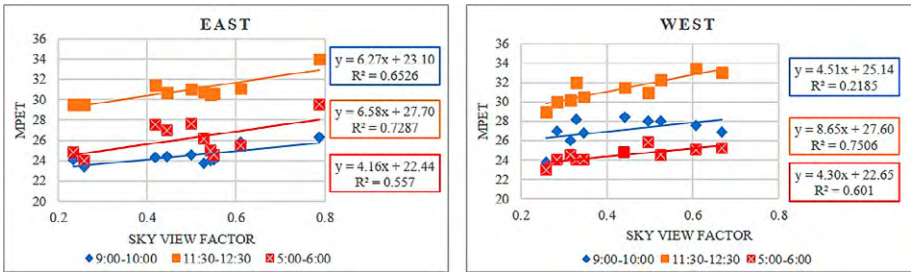

Figure 9. Correlation between SVF and mPET during the Winter

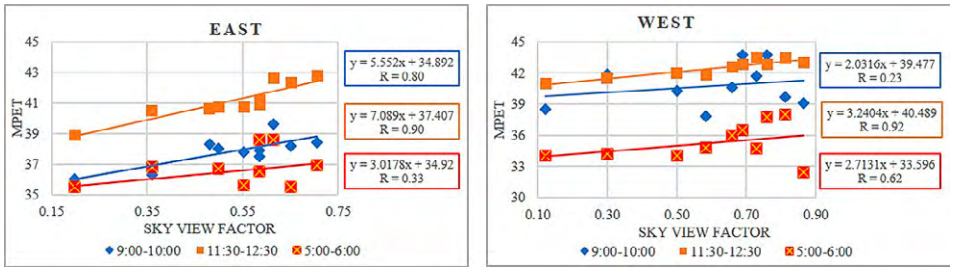

Figure 10. Correlation between SVF and mPET during the Summer

winter) compared to the west side (R^2 value:0.72 for summer and 0.75 for winter) (Fig 9,10).

In the summer season, during the evening (5:00 pm - 6:00 pm), the west side of the street has adjacent buildings blocking solar radiation, while the eastern side remains exposed to it. Therefore, the western side experiences minimum MRT and mPET compared with the eastern side. Thus, the correlation on the west side is strong (R^2 value: 0.62) (Fig 9), whereas on the east side, it is weak (R^2 value: 0.33) (Fig 10). In the winter season, as the sun's azimuth angle is lower, the buildings on the west side block solar radiation for both sides of the street, resulting in minimum mPET values for both sides. Thus, there is no significant difference in the correlation for both sides of the street (R^2 value: 0.55 for the east and 0.60 for the west) (Fig 9,10).

Change in TSV with mPET

The correlation between TSV and mPET can help establish a relationship between the perceived thermal comfort of individuals and the quantified thermal conditions based on mPET. The correlation indicates that people's thermal sensation votes are in agreement with the calculated mPET values (Fig.11).

Although TSV and mPET correlate positively, it is important to evaluate if the physiological stress associated with the mPET index is the same as the actual thermal sensation experienced by people. Thus, the neutral PET was determined using mTSV = 0 in the regression equation. The regression equation for the street in both seasons is described below:

$$y = 0.42x - 11.87 \text{ (East\_Winter)} \quad (3)$$

$$y = 0.38x - 10.74 \text{ (West\_Winter)} \quad (4)$$

$$y = 0.28x - 8.90 \text{ (East\_Summer)} \quad (5)$$

$$y = 0.39x - 12.67 \text{ (West\_Summer)} \quad (6)$$

Where,

- y = mTSV
- x = mPET

The results show that for winter, the neutral mPET values for the Eastern sidewalk is 28.1°C and for the western sidewalk is 27.9°C, respectively. Therefore, the average neutral mPET value for the winter is 28°C. Similarly, for summer, the neutral mPET values for the eastern and western sidewalk are 31.7°C and 32.4°C, respectively. Therefore, the average neutral mPET value for the summer is 32°C. According to the mPET index, the neutral thermal stress varies between 26-30°C (Chen et al., 2018). Whereas for Nagpur city, it is 32°C in summer. This shows an increase in adaptive tolerance to higher temperatures in the summer season, that is, the ability of individuals to adapt and adjust their comfort perceptions and responses based on changing environmental conditions.

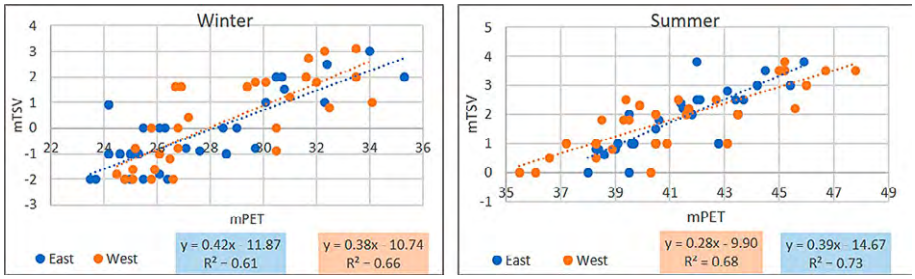

Figure 11. Correlation between mTSV and mPET for winter and summer

Discussion

The study was conducted in Nagpur city, which has a tropical Savannah climate. This study analyzes the seasonal and spatio-temporal behaviors of PTCs on an oriented street as a pilot study in the summer of 2022 and winter of 2023. The results show that urban geometry has an essential effect on the urban microclimate. Urban geometry governs the level of solar radiation, which influences ground Ts and Ta directly above it. The N– S orientation of the street is parallel to the solar path; thus, the building adjacent to the street effectively blocks solar radiation throughout the day and provides shade for pedestrians on the sidewalk. The correlation between SVF and mPET showed that the influence of SVF on microclimate and PTC varied throughout the day. In the morning, the minimum SVF is effective for the eastern sidewalks, whereas in the evening, it is effective for the western sidewalks because the building adjacent to the sidewalk blocks solar radiation. In the afternoon, due to the angle of solar radiation being approximately 90 degrees from the ground, trees or other shading devices block solar radiation. Thus, minimum SVF is effective. These findings are associated with previous studies that show a significant correlation between SVF and thermal comfort index and reported that N– S orientation streets with buildings adjacent to sidewalks are beneficial to PTC (Acero et al., 2019; Achour-Younsi & Kharrat, 2016; Bourbia & Awbi, 2004; Ketterer & Matzarakis, 2014; Narimani et al., 2022; Pearlmutter et al., 2007).

The thermal walk observations in both seasons showed a significant difference in thermal sensation results with respect to microclimatic parameters. It was observed that people's thermal sensations vary spatially with the level of solar radiation and temporally with temperature and wind. The results are aligned with previous studies that show that people overestimate their thermal sensation under direct sunlight and wind speed (Azegami et al., 2023; Kotharkar et al., 2024; Lam & Hang, 2017; Lau et al., 2019; Peng et al., 2022; Sanusi et al., 2016). The presence or absence of wind can significantly impact how cold individuals feel, even at the same temperature. Wind increases the rate of heat loss from the body through convection, making the surroundings feel colder than the actual temperature (Lau et al., 2019; Yu et al., 2021).

The neutral mPET value for winter is 28°C, and that for summer is 32°C. This indicates the dynamic nature of human comfort preferences, showcasing the ability of individuals to adjust their thermal expectations following seasonal variations. The neutral mPET values for Nagpur are similar to a research conducted in in Kolkata, where the neutral PET was calculated and the resultant values were 27.5 °C for winter and 30 °C (summer) (Banerjee et al., 2020). The neutral mPET value also indicated that it is crucial to calibrate the thermal comfort index according to the local conditions to mark the actual thermal sensation through an objective assessment of the outdoor environment.

Conclusion

Walkability is a sustainable mode of transportation and an efficient last-mile connectivity option. In tropical countries, climate is an essential barrier to walkability. This paper presents a pilot study conducted on Nagpur's commercial street as a methodological approach for assessing pedestrian thermal comfort. This study shows the relationship between urban street geometry, microclimate, and pedestrian thermal comfort. This study highlights the importance of a multidimensional approach for understanding pedestrian thermal comfort's spatiotemporal dynamics. It emphasizes the need for a multi-duration study to identify issues concerning the time of day when pedestrians experience maximum thermal stress and the combination of urban geometry that affects pedestrian thermal comfort.

This study shows a strong correlation between urban geometry and pedestrian thermal comfort. For streets with a North– South orientation, the aspect ratio and sky view factor play essential roles, and their influence on pedestrian thermal comfort changes throughout the day. Maximum comfort is experienced on the eastern sidewalk in the morning and on the western sidewalk in the evening due to the shading effect. Both sidewalks have the same comfort level in the afternoon, except for places with direct shading. The ANOVA test outcomes highlight the important role of solar radiation in influencing thermal sensation votes (TSV), demonstrating the importance of shading strategies in mitigating discomfort. The determination of neutral mPET values indicates the need for area-specific calibration of thermal comfort indices at the local level, enabling the identification of critical areas that require specific interventions based on objective assessments.

This study advocates including objective and subjective parameters in comprehensively assessing pedestrian thermal comfort. This study explains the behavior of N–S oriented streets; thus, the results can be applied to N– S oriented streets in similar climatic conditions. Further study will be conducted using the same method for a large data sample in terms of the number of participants for the thermal walk and the streets of different orientations. This method can help urban planners and researchers identify critical areas for pedestrian thermal comfort and develop context-specific mitigative strategies

Acknowledgement

Authors would like to express a sincere gratitude to climatology and photography lab of department of architecture and Planning VNIT Nagpur, for their support in providing the necessary instruments for the data collection. The authors are thankful to all respondents participated in the thermal walk survey.

References

Acero, J. A., Koh, E. J. Y., Li, X. X., Ruefenacht, L. A., Pignatta, G., & Norford, L. K. (2019). Thermal impact of the orientation and height of vertical greenery on pedestrians in a tropical area. *Building Simulation*, 12(6), 973–984. https://doi.org/10.1007/s12273-019-0537-1

Achour-Younsi, S., & Kharrat, F. (2016). Outdoor Thermal Comfort: Impact of the Geometry of an Urban Street Canyon in a Mediterranean Subtropical Climate – Case Study Tunis, Tunisia. *Procedia - Social and Behavioral Sciences*, 216, 689–700. https://doi.org/10.1016/j.sbspro.2015.12.062

Ahmadi Venhari, A., Tenpierik, M., & Taleghani, M. (2019). The role of sky view factor and urban street greenery in human thermal comfort and heat stress in a desert climate. *Journal of Arid Environments*, 166, 68–76. https://doi.org/10.1016/j.jaridenv.2019.04.009

Anupriya, R. S., & Rubeena, T. A. (2023). Spatio-temporal urban land surface temperature variations and heat stress vulnerability index in Thiruvananthapuram city of Kerala, India. *Geology, Ecology, and Landscapes*. https://doi.org/10.1080/24749508.2023.2182088

Arif, V., & Yola, L. (2020). The Primacy of Microclimate and Thermal Comfort in a Walkability Study in the Tropics: A Review. *Journal of Strategic and Global Studies*, 3(1). https://doi.org/10.7454/jsgs.v3i1.1025

ASHRAE (2013). *ANSI/ASHRAE Addendum h to ANSI/ASHRAE Standard 55-2012*. 8400. www.ashrae.org

ASHRAE (2023). *Standard 55*. https://ashrae.iwrapper.com/ASHRAE_PREVIEW_ONLY_STANDARDS/STD_55_2023

Azegami, Y., Imanishi, M., Fujiwara, K., & Kusaka, H. (2023). Effects of solar radiation in the streets on pedestrian route choice in a city during the summer season. *Building and Environment*, 235, 110250. https://doi.org/10.1016/j.buildenv.2023.110250

Baghaeipoor, G., & Nasrollahi, N. (2019). The effect of sky view factor on air temperature in high-rise urban residential environments. *Journal of Daylighting*, 6(2), 42–51. https://doi.org/10.15627/jd.2019.6

Banerjee, S., Ching N. Y, G., Yik, S. K., Dzyuban, Y., Crank, P. J., Pek Xin Yi, R., & Chow, W. T. L. (2022). Analysing impacts of urban morphological variables and density on outdoor microclimate for tropical cities: A review and a framework proposal for future research directions. *Building and Environment*, 225, 109646. https://doi.org/10.1016/j.buildenv.2022.109646

Banerjee, S., Middel, A., & Chattopadhyay, S. (2020). Outdoor thermal comfort in various microentrepreneurial settings in hot humid tropical Kolkata: Human biometeorological assessment of objective and subjective parameters. *Science of the Total Environment*, 721. https://doi.org/10.1016/j.scitotenv.2020.137741

Błazejczyk, K., Jendritzky, G., Bröde, P., Fiala, D., Havenith, G., Epstein, Y., Psikuta, A., & Kampmann, B. (2013). An introduction to the Universal thermal climate index (UTCI). *Geographia Polonica*, 86(1), 5–10. https://doi.org/10.7163/GPol.2013.1

Bourbia, F., & Awbi, H. B. (2004). Building cluster and shading in urban canyon for hot dry climate Part 1: Air and surface temperature measurements. *Renewable Energy*, 29(2), 249–262. https://doi.org/10.1016/S0960-1481(03)00170-8

Chen, L., & Ng, E. (2012). Outdoor thermal comfort and outdoor activities: A review of research in the past decade. *Cities*, 29(2), 118–125. https://doi.org/10.1016/j.cities.2011.08.006

Chen, Y. C., Matzarakis, A., Chen, Y. C., & Matzarakis, A. (2018). Modified physiologically equivalent temperature—basics and applications for western European climate. *ThApC*, 132(3–4), 1275–1289. https://doi.org/10.1007/S00704-017-2158-X

Chen, Y. C., Chen, W. N., Chou, C. C. K., & Matzarakis, A. (2020). Concepts and new implements for modified physiologically equivalent temperature. *Atmosphere*, 11(7), 1–17. https://doi.org/10.3390/atmos11070694

Chidambara. (2019). Walking the first/last mile to/from transit: Placemaking a key determinant. *Urban Planning*, 4(2), 183–195. https://doi.org/10.17645/up.v4i2.2017

Chidambaranath, P., & Bitossi, T. (2018). Final *Project Summary*. Transsolar Academy 2017-2018

Clean air initiative for Asian cities center (2011). *Walkability in Indian Cities*. Philippines; Pasig city. http://cleanairasia.org/wp-content/uploads/portal/files/Walkability-India_SEP.pdf

Moughtin, C. (2007). *Urban design: street and square*. Routledge.

Dai, Q., & Schnabel, M. A. (2013). Pedestrian Thermal Comfort in Relation to Street Zones with Different Orientations - A Pilot-Study of Rotterdam (Version 1). Open Access Te Herenga Waka-Victoria University of Wellington. https://doi.org/10.25455/wgtn.16418127.v1

Deevi, B., & Chundeli, F. A. (2020). Quantitative outdoor thermal comfort assessment of street: A case in a warm and humid climate of India. *Urban Climate*, 34, 100718. https://doi.org/10.1016/j.uclim.2020.100718

ESAF (2017). *Walkability and Pedestrian Facilities in Nagpur.* https://healthbridge.ca/images/uploads/library/Walkability__Pedestrian_Facilities_in_Nagpur_ESAF_HealthBridge_2017.pdf

Jamei, E., & Rajagopalan, P. (2015). Jamei, E., & Rajagopalan, P. (2015). Urban growth and pedestrian thermal comfort. In *The Proceedings of the 49th International Conference of the Architectural Science Association 2015* (pp. 907-918). http://anzasca.net/category/conference-papers/2015-conference-papers

Jamei, E., & Rajagopalan, P. (2019). Effect of street design on pedestrian thermal comfort. *Architectural Science Review*, 62(2), 92–111. https://doi.org/10.1080/00038628.2018.1537236

Katpatal, Y. B., Kute, A., & Satapathy, D. R. (2008). *Katpatal, Y. B., Kute, A., & Satapathy, D. R. (2008). Surface-and air-temperature studies in relation to land use/land cover of Nagpur urban area using Landsat 5 TM data. Journal of urban planning and development*, 134(3), 110-118. https://doi.org/10.1061/(ASCE)0733-9488(2008)134

Ketterer, C., & Matzarakis, A. (2014). Human-biometeorological assessment of heat stress reduction by replanning measures in Stuttgart, Germany. *Landscape and Urban Planning*, 122, 78–88. https://doi.org/10.1016/J.LANDURBPLAN.2013.11.003

Kim, Y., & Brown, R. (2022). Effect of meteorological conditions on leisure walking: a time series analysis and the application of outdoor thermal comfort indexes. *International Journal of Biometeorology*, 66(6), 1109–1123. https://doi.org/10.1007/s00484-022-02262-w

Kotharkar, R., Bagade, A., & Agrawal, A. (2019). Investigating local climate zones for outdoor thermal comfort assessment in an Indian city. *Geographica Pannonica*, 23(4), 318–328. https://doi.org/10.5937/GP23-24251

Kotharkar, R., Dongarsane, P., & Ghosh, A. (2024). Urban Climate Quantification of summertime thermal stress and PET range in a tropical Indian city. *Urban Climate*, 53, 101758. https://doi.org/10.1016/j.uclim.2023.101758

Kotharkar, R., Dongarsane, P., Ghosh, A., & Kotharkar, V. (2024). Numerical analysis of extreme heat in Nagpur city using heat stress indices, all-cause mortality and local climate zone classification. *Sustainable Cities and Society*, 101, 105099. https://doi.org/10.1016/j.scs.2023.105099

Kotharkar, R., Dongarsane, P., & Keskar, R. (2023). Determining influence of urban morphology on air temperature and heat index with hourly emphasis. *Building and Environment*, 233, 110044. https://doi.org/10.1016/j.buildenv.2023.110044

Kotharkar, R., Ramesh, A., & Bagade, A. (2018). Urban Heat Island studies in South Asia: A critical review. *Urban Climate*, 24, 1011–1026. https://doi.org/10.1016/J.UCLIM.2017.12.006

Kottek, M., Grieser, J., Beck, C., Rudolf, B., & Rubel, B. (2006). World Maps of Köppen-Geiger Climate Classification. *Meteorologische Zeitschrift*, 15(3),259-263. https://koeppen-geiger.vu-wien.ac.at/

Krüger, E. L., Minella, F. O., & Rasia, F. (2011). Impact of urban geometry on outdoor thermal comfort and air quality from field measurements in Curitiba, Brazil. *Building and Environment*, 46(3), 621-634. https://doi.org/10.1016/j.buildenv.2010.09.006

Kumar, P., Rai, A., Upadhyaya, A., & Chakraborty, A. (2022). Analysis of heat stress and heat wave in the four metropolitan cities of India in recent period. *Science of the Total Environment*, 818. https://doi.org/10.1016/j.scitotenv.2021.151788

Lam, C. K. C., & Hang, J. (2017). Solar Radiation Intensity and Outdoor Thermal Comfort in Royal Botanic Garden Melbourne during Heatwave Conditions. *Procedia Engineering*, 205, 3456–3462. https://doi.org/10.1016/j.proeng.2017.09.877

Laskar, S. I., Jaswal, K., Bhatnagar, M. K., & Rathore, L. S. (2016). India meteorological department. *Proceedings of the Indian National Science Academy*, 83(3), 1021-1037. https://doi.org/10.16943/ptinsa/2016/48501

Lau, K. K. L., Shi, Y., & Ng, E. Y. Y. (2019). Dynamic response of pedestrian thermal comfort under outdoor transient conditions. *International Journal of Biometeorology*, 979–989. https://doi.org/10.1007/s00484-019-01712-2

Mahmoud, H., Ghanem, H., & Sodoudi, S. (2021). Urban geometry as an adaptation strategy to improve the outdoor thermal performance in hot arid regions: Aswan University as a case study. *Sustainable Cities and Society*, 71, 102965. https://doi.org/10.1016/j.scs.2021.102965

Manavvi, S., & Rajasekar, E. (2020). Semantics of outdoor thermal comfort in religious squares of composite climate: New Delhi, India. *International Journal of Biometeorology*, 64(2), 253–264. https://doi.org/10.1007/s00484-019-01708-y

Mayer, H., & Höppe, P. (1987). Thermal comfort of man in different urban environments. *Theoretical and Applied Climatology*, 38(1), 43–49. https://doi.org/10.1007/BF00866252

Ministry of Urban Development. (2008). *Study on Traffic and Transport Policies and Strategies in Urban Areas in India*. Final Report May. https://mohua.gov.in/upload/uploadfiles/files/final_Report.pdf

Nagpur Metro Rail Corporation. (2023). *NMRCL - Project Profile*. https://www.metrorailnagpur.com/project-profile.aspx

Narimani, N., Karimi, A., & Brown, R. D. (2022). Effects of street orientation and tree species thermal comfort within urban canyons in a hot, dry climate. *Ecological Informatics*, 69, 101671. https://doi.org/10.1016/j.ecoinf.2022.101671

Nikolopoulou, M., Baker, N., & Steemers, K. (2001). Thermal comfort in outdoor urban spaces: Understanding the Human parameter. *Solar Energy*, 70(3), 227–235. https://doi.org/10.1016/S0038-092X(00)00093-1

Nikolopoulou, M., & Lykoudis, S. (2006). Thermal comfort in outdoor urban spaces: Analysis across different European countries. *Building and Environment*, 41(11), 1455–1470. https://doi.org/10.1016/J.BUILDENV.2005.05.031

Oke, T. R. (1988). Street design and urban canopy layer climate. *Energy and Buildings*, 11(1–3), 103–113. https://doi.org/10.1016/0378-7788(88)90026-6

Pearlmutter, D., Berliner, P., & Shaviv, E. (2007). Integrated modeling of pedestrian energy exchange and thermal comfort in urban street canyons. *Building and Environment*, 42(6), 2396–2409. https://doi.org/10.1016/J.BUILDENV.2006.06.006

Pecelj, M., Matzarakis, A., Vujadinović, M., Radovanović, M., Vagić, N., Đurić, D., & Cvetkovic, M. (2021). Temporal analysis of urban-suburban pet, mpet and utci indices in belgrade (Serbia). *Atmosphere*, 12(7), 1–21. https://doi.org/10.3390/atmos12070916

Peng, Z., Bardhan, R., Ellard, C., & Steemers, K. (2022). Urban climate walk: A stop-and-go assessment of the dynamic thermal sensation and perception in two waterfront districts in Rome, Italy. *Building and Environment*, 221, 109267. https://doi.org/10.1016/j.buildenv.2022.109267

Salal Rajan, E. H., & Amirtham, L. R. (2021). Impact of building regulations on the perceived outdoor thermal comfort in the mixed-use neighbourhood of Chennai. *Frontiers of Architectural Research*, 10(1), 148–163. https://doi.org/10.1016/j.foar.2020.09.002

Sanusi, R., Johnstone, D., May, P., & Livesley, S. J. (2016). Street Orientation and Side of the Street Greatly Influence the Microclimatic Benefits Street Trees Can Provide in Summer. *Journal of Environmental Quality*, 45(1), 167–174. https://doi.org/10.2134/JEQ2015.01.0039

Shamsuddin, S., Hassan, N. R. A., & Bilyamin, S. F. I. (2012). Walkable Environment in Increasing the Liveability of a City. *Procedia - Social and Behavioral Sciences*, 50, 167–178. https://doi.org/10.1016/j.sbspro.2012.08.025

India Smart City Mission (2015). *The Smart City Mission: Mission Transform-Nation*. https://smartcities.gov.in/

Surawar, M., & Kotharkar, R. (2017). Assessment of urban heat island through remote sensing in Nagpur urban area using landsat 7 ETM+ Satellite Images. *International Journal of Urban and Civil Engineering*, 11(7), 868-874. https://doi.org/10.5281/ZENODO.1131073

Svensson, M. K. (2004). Sky view factor analysis - Implications for urban air temperature differences. *Meteorological Applications*, 11(3), 201–211. https://doi.org/10.1017/S1350482704001288

Van Hoof, J. (2008). Forty years of Fanger's model of thermal comfort: Comfort for all? *Indoor Air*, 18(3), 182–201. https://doi.org/10.1111/j.1600-0668.2007.00516.x

Vasilikou, C., & Nikolopoulou, M. (2013). Thermal walks: identifying pedestrian thermal comfort variations in the urban continuum of historic city centres. In *Proceeding of PLEA2013-29th Conference, Sustainable architecture for a renewable future, Munich, Germany* (pp. 10-12).

Vasilikou, C., & Nikolopoulou, M. (2020). Outdoor thermal comfort for pedestrians in movement: thermal walks in complex urban morphology. *International Journal of Biometeorology*, 64(2), 277–291. https://doi.org/10.1007/s00484-019-01782-2

Yahia, M. W., Johansson, E., Thorsson, S., Lindberg, F., & Rasmussen, M. I. (2018). Effect of urban design on microclimate and thermal comfort outdoors in warm-humid Dar es Salaam, Tanzania. *International Journal of Biometeorology*, 62(3), 373–385. https://doi.org/10.1007/s00484-017-1380-7

Yu, Y., de Dear, R., Chauhan, K., & Niu, J. (2021). Impact of wind turbulence on thermal perception in the urban microclimate. *Journal of Wind Engineering and Industrial Aerodynamics*, 216, 104714. https://doi.org/10.1016/J.JWEIA.2021.104714

Zhang, Y., Du, X., & Shi, Y. (2017). Effects of street canyon design on pedestrian thermal comfort in the hot-humid area of China. *International Journal of Biometeorology*, 61(8), 1421–1432. https://doi.org/10.1007/S00484-017-1320-6

Zhou, X., & Chen, H. (2018). Impact of urbanization-related land use land cover changes and urban morphology changes on the urban heat island phenomenon. *Science of the Total Environment*, 635, 1467–1476. https://doi.org/10.1016/j.scitotenv.2018.04.091